TOPICS IN VORTEX MOTION

Thesis by

John Steven Sheffield

In Partial Fulfillment of the Requirements

For the Degree of

Doctor of Philosophy

California Institute of Technology

Pasadena, California

1978

(Submitted June 20, 1977)

ACKNOWLEDGMENTS

I would like to express my sincere gratitude to Professor P. G. Saffman for his guidance as my advisor and thesis supervisor. He not only suggested the problems considered in this work, but offered timely advice and encouragement during its completion.

Financial support during my stay as a graduate student was provided by the National Science Foundation and the California Institute of Technology.

I also want to thank Ruth Stratton for doing the typing on last minute notice, Daryl Madura for his help with the graphics, and the faculty and fellow graduate students who were always willing to take the time to discuss another's work. Finally, my thanks go to Lisa Anderson for her cheerful encouragement.

ABSTRACT

Six topics in incompressible, inviscid fluid flow involving vortex motion are presented. The stability of the unsteady flow field due to the vortex filament expanding under the influence of an axial compression is examined in the first chapter as a possible model of the vortex bursting observed in aircraft contrails. The filament with a stagnant core is found to be unstable to axisymmetric disturbances. For initial disturbances with the form of axisymmetric Kelvin waves, the filament with a uniformly rotating core is neutrally stable, but the compression causes the disturbance to undergo a rapid increase in amplitude. The time at which the increase occurs is, however, later than the observed bursting times, indicating the bursting phenomenon is not caused by this type of instability.

In the second and third chapters the stability of a steady vortex filament deformed by two-dimensional strain and shear flows, respectively, is examined. The steady deformations are in the plane of the vortex cross-section. Disturbances which deform the filament centerline into a wave which does not propagate along the filament are shown to be unstable and a method is described to calculate the wave number and corresponding growth rate of the amplified waves for a general distribution of vorticity in the vortex core.

In Chapter Four exact solutions are constructed for two-dimensional potential flow over a wing with a free ideal vortex standing over the wing. The loci of positions of the free vortex are found and the lift is calculated. It is found that the lift on the wing can be

significantly increased by the free vortex.

The two-dimensional trajectories of an ideal vortex pair near an orifice are calculated in Chapter Five. Three geometries are examined, and the criteria for the vortices to travel away from the orifice are determined.

Finally, Chapter Six reproduces completely the paper, "Structure of a linear array of hollow vortices of finite cross-section," co-authored with G. R. Baker and P. G. Saffman. Free streamline theory is employed to construct an exact steady solution for a linear array of hollow, or stagnant cored vortices. If each vortex has area A and the separation is L, then there are two possible shapes if $A^{1/2}/L$ is less than 0.38 and none if it is larger. The stability of the shapes to two-dimensional, periodic and symmetric disturbances is considered for hollow vortices. The more deformed of the two possible shapes is found to be unstable, while the less deformed shape is stable.

TABLE OF CONTENTS

INTRODUCTION

This work is presented in six chapters corresponding to the separate topics considered. With the exception of the third, the chapters are each self contained. The unifying theme is that each chapter examines some model of a physical phenomenon in which a major contribution to the flow is from a vortex, either a three-dimensional filament or a point vortex or hollow vortex in two dimensions. An incompressible, inviscid fluid with constant density is assumed in all cases.

The first chapter examines the stability of the unsteady flow field due to a vortex filament expanding under the influence of an axial compression. The structure of the filament core is either a uniform distribution of vorticity or a stagnant core with the vorticity concentrated on a cylindrical vortex sheet.

In the second and third chapters the stability of steady vortex filaments is examined, when they are deformed by small two-dimensional strain and shear flows in the plane of the filament cross-section. The motivation for examining the two deformations arises from separate physical phenomena and for that reason they are presented in separate chapters.

The exact solutions for two-dimensional potential flow over a wing with a free vortex standing over the wing are constructed in the fourth chapter. The possible positions of the free vortex and the effect of the vortex on the lift are examined.

Chapter Five makes use of complex variables to examine the trajectories of a pair of point vortices in the geometry modeling the

apparatus to generate vortex rings or pairs from a piston pushing fluid out a tube or channel.

Finally, the sixth chapter reproduces in total the paper, "Structure of a linear array of hollow vortices of finite cross-section," co-authored with G. R. Baker and P. G. Saffman.* The contributions to the paper from this author are the mappings in Section 6.3, the calculation of the curve in Figure 6.3, and the analysis of the recursion relation for finite β given in Section 6.5.

*This paper has been published in the Journal of Fluid Mechanics (1976), volume 74, part 3, pages 469-476.

CHAPTER 1

BURSTING OF A VORTEX UNDER COMPRESSION

1.1 Introduction

The study of the aircraft wake vortex system has been stimulated in the last decade by the increase in airport traffic and the introduction of the jumbo jets and the hazardous wake conditions they can produce. The vorticity shed from the trailing edge of the wings rolls up into a pair of counter-rotating trailing vortices. Under calm conditions this sytem remains strong for several miles behind the aircraft and presents a hazard to lighter aircraft. Chigier (1974) gives a popular presentation on this phenomenon and its effect on airport traffic. An understanding of the processes leading to the deterioration of the vortex system is needed in order to help develop means to accelerate the decay.

Crow (1970) examines the interaction of a pair of parallel line vortices in a perfect fluid, and finds that initially the most unstable disturbance is that with the center lines of the line vortices deformed into symmetric sinusoidal curves in planes tilted about 45 degrees from vertical, as shown in Figure 1.1. This disturbance is followed numerically by Moore (1972) to the touching of vortex cores. The curved vortex filaments for the finite amplitude waves remain close to the linear behavior of Crow's case.

Flight test studies by Chevalier (1973), Tombach (1973) and others use some tracers such as colored smoke released near the wingtips

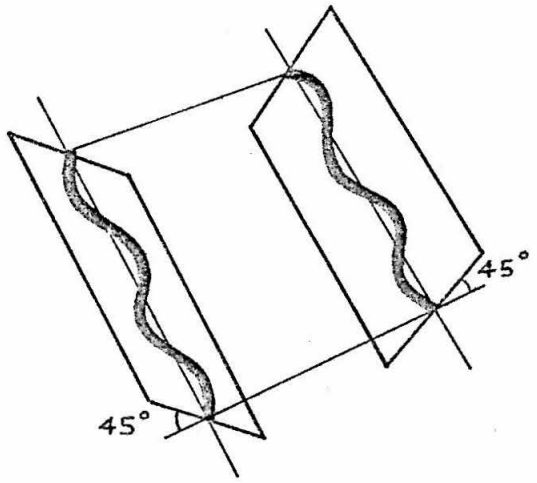

Figure 1.1 Section of the trailing vortices deformed by Crow instability, taken from Crow (1972).

to mark the position of the vortex core. For relatively calm conditions, both Chevalier and Tombach notice two predominant forms for the disruption of the vortex system. For one form the sinusoidal disturbances (Crow instability) grow in amplitude until the vortices link and form rings. The second form is characterized by an isolated bursting of the smoke marked vortex core. This second instability cannot arise in the analysis of Crow or Moore as they do not allow the core radius to vary along the filament.

The analysis of the stability of a single line vortex is done by Kelvin (1880). The dispersion relation for waves on the core boundary is found for a cylindrical vortex core in solid body rotation, surrounded by potential flow. These Kelvin waves are found to be stable for axisymmetric disturbances. Criteria for the stability of general

rotating flows to axisymmetric disturbances are established by Rayleigh (1916). The flow is unstable if at any distance from the axis of rotation the circulation decreases outward.

Uberoi, Chow and Narain (1972) extend the stability analysis to include vortices with axial flow and density discontinuities. Cases in which the axial flow is discontinuous across the vortex core boundary are expected to exhibit the Kelvin-Helmholtz instability for vortex sheets, so that waves in the axial direction are unstable. The effect of surface tension, rotation and density differences on these unstable waves are examined by Uberoi, et al.

The experimental work of Sarpkaya (1971) demonstrates the phenomenon known as vortex breakdown. A vortex in a diverging cylindrical duct develops instabilities of several forms. Under some conditions the dye-marked center line undergoes spiral displacements which grow and eventually lead to turbulent mixing. Other conditions produce a near axisymmetric bubble expanding at a stagnation point in the flow. Downstream from the bubble the vortex appears to have lost its tight structure and decays rapidly. These forms of vortex breakdown are also seen in Lambourne and Bryer (1961) for vortices formed over a delta wing at a high angle of attack. The axisymmetric form of vortex breakdown offers a possible explanation for the bursting seen in trailing vortices. Both are characterized by the rapid growth of the core in a small section of the vortex.

Hall (1972) gives a discussion of several of the explanations of the vortex breakdown phenomenon, and proposes a theory combining

features of some of them. He views the formation of the bubble as a strongly nonlinear phenomenon in which the flow tends to some critical state near an axial stagnation point. For sufficiently high swirl velocities the flow field jumps from a supercritical to a subcritical state. The distinction between states is that only the subcritical flow can support standing waves which do not propagate relative to the jump. The rapid local growth of the core results from the transition. While no theory for vortex breakdown is widely accepted, numerical work by Grabowski and Berger (1976) supports Hall's explanation. The numerical solutions are restricted to axisymmetric flows, modelling only the bubble form of breakdown.

Vortex breakdown is only a possible explanation for the bursting phenomenon seen in the aircraft wake vortices. Other mechanisms may be responsible for the observed bursting. From the range of phenomena observed, it seems feasible that bursting could be the result of more than a single mechanism. Widnall, Bliss and Zalay (1971) state that in towing tank experiments the bursts occur at the crests on the sinusoidally deformed filaments, the points of greatest separation. Scorer and Davenport (1970) give the location of the bursts as the troughs of the wave, the points of minimum separation. The flight experiments of Tombach show bursting at positions along the vortex seemingly independent of the sinusoidal deformation. The relationship between the core bursting and the Crow instability is mentioned by Chevalier (1973). He induces core bursting by producing small oscillations in the angle of attack. The bursts appear at even intervals along the trailing

vortices, corresponding to the wavelength of the Crow instability.

The effect of the growth of the Crow instability on the vortex filament may offer some insight into the bursting phenomenon. The numerical work of Moore (1972) follows the Crow instability to finite amplitudes. The two vortex filaments are found to be stretched in the troughs and compressed at the crests. The amount of compression or extension due to the sinusoidal deformation of the vortices can be estimated from Moore's calculation. These estimates neglect axial flow in the filament, variations in the core radius along the filament, and variations from the uniform vorticity in the vortex filament, but give a qualitative description of the deformed filament.

Saffman (1974) suggests the axial compression of the vortices as a possible mechanism responsible for the observed bursting. In order to examine this possibility, Section 1.2 defines a flow field modelling the compressed section of the vortex and discusses the stability criterion for that model. In Sections 1.3 through 1.6 the stability of the model is examined for the case with the vorticity concentrated on a vortex sheet at the core boundary. In Sections 1.7 through 1.9 the filament core contains constant vorticity.

1.2 Model Problem

As a simplified model of the flow in the deformed vortex filament, the straight filament with axial compression in an unbounded perfect fluid can be examined. The equations of motion governing this system

are the Euler equations and the equation of continuity. For brevity the density is put equal to unity. Define a cylindrical coordinate system (r,θ,z) with the z axis as the center line for the vortex filament. The radial, azimuthal and axial velocities are denoted by U, V and W for the undisturbed flow. The governing equations for the velocities and pressure, P, in this system are

$$\frac{\partial U}{\partial t}+U\frac{\partial U}{\partial r}-\frac{1}{r}V^2+\frac{1}{r}V\frac{\partial U}{\partial \theta}+W\frac{\partial U}{\partial z}=-\frac{\partial P}{\partial r}\ , \tag{1.2.1a}$$

$$\frac{\partial V}{\partial t}+U\frac{\partial V}{\partial r}+\frac{1}{r}UV+\frac{1}{r}V\frac{\partial V}{\partial \theta}+W\frac{\partial V}{\partial z}=-\frac{1}{r}\frac{\partial P}{\partial \theta}\ , \tag{1.2.1b}$$

$$\frac{\partial W}{\partial t}+U\frac{\partial W}{\partial r}+\frac{1}{r}V\frac{\partial W}{\partial \theta}+W\frac{\partial W}{\partial z}=-\frac{\partial P}{\partial z}\ , \tag{1.2.1c}$$

$$\frac{\partial U}{\partial r}+\frac{1}{r}U+\frac{1}{r}\frac{\partial V}{\partial \theta}+\frac{\partial W}{\partial z}=0\ . \tag{1.2.1d}$$

For the vortex core of radius a, the azimuthal or swirl velocity is assumed to be of the form

$$V=\begin{cases}\dfrac{\tilde{\kappa} r}{2\pi a^2} & \text{for } r<a\\[2ex] \dfrac{\kappa}{2\pi r} & \text{for } r>a\ .\end{cases} \tag{1.2.2}$$

The two cases to be considered have $\tilde{\kappa}=0$ and $\tilde{\kappa}=\kappa$. The first case, the stagnant core vortex, has the vorticity concentrated on the vortex sheet at $r=a$. The second has constant vorticity in the core and continuous velocities everywhere. This will be called the uniform core vortex. The Kelvin circulation theorem requires that κ be constant.

To model the compression, the flow field with velocities

$$U = \alpha r \quad \text{and} \quad W = -2\alpha z \tag{1.2.3}$$

is superimposed on the vortex. The factor $\alpha = \alpha(t)$ is a function of time, t. In order that the full flow field satisfy the Euler equations, the core radius, a, must also be a function of time. Substituting the velocities into the aximuthal momentum equation gives

$$\frac{da}{dt} - \alpha a = 0$$

or, integrating from some initial time,

$$a(t) = a_0 \exp\left(\int_{t_0}^{t} \alpha(\tau) d\tau \right) , \tag{1.2.4}$$

where a_0 is the core radius at the initial time, t_0. In the work presented here, $\alpha(t)$ is taken either as a constant or proportional to t^{-1}. For the case α a constant, it is convenient to take $t_0 = 0$. The core radius a(t) is then of the form

$$a(t) = a_0 e^{\alpha t} . \tag{1.2.5}$$

The increase in the core radius can be limited to algebraic growth by choosing a compression

$$\alpha(t) = \nu/t , \tag{1.2.6}$$

where ν is a constant. For $t_0 = 1$, the core radius is defined by the relation

$$a(t) = a_o t^{\nu} . \qquad (1.2.7)$$

If the above is to model the deformation of the vortex responsible for core bursting, then disturbances on the core boundary should grow much faster than the expansion given in equations (1.2.5) and (1.2.7). Waves on the core are expected to grow for sufficiently large compression, as they cannot escape outward along the filament. In opposition to these trapped waves, the rotation of the vortex core (for the uniform core vortex) tends to have a stabilizing effect.

The growth of disturbance along the vortex filament can be analyzed by adding an infinitesimal disturbance to the exact solution for the velocities and pressure and substituting into the equations of motion. Retaining only terms linear in the disturbance quantities gives the equations for the linearized stability of the compressed vortex. In some regions the undisturbed flow field is described by potential flow. The disturbance can be expressed as a velocity potential in these regions. The length scale of the system is increasing, so that some care must be taken in defining stability. For steady flows, stability to infinitesimal disturbances is determined by the growth or decay of the initial disturbance. Moore and Griffith-Jones (1974) examine the two-dimensional stability of an expanding cylindrical vortex sheet. They initially choose to define stability by requiring that disturbances to the sheet remain bounded, but modify the interpretation by noting that for algebraic growth, initially small disturbances remain small over the time scale of an experiment. The expansion at which the growth rate of disturbances changes from exponential

to algebraic is the stability boundary for their problem.

A similar approach to the definition is used here. The deflection of the vortex core radius seems an appropriate quantity on which to base the stability analysis. The disturbed core radius, $R(\theta,z,t)$, can be written as

$$R(\theta,z,t) = a(t)\left(1+\tilde{\delta}(\theta,z,t)\right). \qquad (1.2.8)$$

The deflection function $\tilde{\delta}$ gives a measure for the stability. If $\tilde{\delta}$ decreases in time, the system will be considered stable, even when the product $a(t)\tilde{\delta}$ increases.

The existence of unstable solutions is not sufficient to demonstrate that the compressed vortex models the bursting phenomenon. The disturbance must grow rapidly on a time scale comparable with the linking of the pair of trailing vortices. The calculation of finite amplitude waves on the pair of vortex filaments by Moore (1972) gives estimates for the parameters in the model. These values are used to examine the behavior of the deflection, $\tilde{\delta}$. The disturbances considered are often restricted to be axisymmetric, as this simplification appears physically justified from the observed bursting.

1.3 Stagnant Core Vortex

The disturbance velocities and pressure for the compressed stagnant core vortex can be written in terms of a velocity potential in the core region and outside the core. This simplification to the stability analysis arises from the constraint that the vorticity is non-zero only

on the cylindrical vortex sheet at the core boundary. If $R(\theta,z,t)$ is the core radius, then the equations describing the behavior of the disturbance velocity potential $\tilde{\phi}$ are

$$\begin{aligned} \nabla^2\tilde{\phi}_1 &= 0 \qquad \text{for} \quad r<R, \\ \nabla^2\tilde{\phi}_2 &= 0 \qquad \text{for} \quad r>R, \end{aligned} \tag{1.3.1}$$

where the subscript 1 is used to denote quantities defined in the core region and the subscript 2 outside the core. The disturbance potentials must satisfy the conditions that $\tilde{\phi}_2$ tends to zero far from the vortex and $\tilde{\phi}_1$ is bounded at the core center.

The vortex sheet must move as a material surface. This constraint gives the kinematic condition for the position of the sheet,

$$\frac{D}{Dt}(r-R) = 0 \quad \text{on} \quad r=R, \tag{1.3.2}$$

where D/Dt is the material derivative. Substituting the velocities given in equations (1.2.2) and (1.2.3) and the form of the core radius given in equation (1.2.8) into the kinematic sheet condition gives two equations for the motion of the sheet. Linearized stability theory dictates that only terms linear in the disturbance quantities be retained and all quantities be evaluated at the undisturbed position of the sheet. The resulting pair of equations for the kinematic sheet condition in terms of the deflection, $\tilde{\delta}$, and disturbance potentials, $\tilde{\phi}_1$ and $\tilde{\phi}_2$, are

$$\frac{\partial \tilde{\delta}}{\partial t} - 2\alpha z \frac{\partial \tilde{\delta}}{\partial z} = \frac{\partial \tilde{\phi}_1}{\partial r},$$
$$\frac{\partial \tilde{\delta}}{\partial t} + \frac{K}{2\pi a^2} \frac{\partial \tilde{\delta}}{\partial \theta} - 2\alpha z \frac{\partial \tilde{\delta}}{\partial z} = \frac{\partial \tilde{\phi}_2}{\partial r}. \qquad (1.3.3)$$

A second constraint on the vortex sheet position is the dynamic condition that the pressure be continuous across the sheet. The discontinuity of the swirl velocity that accounts for the vortex sheet creates pressure deviations when the sheet is deformed, which must be balanced by the disturbance pressures due to the velocity potentials. The change in the pressure across the sheet due to the deflection is

$$P_2(R) - P_1(R) = -\tfrac{1}{2}\left(\frac{K}{2\pi a}\right)^2 \left((1+\tilde{\delta})^2 - 1 \right). \qquad (1.3.4)$$

The disturbance pressure, p, due to the disturbed velocity potential can be written from Bernoulli's integral, linearized in the disturbance quantities,

$$p = -\frac{\partial \tilde{\phi}}{\partial t} - U \frac{\partial \tilde{\phi}}{\partial r} - \tfrac{1}{r} V \frac{\partial \tilde{\phi}}{\partial \theta} - W \frac{\partial \tilde{\phi}}{\partial z}, \qquad (1.3.5)$$

where U, V and W are the undisturbed velocities and the subscripts 1 and 2 both apply. The continuity of pressure across the sheet requires the disturbance pressure to satisfy

$$p_2 - p_1 = -\left(\frac{K}{2\pi a}\right)^2 \tilde{\delta} \quad \text{on the sheet.} \qquad (1.3.6)$$

Substituting the form of p from equation (1.3.5) into the above and using the kinematic sheet condition to simplify the resulting expression yields the dynamic sheet condition

$$\left(\frac{\partial}{\partial t} - 2\alpha z \frac{\partial}{\partial z}\right)\left(\tilde{\phi}_2 - \tilde{\phi}_1\right) + \frac{K}{2\pi a^2}\tilde{\phi}_2$$
$$= \left(\frac{K}{2\pi a}\right)^2 \tilde{\delta} - \frac{K}{2\pi a^2}\frac{\partial \tilde{\delta}}{\partial \theta} \quad \text{on} \quad r = a. \tag{1.3.7}$$

The axial and azimuthal dependence can each be separated from the equation by examining the growth of normal modes of the initial conditions. The form of the potentials and deflection can be written as

$$\begin{aligned} \tilde{\phi}_1 &= \phi_1(r,t)\exp(ikz + in\theta), \\ \tilde{\phi}_2 &= \phi_2(r,t)\exp(ikz + in\theta), \\ \tilde{\delta} &= \delta(t)\exp(ikz + in\theta), \end{aligned} \tag{1.3.8}$$

where n is an integer and k = k(t) is a function of time. The form for the time dependent wave number in order that the axial dependence separates is

$$k(t) = k_o \exp\left(2\int_{t_o}^{t} \alpha(\tau)\, d\tau\right), \tag{1.3.9}$$

where k_o is the initial crucial wave number. Allowing k to be time dependent is equivalent to replacing z by a new variable,

$$\xi = kz/k_o, \tag{1.3.10}$$

and separating the dependence on ξ.

Since the disturbance velocity potentials satisfied Laplace's equation, both ϕ_1 and ϕ_2 satisfy

$$\frac{1}{r}\frac{\partial}{\partial r}\left(r\frac{\partial\phi}{\partial r}\right)-\left(k^2+\frac{n^2}{r^2}\right)\phi=0 \tag{1.3.11}$$

and the radial dependence is determined by invoking the conditions at infinity and the origin. The solutions to equation (1.3.11) are the modified Bessel functions, I_n and K_n, giving potentials of the form

$$\begin{aligned}\phi_1 &= A_1(t)\,I_n(kr),\\ \phi_2 &= A_2(t)\,K_n(kr),\end{aligned} \tag{1.3.12}$$

where A_1 and A_2 need be determined from the sheet conditions.

Substituting for $\tilde{\phi}_1$, $\tilde{\phi}_2$ and $\tilde{\delta}$ in the kinematic and dynamic conditions on the sheet (equations (1.3.7) and (1.3.3)) gives a set of three ordinary differential equations for the functions A_1, A_2 and δ. These can be written as

$$\begin{aligned}&\frac{d\delta}{dt}-\frac{k}{a}I_n'(ka)A_1=0,\\ &\frac{d\delta}{dt}-\frac{k}{a}K_n'(ka)A_2-in\Omega\delta=0,\\ &\frac{d}{dt}\left(A_1I_n(kr)-A_2K_n(kr)\right)\Big|_{r=a}-in\Omega K_n(ka)A_2\\ &\qquad=(in\alpha-\Omega)\Omega a^2\delta,\end{aligned} \tag{1.3.13}$$

where the primes indicate differentiation with respect to the arguments and Ω is the maximum rotational velocity defined by

$$\Omega=\frac{K}{2\pi a^2}. \tag{1.3.14}$$

Eliminating A_1 and A_2 in the above gives a single ordinary differential equation for $\delta(t)$. This equation can be written as

$$\frac{d^2\delta}{dt^2} + p(t)\frac{d\delta}{dt} + q(t)\delta = 0 , \qquad (1.3.15)$$

where

$$\left.\begin{aligned} p(t) &= -\alpha - 3\alpha k^2 a^2 \left(\frac{I_n' K_n K_n''}{K_n'} - \frac{I_n K_n' I_n''}{I_n'} \right) \\ &\quad - 2in\Omega ka I_n' K_n , \\ q(t) &= -\Omega^2 k^2 a^2 I_n' \left(K_n' + \frac{n^2}{ka} K_n \right) - 3i\alpha n \Omega ka I_n' \left(K_n \right. \\ &\quad \left. + ka K_n K_n''/K_n' - ka K_n' \right), \end{aligned}\right\} \qquad (1.3.16)$$

and the argument of the modified Bessel functions is always ka.

The equation for axisymmetric disturbances (n=0) reduces to

$$\frac{d^2\delta}{dt^2} + \left[2\alpha - 3\alpha ka \left(\frac{I_0}{I_1} - \frac{K_0}{K_1} \right) \right] \frac{d\delta}{dt} + \Omega^2 k^2 a^2 I_1 K_1 \delta = 0 . \qquad (1.3.17)$$

Even for this simple case, an exact solution is not found. The equation needs to be examined further.

For the limiting case of zero compression, equation (1.3.17) has constant coefficients and can be solved. These solutions are discussed in the next section.

The asymptotic behavior of the solutions to equation (1.3.17) for large time can be determined using the WKBJ method. If strongly unstable solutions exist, they should demonstrate appropriate asymptotic growth. This analysis is contained in Section 1.5.

The estimates of the size of α/Ω_0 (where Ω_0 is the initial value of the maximum rotation rate, Ω) for constant compression suggest examining the solution for $\alpha/\Omega_0 << 1$. The stability problem is

formulated in terms of a variational principle in Section 1.6, and approximations to the solution found for small α/Ω_0.

In Section 1.7 the results of integrating equation (1.3.17) numerically are given for the case of constant compression. The growth of the solutions for the small compression can be compared with the values from Section 1.6. The dependence of the asymptotic solutions found in Section 1.5 on the initial parameters is also examined by the numerical integration.

1.4 Undeformed Stagnant Core

Before trying to examine the stability of the compressed stagnant core vortex deformed by a small compression, the solution in the limit of zero compression should be determined. The governing equation for $\alpha = 0$ is deduced from equation (1.3.15) to be

$$\frac{d^2\delta}{dt^2} + 2in\Omega ka I_n' K_n \frac{d\delta}{dt} - \Omega^2 k^2 a^2 I_n' \left(K_n' + \frac{h^2}{ka} K_n\right)\delta = 0, \qquad (1.4.1)$$

where k, a and Ω are constants and the argument of the modified Bessel function is ka. Substituting the expression

$$\delta(t) = \delta_0 e^{i\omega t} \qquad (1.4.2)$$

into the differential equation gives the dispersion relation for waves on the vortex sheet in terms of the dimensionless axial wave number, ka, the azimuthal wave number, n, and the dimensionless frequency, ω/Ω. The dispersion relation is a quadratic equation in the frequency of the form

$$\left(\frac{\omega}{\Omega}\right)^2 - 2n\,ka\,I_n' K_n \left(\frac{\omega}{\Omega}\right) + k^2a^2\, I_n' \left(K_n' + \frac{n^2}{ka} K_n\right) = 0 \qquad (1.4.3)$$

and the sign of the imaginary part of the solution for ω/Ω determines stability. The coefficients of equation (1.4.3) are real, so the pair of roots must be complex conjugates if the imaginary part is to be non-zero. The resulting criterion for stability is that the roots of the dispersion relation be real. Substituting the coefficients into the quadratic formula gives the relation

$$\frac{\omega}{\Omega} = -ka\left(n \pm \left[I_n' K_n' (n^2 I_n K_n - 1)\right]^{\frac{1}{2}}\right). \qquad (1.4.4)$$

Since I_n' and $-K_n'$ are positive for real positive ka, the solutions are unstable for axial and azimuthal wave numbers satisfying

$$I_n(ka)\, K_n(ka) > 1/n^2. \qquad (1.4.5)$$

These solutions grow exponentially with the amplification rate given by the imaginary part in equation (1.4.4).

In order to determine the nature of the stability boundary given in terms of the modified Bessel functions, examine the long and short axial wave limits,

$$I_n(ka) K_n(ka) \sim 1/2|n| \qquad \text{as } ka \to 0, \qquad (1.4.6)$$

$$I_n(ka) K_n(ka) \sim 1/2ka \qquad \text{as } ka \to \infty. \qquad (1.4.7)$$

For two-dimensional disturbances the stability is given by the ka = 0

limit. Combining equations (1.4.5) and (1.4.6) determines that the two-dimensional waves are unstable for the azimuthal wave numbers, $n \geq 3$. For sufficiently large axial wave number, the solutions are stable for a given value of n. Similarly, for a fixed value of ka, solutions are unstable for sufficiently large n. In general, for a fixed $n \geq 3$ there is a critical axial wave number, ka*, at which there is a change of stability. As a function of n, the critical axial wave number increases as n increases. The first few values of ka*, calculated numerically from equation (1.4.5) are given in Table 1.1 below:

Table 1.1

n	3	4	5	6	7	8	9	10
ka*	3.33	6.93	11.5	17.0	23.5	31.0	39.5	49.0

Using an asymptotic expansion for large n in the modified Bessel functions, the critical axial wave number can be approximated by

$$ka^*(n) \sim n\left(\frac{n^2}{4}-1\right)^{1/2} \quad \text{for } n \text{ large.} \tag{1.4.8}$$

Disturbances are unstable for $ka < ka^*(n)$ and $n \geq 3$, and stable otherwise.

The axisymmetric disturbance waves along the stagnant core are stable for all wave numbers. The effect of the compression on these stable waves is investigated in the next three sections.

1.5 Asymptotic Behavior for Stagnant Core

Even though the asymptotic behavior of the deflection does not give exact information about the initial growth, it can help to point out the stable and unstable disturbances. The procedure is to consider disturbances, which grow asymptotically faster than the undisturbed core radius, as unstable. The analysis presented here is restricted to axisymmetric disturbances. The algebra involved for the higher modes is lengthy to present, and since the procedure is identical, only results will be given.

For constant compression α , the asymptotic behavior of the scaled amplitude δ is determined by the WKBJ method. Equation (1.3.17) describing the behavior of δ, is transposed into the standard form by defining the scaled function

$$f(t) = \Omega (I_1 K_1)^{\frac{1}{2}} \delta(t) \ , \tag{1.5.1}$$

where the argument of the modified Bessel functions is the time dependent, nondimensional wave number, ka. The equation for the growth of f is

$$\frac{d^2 f}{dt^2} - \hat{q}(t) f = 0 \ , \tag{1.5.2}$$

where

$$\hat{q}(t) = \alpha^2 - \Omega^2 k^2 a^2 I_1 K_1 - 12 \left(\frac{I_0}{I_1} - \frac{K_0}{K_1} \right. \\ \left. - 9\alpha^2 k^2 a^2 \left(1 + \tfrac{1}{2} \frac{I_0 K_0}{I_1 K_1} - \tfrac{3}{4} \left(\frac{I_0^2}{I_1^2} + \frac{K_0^2}{K_1^2} \right) \right) \right. . \tag{1.5.3}$$

For α positive, ka grows like $e^{3\alpha t}$ and Ω is proportional to $e^{-2\alpha t}$. By substituting the asymptotic behavior of the Bessel functions into equation (1.5.3) and retaining only the leading two orders, the coefficient $\hat{q}(t)$ is shown to be bounded, and

$$\hat{q}(t) = \alpha^2/4 - \tfrac{1}{8}\Omega^2 ka + O(e^{-6\alpha t}) \quad \text{as } t \to \infty. \tag{1.5.4}$$

The WKBJ approximation applied to equation (1.5.2) gives the asymptotic form for f(t) as

$$f(t) \sim \text{constant} \cdot \hat{q}^{-\frac{1}{4}} \exp\left(\int \hat{q}^{\frac{1}{2}}\, dt\right) \quad \text{as } t \to \infty. \tag{1.5.5}$$

The behavior of $\hat{q}$, f and the modified Bessel functions for large time, t, substituted into equation (1.5.1), give the asymptotic behavior of the deflection, δ. The dominant term in the expansion,

$$\delta(t) \sim \text{constant} \cdot e^{\alpha t} \quad \text{as } t \to \infty, \tag{1.5.6}$$

is unbounded, implying that the stagnant core vortex for constant compression is unstable to axisymmetric disturbances.

For a non-zero azimuthal mode n, the procedure above can be duplicated with the same result. The amplitude of waves on the vortex increases like the square of the magnitude of the exponentially increasing core radius, a(t). This amplification is examined on the time scale of the bursting phenomenon in Section 1.7.

For that compression leading to the algebraically expanding core, the analysis of the asymptotic behavior of the deflection is facilitated by defining a new function of time, y(t), as

$$y(t) = \Omega^2 \, (I_1 K_1)^{-1} \, \frac{d\delta}{dt} \, . \tag{1.5.7}$$

The argument of the modified Bessel functions, ka, increases as $t^{3\nu}$. Combining equations (1.5.7) and (1.3.17) gives the relation between dy/dt and δ as

$$\frac{dy}{dt} + \Omega^4 k^2 a^2 \delta = 0. \tag{1.5.8}$$

The small compression values are of interest from physical considerations. By limiting the initial compression, $\alpha(1) < 1/2$, or equivalently, $\nu < 1/2$, the time can be replaced by the dimensionless time, s, using

$$s = \frac{\Omega t}{1-2\nu} \, . \tag{1.5.9}$$

The time dependence of $\Omega(t) = \Omega_0 t^{-2\nu}$ does not affect the direction of increasing time for the restricted range of ν. In terms of the new time, the pair of equations for y(s) and δ(s) are

$$\begin{aligned} \frac{d\delta}{ds} - \Omega^{-3} I_1 K_1 y &= 0, \\ \frac{dy}{ds} + \Omega^3 k^2 a^2 \delta &= 0. \end{aligned} \tag{1.5.10}$$

The coefficient $\Omega^3 k^2 a^2$ is independent of time and allows equations

(1.5.10) to be easily combined into a single equation for y(s), written

$$\frac{d^2\gamma}{ds^2} + k^2a^2 I_1 K_1 \gamma = 0. \qquad (1.5.11)$$

The WKBJ method applied to this equation gives the asymptotic result

$$\gamma(s) \sim \text{constant} \cdot (ka)^{\frac{1}{4}} \exp\left(\pm i \int ka\,(I_1K_1)^{\frac{1}{2}}\,ds\right) \qquad (1.5.12)$$

for large values of s. The behavior of $\delta(t)$ follow directly from equation (1.5.9) as

$$\delta(t) \sim \text{constant} \cdot t^{\frac{3\nu}{2}} \exp\left(\pm i \int \Omega ka\,(I_1K_1)^{1/2}\,dt\right). \qquad (1.5.13)$$

This expression agrees with the bounded wave behavior for the limiting case of $\nu = 0$ given in the previous section. The introduction of the compression causes the waves to become unstable.

1.6 Small Compression for the Stagnant Core

The initial growth of disturbances to the stagnant core vortex under constant compression can be determined when the compression is sufficiently small. In this context small compression means that α is small compared with the initial maximum rotation, $\Omega = \kappa/2\pi a^2$. Define the parameter ε as the ratio

$$\varepsilon = \alpha/\Omega_o \,, \qquad (1.6.1)$$

then for this section the range of ε is $0 < \varepsilon << 1$.

The stable, axisymmetric waves on the stagnant core discussed in Section 1.4 are the solutions for the limit of $\varepsilon = 0$. The effect of $\varepsilon > 0$ on these waves can be investigated by noting that the form of the wave changes only slightly over a period of the oscillation. Whitham (1974) demonstrates a method for finding the slowly varying wave behavior by formulating the problem in terms of a variational principle. Conservation laws governing the behavior of the slowly varying amplitude and phase of the wave are generated from the variational equations of the averaged Lagrangian.

Define the Lagrangian density, L, by the integrals

$$L = \int_0^R \left(\frac{\partial \phi_1}{\partial t} + \frac{1}{2}(\nabla \phi_1)^2 + \alpha r \frac{\partial \phi_1}{\partial r} - 2\alpha z \frac{\partial \phi_1}{\partial z} + \frac{\kappa^2}{8\pi a^2} \right) r\,dr + \int_R^\infty \left(\frac{\partial \phi_2}{\partial t} + \frac{1}{2}(\nabla \phi_2)^2 + \alpha r \frac{\partial \phi_2}{\partial r} + \frac{\kappa}{2\pi r^2} \frac{\partial \phi_2}{\partial \theta} - 2\alpha z \frac{\partial \phi_2}{\partial z} + \frac{\kappa^2}{8\pi r^2} \right) r\,dr, \quad (1.6.2)$$

where

$$R(\theta, z, t) = a_0 e^{\alpha t} + \tilde{\eta}(\theta, z, t). \quad (1.6.3)$$

A factor of $-\rho$, usually included in formulations in which the pressure acts as the Lagrangian, is deleted for this calculation. The form of the disturbed radius is changed slightly from Section 1.3. In terms of the displacement $\tilde{\delta}$, the wave amplitude $\tilde{\eta}$ satisfies

$$\tilde{\eta} = a(t)\,\tilde{\delta}. \quad (1.6.4)$$

The confusion with the variation symbol, δ, is also eliminated by using

$\tilde{\eta}$ for core deflections.

For the linearized stability equations, only terms in equation (1.6.2) quadratic in the disturbance quantities need be retained. After dropping higher order terms, exact derivatives, and constants from the expanded form, the Lagrangian density is equivalent to

$$\begin{aligned} L = \; & \tfrac{1}{2}\int_0^a (\nabla\phi_1)^2 r\,dr + \tfrac{1}{2}\int_a^\infty (\nabla\phi_2)^2 r\,dr \\ & + a\tilde{\eta}\left[\left(\frac{\partial\phi_1}{\partial t} + \alpha r\frac{\partial\phi_1}{\partial r} - 2\alpha z\frac{\partial\phi_1}{\partial z}\right)\Big|_{r=a} + \frac{K^2}{8\pi^2 a^2}\left(1+\frac{\tilde{\eta}}{2a}\right)\right] \\ & - a\tilde{\eta}\left[\left(\frac{\partial\phi_2}{\partial t} + \alpha r\frac{\partial\phi_2}{\partial r} + \frac{K}{2\pi a^2}\frac{\partial\phi_2}{\partial\theta} - 2\alpha z\frac{\partial\phi_2}{\partial z}\right)\Big|_{r=a} + \frac{K^2}{8\pi^2 a^2}\left(1-\frac{\tilde{\eta}}{2a}\right)\right]. \end{aligned} \tag{1.6.5}$$

Define the functional $J[\phi_1,\phi_2,\tilde{\eta}]$ by the integration of L over the independent variables, that is

$$J = \iiint L\,d\theta\,dz\,dt. \tag{1.6.6}$$

If L is an appropriate Lagrangian density, then setting the variations of J with respect to ϕ_1, ϕ_2 and $\tilde{\eta}$ equal to zero should generate the equations governing the disturbance behavior, in particular, equations (1.3.1), (1.3.3) and (1.3.7).

The variation in J with respect to ϕ_1 is denoted

$$\delta\phi_1: \qquad \delta J = J[\phi_1+\delta\phi_1,\phi_2,\tilde{\eta}] - J[\phi_1,\phi_2,\tilde{\eta}], \tag{1.6.7}$$

where only terms linear in $\delta\phi_1$ are retained. Integration by parts is used to eliminate derivatives of $\delta\phi_1$, and the resulting integrand is set equal to zero. The variations with respect to ϕ_2 and $\tilde{\eta}$ are denoted in the same fashion.

In taking the variation with respect to ϕ_1 and ϕ_2, the following identity is used:

$$\tfrac{1}{2}\left(\nabla(\phi+\delta\phi)\right)^2-\tfrac{1}{2}(\nabla\phi)^2=\nabla\cdot(\delta\phi\,\nabla\phi)-\delta\phi\,\nabla^2\phi\,, \qquad (1.6.8)$$

where terms $O(\delta\phi)^2$ have been dropped. Taking the variation of J with respect to ϕ_1, ϕ_2 and $\tilde{\eta}$ gives

$$\delta\phi_1: \quad \begin{aligned} &\nabla^2\phi_1=0 \qquad \text{for} \quad 0<r<a\,,\\ &\frac{\partial\phi_1}{\partial r}=\frac{\partial\tilde{\eta}}{\partial t}-\alpha\tilde{\eta}-2\alpha z\frac{\partial\tilde{\eta}}{\partial z} \qquad \text{on } r=a\,, \end{aligned} \qquad (1.6.9)$$

$$\delta\phi_2: \quad \begin{aligned} &\nabla^2\phi_2=0 \qquad \text{for} \quad r>a\,,\\ &\frac{\partial\phi_2}{\partial r}=\frac{\partial\tilde{\eta}}{\partial t}-\alpha\tilde{\eta}+\frac{K}{2\pi a^2}\frac{\partial\tilde{\eta}}{\partial\theta}-2\alpha z\frac{\partial\tilde{\eta}}{\partial z} \qquad \text{on } r=a\,, \end{aligned} \qquad (1.6.10)$$

$$\delta\tilde{\eta}: \quad \left(\frac{\partial}{\partial t}+\alpha a\frac{\partial}{\partial r}-2\alpha z\frac{\partial}{\partial z}\right)(\phi_2-\phi_1)=\frac{K^2}{4\pi^2a^2}\tilde{\eta} \qquad \text{on } r=a. \qquad (1.6.11)$$

These are equivalent to the expressions from Section 1.3.

The solution to the above system for the limiting case of no compression is given in Section 1.4. The form of the solution for an initial axial wave number, k, and azimuthal mode, n, is given by

$$\begin{aligned} \phi_1 &= A_1 I_n(kr)\cos(\psi+n\theta)\,,\\ \phi_2 &= A_2 K_n(kr)\cos(\psi+n\theta)\,,\\ \tilde{\eta} &= \eta\,\sin(\psi+n\theta), \end{aligned} \qquad (1.6.12)$$

where

$$\psi = kz-\omega t \qquad (1.6.13)$$

and ω satisfies the dispersion relation in equation (1.4.4). For α non-zero, the amplitudes A_1, A_2, and η are allowed to vary slowly over the period of the oscillation. The local axial wave number and frequency, defined by the relations

$$k = \frac{\partial \psi}{\partial z} \qquad \text{and} \qquad \omega = -\frac{\partial \psi}{\partial t} \,, \tag{1.6.14}$$

are also considered slowly varying. The phase ψ is determined from equation (1.6.14) and the initial condition.

To find the averaged Lagrangian, $\mathcal{L}$, substitute the form of the ϕ_1, ϕ_2 and η given in equation (1.6.12) into the Lagrangian density L, then average over one period of the oscillation by integrating in ψ over an interval of length 2π. After carrying out the integrations of the modified Bessel functions, the form of the averaged Lagrangian becomes

$$\begin{aligned} \mathcal{L} = \tfrac{1}{2}\Big[\tfrac{1}{2} ka \left(I_n I_n' A_1^2 - K_n K_n' A_2^2 \right) + \tfrac{1}{2}\Omega^2 a^2 \eta^2 \\ + a(\omega + 2\alpha k z)(I_n A_1 - K_n A_2)\eta + n\Omega a K_n A_2 \eta \Big], \end{aligned} \tag{1.6.15}$$

where Ω is the rotational velocity given by equation (1.3.14).

The variational equations for variations in A_1 and A_2 give the amplitudes of the potentials in terms of the core displacement as

$$\begin{aligned} A_1 &= \frac{n\Omega - (\omega + 2\alpha k z)}{k K_n'} \eta \,, \\ A_2 &= -\frac{\omega + 2\alpha k z}{k I_n'} \eta \,. \end{aligned} \tag{1.6.16}$$

Substituting these into equation (1.6.15) gives the averaged Lagrangian as

$$\mathcal{L} = \tfrac{1}{4} G(\omega,k)\eta^2 , \tag{1.6.17}$$

where

$$G(\omega,k) = \Omega^2 a^2 + (\omega + 2\alpha k z - n\Omega)^2 \frac{a K_n}{k K_n'} - (\omega+2\alpha k z)^2 \frac{a I_n}{k I_n'} . \tag{1.6.18}$$

The variational equation for variations in η gives the dispersion relation for the slowly varying wave

$$G(\omega,k) = 0 \tag{1.6.19}$$

or solving for the frequency

$$\omega = -2\alpha k z + ka\Omega\left(nI_n'K_n + [(n^2 I_n K_n - 1) I_n' K_n']^{\frac{1}{2}}\right) . \tag{1.6.20}$$

The frequency and axial wave number are also related through the phase ψ . From equation (1.6.14) they must satisfy

$$\frac{\partial k}{\partial t} + \frac{\partial \omega}{\partial z} = 0 , \tag{1.6.21}$$

the equation for conservation of wave crests. Substituting for ω from equation (1.6.20) in the above gives a first order wave equation for k,

$$\frac{\partial k}{\partial t} + c_g \frac{\partial k}{\partial z} = 2\alpha k , \tag{1.6.22}$$

where $C_g = \frac{\partial \omega}{\partial k}$ is the group velocity. If the axial dependence of the initial condition consists of a single Fourier mode, then the initial wave number k_o is a constant and the solution to equation (1.6.22) is

$$k(t) = k_o e^{2\alpha t} . \tag{1.6.23}$$

The phase of the slowly varying wave is determined by the axial wave number, the frequency and the initial phase. Substituting the solutions for k(t) and $\omega(z,t)$ into equation (1.6.14) gives

$$\Psi(z,t) = \Psi_o + kz - \int_o^t \Omega ka \left(n K_n I_n' + \left[I_n' K_n' (n^2 I_n K_n - 1) \right]^{\frac{1}{2}} \right) d\tau , \tag{1.6.24}$$

where ψ_o is the initial phase of the wave.

The variational equation for variations in ψ gives an equation for the amplitude η ,

$$\frac{\partial}{\partial t}\left(\eta^2 \frac{\partial G}{\partial \omega}\right) - \frac{\partial}{\partial z}\left(\eta^2 \frac{\partial G}{\partial k}\right) = 0 \tag{1.6.25}$$

or

$$\frac{\partial}{\partial t}\left(\eta^2 \frac{\partial G}{\partial \omega}\right) + \frac{\partial}{\partial z}\left(\eta^2 C_g \frac{\partial G}{\partial \omega}\right) = 0 , \tag{1.6.26}$$

from taking the partial derivative with respect to k in equation (1.6.19). This can be written as a first order wave equation for the amplitude by expanding the derivatives and regrouping to get

$$\frac{\partial \eta}{\partial t} + c_g \frac{\partial \eta}{\partial z} = -\frac{1}{2}\left[\frac{\partial c_g}{\partial z} + \left[\left(\frac{\partial}{\partial t} + c_g \frac{\partial}{\partial z} \right) \frac{\partial G}{\partial \omega} \right] \left(\frac{\partial G}{\partial \omega} \right)^{-1} \right] \eta \quad . \tag{1.6.27}$$

Since the wave number is a function of time alone, equations (1.6.19) and (1.6.18) combine to give

$$\frac{\partial G}{\partial \omega} = 2 \frac{\Omega a^2}{ka} \left(\frac{n^2 I_n K_n - 1}{I_n' K_n'} \right)^{1/2}, \tag{1.6.28}$$

independent of z. For a wave of initial amplitude η_0, composed of a single Fourier mode, the solution to equation (1.6.27) gives

$$\eta(t) = \eta_0 \frac{N(t)}{N(0)} e^{\gamma \alpha t/4} \tag{1.6.29}$$

where

$$N(t) = \left(ka \frac{I_n' K_n'}{n^2 I_n K_n - 1} \right)^{1/4} . \tag{1.6.30}$$

The analysis holds only for $\omega(z,t)$ real, restricting the initial dimensionless wave number, $k_0 a_0$, to

$$k_0 a_0 > ka^*(n) \tag{1.6.31}$$

where ka*(n) is defined in Section 1.4. Since ka is initially greater than the critical value and is an increasing function of time, the denominator in equation (1.6.30) never vanishes. For large n the value of N(t) is a maximum for ka initially near the stability boundary of the zero compression problem. As ka increases, N asymptotes 1/2. The maximum amplification rate for the waves with large azimuthal mode n is given by the exponent in equation (1.6.29) to be $7\alpha/4$.

For the axisymmetric disturbances, the function N(t) reduces to

$$N(t) = [\, ka\, I_1(ka)\, K_1(ka)]^{1/4}. \qquad (1.6.31)$$

In the long wave limit, N is asymptotic to $(ka)^{1/4}$, so that waves are initially amplified at the rate $5\alpha/2$. For increasing ka the rate decreases, resulting in the short wave amplification rate of $7\alpha/4$, as in the case of large n.

The growth of the waves needs to be compared with the increasing core radius, $a_0 e^{\alpha t}$. By dividing η by a, these results can be compared with the asymptotic growth given in the last section. For large wave numbers, the initial growth is slower than the eventual asymptotic growth. For long axisymmetric waves, the growth is faster.

The validity of the slowly varying wave analysis extends to when αt is order one. The asymptotic expansions given in Section 1.5 are valid for αt large compared with one. There is no guaranteed region of overlap for the two expansions. The behavior of the waves is examined numerically in the next section to determine the connection.

The form of the axial wave number in the slowly varying wave is the same as that used in separating the z dependence in Section 1.3. This suggests examining equation (1.3.17) for the deflection $\tilde{\eta}$ as an oscillator with slowly varying amplitude and frequency. This approach can be extended to the uniform core vortex, where the variation principle is considerably more complex.

For axisymmetric waves the deflection can be written as

$$\tilde{\eta}(z,t) = \eta_1(s)\cos(kz) + \eta_2(s)\sin(kz), \tag{1.6.32}$$

where s is the dimensionless time,

$$s = \Omega_0 t \tag{1.6.33}$$

The functions η_1 and η_2 are scaled forms of the deflection given in equation (1.3.17) and satisfy

$$\frac{d^2\eta}{ds^2} - \varepsilon p(\varepsilon s)\frac{d\eta}{ds} + [\mu^2(\varepsilon s) - \varepsilon^2(1-p(\varepsilon s))]\eta = 0, \tag{1.6.34}$$

where

$$\left.\begin{aligned} p(\varepsilon s) &= 3ka\left(\frac{I_0}{I_1} - \frac{K_0}{K_1}\right), \\ \mu^2(\varepsilon s) &= k^2a^2 I_1 K_1 e^{-4\varepsilon s}, \end{aligned}\right\} \tag{1.6.35}$$

and ε is the small ratio α/Ω_0.

Using the previous results to guide the calculation, define a new time variable from equation (1.6.24) as

$$\bar{s} = \int_0^s \mu(\varepsilon\xi)\,d\xi . \tag{1.6.36}$$

In terms of this variable, the equation for η_1 and η_2 becomes

$$\frac{d^2\eta}{d\bar{s}^2} + \frac{\varepsilon}{\mu}\left(\frac{\mu'}{\mu} - p\right)\frac{d\eta}{d\bar{s}} + \left(1 - \frac{\varepsilon^2}{\mu^2}(1-p)\right)\eta = 0. \tag{1.6.37}$$

The solution to this equation can be approximated using the method of two-timing. The slow time variable is defined by

$$\tilde{s} = \varepsilon s \tag{1.6.38}$$

and the form of the solution is assumed to be a regular expansion in functions of the two times,

$$\eta = F_0(\bar{s},\tilde{s}) + \varepsilon F_1(\bar{s},\tilde{s}) + \cdots . \tag{1.6.39}$$

After expanding the derivatives in equation (1.6.37) and grouping terms in powers of ε, a hierarchy of equations is established.

$$\varepsilon^0: \quad \frac{\partial^2 F_0}{\partial \bar{s}^2} + F_0 = 0 , \tag{1.6.40}$$

$$\varepsilon^1: \quad \frac{\partial^2 F_1}{\partial \bar{s}^2} + F_1 = -\frac{1}{\mu}\left(2\frac{\partial^2 F_0}{\partial \bar{s}\partial \tilde{s}} + \frac{\mu'}{\mu}\frac{\partial F_0}{\partial \bar{s}} - P\frac{\partial F_0}{\partial \bar{s}}\right), \tag{1.6.41}$$

$$\varepsilon^2: \quad \frac{\partial^2 F_2}{\partial \bar{s}^2} + F_2 = \cdots , \text{ etc.}$$

The lowest order solution is just the unmodified oscillation,

$$F_0(\bar{s},\tilde{s}) = A_0(\tilde{s})\cos\left(\bar{s} + \Phi_0(\tilde{s})\right), \tag{1.6.42}$$

where $A_0(\tilde{s})$ and $\Phi_0(\tilde{s})$ are functions of the slow time. Substituting this form into equation (1.6.41) gives the equation for F_1 as

$$\frac{\partial^2 F_1}{\partial \bar{s}^2} + F_1 = \frac{1}{\mu}\left(2\frac{dA_0}{d\tilde{s}} + \frac{\mu'}{\mu}A_0 - pA_0\right)\sin(\bar{s}+\Phi_0) + \frac{2}{\mu}A_0\frac{d\Phi_0}{d\tilde{s}}\cos(\bar{s}+\Phi_0) . \tag{1.6.43}$$

The solution for F_1 must be a bounded function of the fast time, $\bar{s}$, in order that the expansion be valid. The coefficients of the sine and cosine terms in equation (1.6.43) must vanish to prevent algebraically growing solutions for $F_1(\bar{s},\tilde{s})$. This gives equations for the slow time behavior of the amplitude and phase

$$\frac{dA_0}{d\tilde{s}} + \tfrac{1}{2}(\mu'/\mu - P)A_0 = 0 , \tag{1.6.44}$$

$$d\Phi_0/d\tilde{s} = 0 , \tag{1.6.45}$$

with solutions

$$A_o(\tilde{s}) = A_o(o)\left[\frac{ka\, I_1(ka)\, K_1(ka)}{k_o a_o I_1(k_o a_o) K_1(k_o a_o)}\right]^{\frac{1}{4}} e^{\frac{\eta \tilde{s}}{4}}, \tag{1.6.46}$$

$$\Phi_o(\tilde{s}) = \Phi_o(o). \tag{1.6.47}$$

If the initial form of the deflection and the rate of the deflection of the core radius are for a travelling wave of amplitude η_o and wave number k_o, then

$$\eta_1(s) = A_o(\tilde{s}) \cos\left(s + \pi/2 - \psi_o\right), \tag{1.6.48}$$

$$\eta_2(s) = A_o(\tilde{s}) \cos\left(\tilde{s} - \psi_o\right), \tag{1.6.49}$$

where $A_o(0) = \eta_o$ and ψ_o is the initial phase of the deflection wave. Substituting in equation (1.6.32) gives

$$\tilde{\eta}(z,t) = \eta_o \frac{N(t)}{N(o)} e^{\frac{\eta \alpha t}{4}} \sin\left(\psi(z,t)\right). \tag{1.6.50}$$

$N(t)$ and $\psi(z,t)$ are defined in equations (1.6.31) and (1.6.24) and the form of the approximate solution agrees with that found using the averaged Lagrangian.

1.7 Numerical Results for Stagnant Core

Waves on the compressed stagnant core vortex are shown to be unstable in Section 1.5. The asymptotic behavior for constant compression gives

$$\delta \sim G(k_o a_o, \varepsilon, \delta(o), \delta'(o))\, e^{\alpha t} \quad \text{as } t \to \infty. \tag{1.7.1}$$

The dependence of G on the initial parameters needs to be examined. Also, the behavior of $\delta(t)$ for the physically relevant parameters should be computed.

The equations governing the behavior of δ in dimensionless variables can be written

$$\frac{d}{ds}\left(\delta e^{-\varepsilon s}\right) = I_1 K_1 e^{3\varepsilon s} y - \varepsilon\left(\delta e^{-\varepsilon s}\right), \tag{1.7.2}$$

$$\frac{dy}{ds} = -k_o^2 a_o^2 e^{-\varepsilon s}\left(\delta e^{-\varepsilon s}\right), \tag{1.7.3}$$

where

$$s = \Omega_o t \tag{1.7.4}$$

is the dimensionless time. The form $\delta e^{-\varepsilon s}$ is used because it is expected to asymptote to a constant for large s. This system is in an appropriate form to be numerically integrated from some initial conditions. The initial conditions, $\delta(0)$ and $\delta'(0)$, generate the value for $y(0)$. To decrease the number of parameters, the initial form of the disturbance is assumed to be a wave train of unit amplitude with the frequency of the stable uncompressed wave. These can be expressed as

$$\delta(0) = \cos(\psi_o), \tag{1.7.5}$$

$$\delta'(0) = k_o a_o \left[I_1(k_o a_o) K_1(k_o a_o)\right]^{1/2} \sin(\psi_o), \tag{1.7.6}$$

and from equation (1.7.2), $y(0)$ satisfies

$$y(0) = k_o a_o \left(I_1(k_o a_o) K_1(k_o a_o)\right)^{-\frac{1}{2}} \sin(\psi_o). \tag{1.7.7}$$

In these expressions ψ_0 is the initial phase of the wave.

An Adam-Moulton predictor-corrector scheme using the Runge-Kutta-Gill method as a start and restart scheme was used to carry out the numerical integration. The integration step length was varied to maintain the local relative error at less than $.5 \times 10^{-4}$. Care was taken to avoid roundoff error from the difference in equation (1.7.2).

The solution curves for $\varepsilon = .01$, the initial phase $\psi_0 = \pi/2$ and the wave numbers $k_0a_0 = .00001, .0001, .001, .002, .005, .01, .05$ are given in Figure 1.2. For the scaled time s greater than 1000, the solution curves for $\delta e^{-\varepsilon s}$ asymptote $G(k_0a_0, \varepsilon, \delta(0), \delta'(0))$. The initial phase $\psi_0 = \pi/2$ results in the largest value for the asymptote of curves with small wave number. For larger wave numbers, there are many oscillations before the curve levels off and the initial condition required to maximize the asymptote varies with the wave number.

The periods for the stable waves on the undeformed vortex are written in parentheses after the corresponding wave numbers in the figure. For small ka, the period of the oscillation is approximately given by

$$T \sim \frac{2\sqrt{2}\pi}{k_0a_0} \approx \frac{8.89}{k_0a_0} \quad . \tag{1.7.8}$$

Solutions for values of k_0a_0 resulting in periods small compared with the time s = 1000 are initially oscillatory with varying amplitude and phase. If the period is large compared with the time in which curves approach a constant, the solution increases monotonically to that constant. The largest values of the asymptotes are for the smallest wave number. However, for wave numbers sufficiently small that the solution

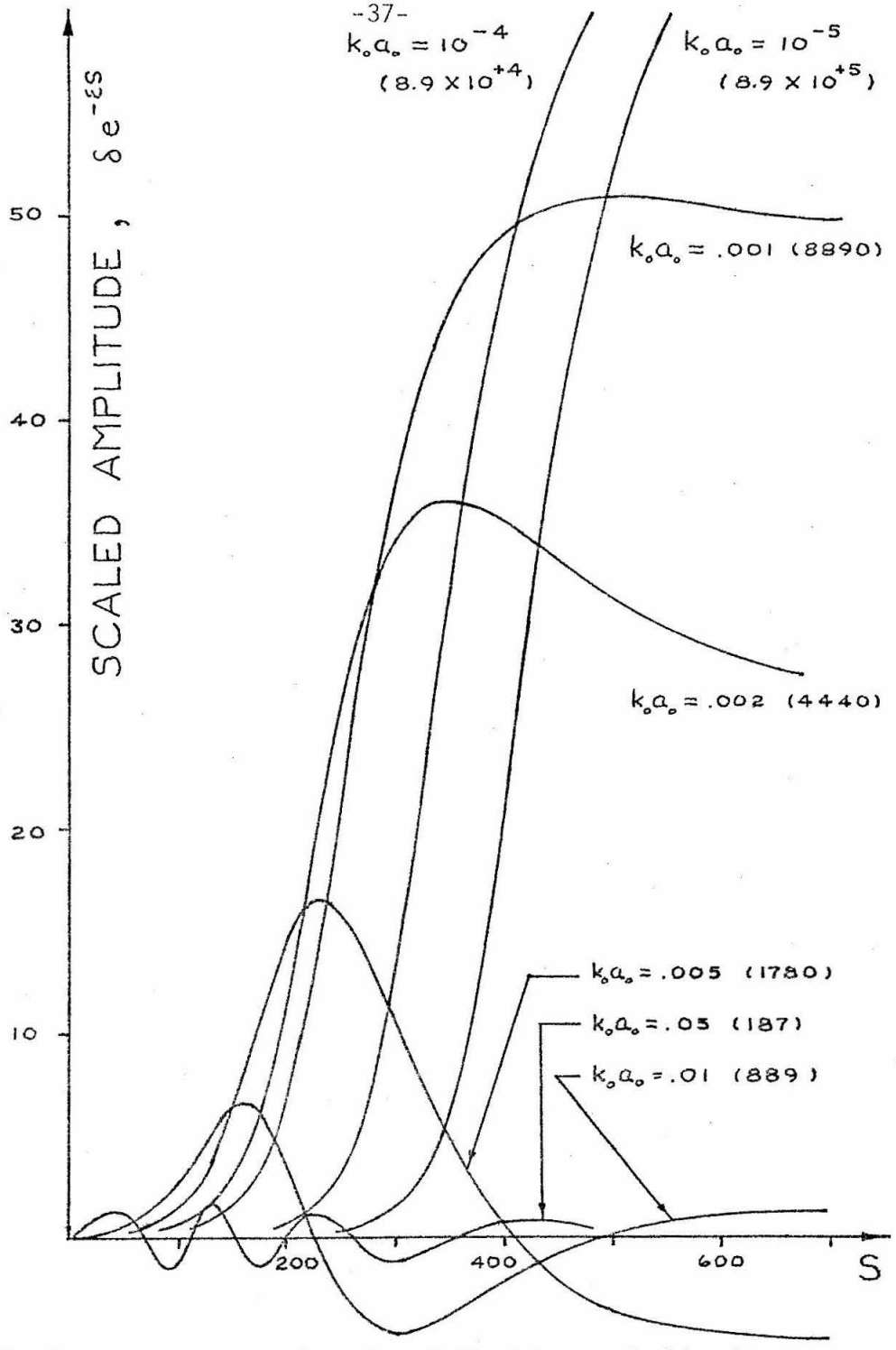

Figure 1.2 The stagnant cored vortex deflection scaled by its asymptotic behavior graphed versus the dimensionless time s for $\varepsilon = 0.01$ and several values of $k_0 a_0$. The curve for $k_0 a_0 = 10^{-5}$ asymptotes 70.7 and for $k_0 a_0 = 10^{-4}$ asymptotes 69.6.

increases monotonically, decreasing the wave number further increases the value of G only slightly.

For smaller values of ε the solutions are similar to those described above. The time in which the solutions asymptote a constant is about $s = 10/\varepsilon$. The wave numbers corresponding to the behavior of the curves in Figure 1.2 need be decreased with ε to maintain the same relation between the period of the zero compression oscillations and the asymptotic time. For the smallest wave numbers, the value of the asymptote G increases as $1/\varepsilon$.

Considering the time scale of the phenomenon, the values of s greater than about 500 are expected to be beyond the range of any experiment. Moore (1972) finds that the vortex pair touch for the value of s at about 250. For values of ε in the range of .001, the rapid increase to the asymptote occurs beyond the experimental time.

The role of the initial conditions in this analysis needs to be examined more closely. The value for $\delta'(0)$ is chosen to give unit amplitude for the case of zero compression. As a result, the value decreases proportional to the wave number when the waves are long. The largest values of G are attained for the smallest values of ka, even though these correspond to the smallest values for $\delta'(0)$. Since the problem is linear,

$$G(k_0 a_0, \varepsilon, 0, \delta'(0)) = \delta'(0)\, G_1(k_0 a_0, \varepsilon)\,. \qquad (1.7.9)$$

If the initial condition $\delta'(0) = 1$ is chosen, the stable waves for the vortex without compression appear to grow rapidly as ka tends to

zero. The effect of the choice of $\delta'(0)$ given in equation (1.7.6) is to scale the amplitude of the waves with the maximum amplitude of the zero compression wave. The stability analysis is to determine the effect of the compression on the stable waves.

Even though the waves on the compressed vortex are unstable, no rapid growth occurs on the scale of the physical problem. If the value of δ increased to 10 in the time of the vortices touching, this would be considered rapid growth. It does not seem to model the bursting. However, this is not too disappointing because the stagnant vortex has no core rotation to resist the wave growth.

The more interesting flow to examine has uniform vorticity in the core. The methods used to examine the stagnant core are extended to the more complicated case in the rest of this chapter.

1.8 Uniform Core Vortex

In the stagnant core vortex filament the vorticity is non-zero only on a vortex sheet bordering the filament core. This requirement allows considering only irrotational disturbances to the flow field. For the vortex filament with core in solid body rotation, the vorticity is constant and non-zero in the core. The disturbance velocity field in the core region cannot be restricted to potential flow.

The governing equations for the infinitesimal disturbances in the core region are the linearized Euler equations. Denote U, V and W as the undisturbed radial, azimuthal and axial velocities, and $\tilde{u}$, $\tilde{v}$, $\tilde{w}$ and $\tilde{p}$ as the disturbance velocities and pressure. The form of

the undisturbed velocity field in the core is given in Section 1.2 as

$$V = \frac{\kappa r}{2\pi a^2} , \tag{1.2.2}$$

$$U = \alpha r \quad \text{and} \quad W = -2\alpha z , \tag{1.2.3}$$

where κ is the constant filament strength and $\alpha(t)$ is the amplitude of the compression. The undisturbed core radius is a function of time given as

$$a(t) = a_0 \exp\left[\int_{t_0}^{t} \alpha(\tau)\, d\tau\right]. \tag{1.2.4}$$

Substituting into the Euler equations and retaining only terms linear in the disturbance quantities gives the equations

$$\frac{\partial \tilde{u}}{\partial t} + \alpha r \frac{\partial \tilde{u}}{\partial r} + \alpha \tilde{u} + \frac{\kappa}{2\pi a^2}\left(\frac{\partial \tilde{u}}{\partial \theta} - 2\tilde{v}\right) - 2\alpha z \frac{\partial \tilde{u}}{\partial z} = -\frac{\partial \tilde{p}}{\partial r} , \tag{1.8.1a}$$

$$\frac{\partial \tilde{v}}{\partial t} + \alpha r \frac{\partial \tilde{v}}{\partial r} + \alpha \tilde{v} + \frac{\kappa}{2\pi a^2}\left(\frac{\partial \tilde{v}}{\partial \theta} + 2\tilde{u}\right) - 2\alpha z \frac{\partial \tilde{v}}{\partial z} = -\frac{1}{r}\frac{\partial \tilde{p}}{\partial \theta} , \tag{1.8.1b}$$

$$\frac{\partial \tilde{w}}{\partial t} + \alpha r \frac{\partial \tilde{w}}{\partial r} + \frac{\kappa}{2\pi a^2}\frac{\partial \tilde{w}}{\partial \theta} - 2\alpha w \frac{\partial \tilde{w}}{\partial z} - 2\alpha \tilde{w} = -\frac{\partial \tilde{p}}{\partial z} , \tag{1.8.1c}$$

$$\frac{\partial \tilde{u}}{\partial r} + \frac{1}{r}\tilde{u} + \frac{1}{r}\frac{\partial \tilde{v}}{\partial \theta} + \frac{\partial \tilde{w}}{\partial z} = 0 . \tag{1.8.1d}$$

These equations govern the flow in the disturbed filament core, where $r < R(\theta,z,t)$. The displacement of the core boundary $\tilde{\delta}$ is defined by the relation

$$R(\theta,z,t) = a(t)\left(1 + \tilde{\delta}(\theta,z,t)\right). \tag{1.8.2}$$

In the region outside the vortex core, the undisturbed flow field is identical to the flow outside the stagnant core vortex. It follows

that a disturbance velocity potential $\tilde{\phi}$ exists and must satisfy

$$\nabla^2 \tilde{\phi} = 0 \qquad \text{for} \quad r > R, \tag{1.8.3}$$

along with the boundary conditions on r = R which arise to insure continuous velocities and pressure.

The core boundary is a vorticity jump, due to the discontinuity in the derivative of the undeformed azimuthal velocity. This moves as a material surface, just as for the vortex sheet, and forms a boundary between the regions of rotational and irrotational flow. The continuity of the velocities across the material surface gives three conditions to replace the dynamic and kinematic conditions. The resulting conditions are equivalent, but velocity continuity is simpler to implement in this problem.

The axial and azimuthal dependence can each be separated by examining a single Fourier mode. As in the stagnant vortex problem, the axial wave number is time dependent for the separation and is of the form

$$k(t) = k_o \exp\left[2\int_{t_o}^{t} \alpha(\tau)\, d\tau\right], \tag{1.8.4}$$

where k_o is the initial wave number. The azimuthal wave number n is a constant integer.

Define the dimensionless independent variables x and s by the relations

$$x = r/a \qquad \text{and} \qquad s = \Omega_o t, \tag{1.8.5}$$

where Ω_0 is the initial rotation rate of the undisturbed core. The scaling for x is chosen to allow the linearized boundary conditions on r = a to be evaluated at a fixed value, x = 1, for all time.

The disturbance velocities and pressure in the vortex core can be expressed in terms of the dimensionless unknown functions of only x and s by the relations

$$\tilde{u} = \frac{\kappa}{2\pi a} u(x,s)\, e^{in\theta + ikz}, \tag{1.8.6a}$$

$$\tilde{v} = \frac{\kappa}{2\pi a} v(x,s)\, e^{in\theta + ikz}, \tag{1.8.6b}$$

$$\tilde{w} = \frac{-i\kappa}{2\pi a} w(x,s)\, e^{in\theta + ikz}, \tag{1.8.6c}$$

$$\tilde{p} = \left(\frac{\kappa}{2\pi a}\right)^2 p(x,s)\, e^{in\theta + ikz}. \tag{1.8.6d}$$

Substituting the above into equation (1.8.1) gives the core equations,

$$\frac{\partial u}{\partial s} + A\left(inu - 2v + \frac{\partial p}{\partial x}\right) = 0, \tag{1.8.7a}$$

$$\frac{\partial v}{\partial s} + A\left(inv + 2u + \frac{in}{x} p\right) = 0, \tag{1.8.7b}$$

$$\frac{\partial w}{\partial s} - 3\varepsilon w + A(inw - kap) = 0, \tag{1.8.7c}$$

$$\frac{\partial u}{\partial x} + \frac{1}{x} u + \frac{in}{x} v + kaw = 0, \tag{1.8.7d}$$

where

$$\varepsilon(s) = \alpha(s/\Omega_0)/\Omega_0, \tag{1.8.8}$$

$$A(s) = a_0^2/a^2 = \exp\left[-2\int_{s_0}^{s} \varepsilon(\xi)\, d\xi\right]. \tag{1.8.9}$$

The velocity potential for the region outside the core is of the form

$$\tilde{\phi} = \phi(s)\, K_n(kax)\, e^{in\theta + ikz}, \tag{1.8.10}$$

where K_n is a modified Bessel function and $\phi(s)$ is determined from the conditions on the core boundary.

The three continuity conditions across the core boundary can be linearized in the disturbances and evaluated at $x = 1$. The dimensionless core displacement $\tilde{\delta}(\theta,z,t)$ appears in the azimuthal equation due to the discontinuity in the derivative of the undisturbed azimuthal velocity. For consistency, define $\delta(s)$ by the relation

$$\tilde{\delta}(\theta,z,t) = \delta(s)\, e^{in\theta + ikz}. \tag{1.8.11}$$

The conditions for continuous velocities on the interface between the rotational and potential flows reduce to the following:

$$\left.\begin{aligned} \tfrac{K}{2\pi a}\, u(1,s) &= k\phi(s)\, K_n'(ka), \\ \tfrac{K}{2\pi a}\, v(1,s) &= -\tfrac{K}{\pi a}\,\delta(s) + \tfrac{in}{a}\,\phi(s) K_n'(ka), \\ \tfrac{K}{2\pi a}\, w(1,s) &= -k\phi(s)\, K_n(ka). \end{aligned}\right\} \tag{1.8.12}$$

The primes denote differentiation with respect to the argument.

The unknown function $\phi(s)$ can be eliminated in the above to give the two independent equations:

$$w(1,s)\, K_n'(ka) + u(1,s)\, K_n(ka) = 0, \tag{1.8.13}$$

$$\delta(s) = -\tfrac{1}{2} v(1,s) - \frac{in}{2ka}\, w(1,s). \tag{1.8.14}$$

The first equation acts as a boundary condition on $x = 1$ for the system of equations (1.8.7). The requirement that the velocities be bounded at the origin gives boundary conditions on $x = 0$. Given initial values for u, v and w, the solution of the system with boundary conditions is determined on the strip $0 < x < 1$, $s > s_0$. The second equation above (1.8.14) then determines the behavior of the disturbance to the core radius.

The system of equations (1.8.7) with its boundary conditions can be solved numerically for given n, $k_0 a_0$, $\varepsilon(s)$, and the initial conditions, $u(x,s_0)$, $v(x,s_0)$, $w(x,s_0)$. The analysis of the system can be extended by assuming the disturbances to be axisymmetric (n=0). From the consideration of experimental observations (see Section 1.1), this assumption is not expected to be too restrictive.

The equations for the axisymmetric disturbances can be written as a single partial differential equation for $u(x,s)$ on $0 < x < 1$, $s > s_0$, of the form

$$\left(\frac{\partial^2}{\partial s^2} + 2\varepsilon\frac{\partial}{\partial s} + 4A^2\right)u - \left(\frac{\partial^2}{\partial s^2} + 2\varepsilon\frac{\partial}{\partial s}\right)\left(\frac{\partial^2}{\partial x^2} + \frac{1}{x}\frac{\partial}{\partial x} - \frac{1}{x^2}\right)\frac{u}{(ka)^2} = 0, \qquad (1.8.15)$$

where the boundary conditions on $x = 0$ and $x = 1$ are

$$u(0,s) = 0, \qquad (1.8.16)$$

$$\frac{\partial u}{\partial x} + \left(1 + ka\frac{K_0(ka)}{K_1(ka)}\right)u = 0 \quad \text{on } x = 1. \qquad (1.8.17)$$

The solution to the above is uniquely determined, given the initial func-

tion $u(x,s_o)$.

The dependence of u on the independent variable x can be separated in discrete modes by defining

$$u_n(x,s) = f_n(s)\, J_1(\lambda_n(s)\, x)\,, \quad n = 1,2,\cdots\,, \tag{1.8.18}$$

where J_1 is a Bessel function of the first kind. The boundary condition at x = 1, along with the choice of ordering that the λ_n be an increasing sequence at a fixed time, determine the relations

$$\lambda_n \frac{J_o(\lambda_n)}{J_1(\lambda_n)} + ka \frac{K_o(ka)}{K_1(ka)} = 0\,, \tag{1.8.19}$$

$$j_{o,n} < \lambda_n < j_{1,n}\,. \tag{1.8.20}$$

The numbers $j_{o,n}$ and $j_{1,n}$ are the n^{th} largest positive roots of J_o and J_1. Notice that as ka varies from zero to infinity, λ_n varies from $j_{o,n}$ to $j_{1,n}$.

The $\lambda_n(s)$ and $J_1(\lambda_n(s)x)$ are the eigenvalues and eigenfunctions of the Sturm-Liouville system

$$\left.\begin{aligned} &\frac{d}{dx}\left(x \frac{dy_n}{dx}\right) + \left(\lambda_n^2 x - 1/x\right) y_n = 0\,, \\ &y_n(0) = 0\,, \quad \frac{d}{dx} y_n(1) + \left(1 + ka \frac{K_o(ka)}{K_1(ka)}\right) y_n(1) = 0. \end{aligned}\right\} \tag{1.8.21}$$

The $J_1(\lambda_n(s_o)x)$ form a complete set of orthogonal functions spanning the set of continuously differentiable functions on $0 < x < 1$. The initial function $u(x,s_o)$ can be expressed as a series in these eigenfunctions by

$$u(x,s_o) = \sum a_n J_1(\lambda_n(s_o)x) \ . \qquad (1.8.22)$$

In this way an initial value, $f_n(s_o)$, can be determined for each of the $u_n(x,s_o)$.

Substituting the form of the solution, u_n, into equation (1.8.15) gives the equation,

$$\frac{\partial}{\partial s}\left(\frac{1}{A}\frac{\partial}{\partial s}\left[\left(1+\left(\frac{\lambda_n}{ka}\right)^2\right)u_n\right]\right) + 4A u_n = 0 \ . \qquad (1.8.23)$$

The x dependence of the equation has been suppressed in that it acts as a parameter in the solution.

The quantity of interest is the core radius deflection, $\delta_n(s)$, corresponding to u_n. Equations (1.8.7) and (1.8.14) can be combined to give

$$\delta_n(s) = -\tfrac{1}{2}V_n(1,s) = \frac{-1}{4A}\frac{d}{ds}\left(\left[1+\left(\frac{\lambda_n}{ka}\right)^2\right]u_n(1,s)\right) \ . \qquad (1.8.24)$$

In this formulation, once the values of the initial condition have been transformed to the coefficient in the Bessel function series, the expression need only be evaluated at x = 1. A convenient form of the equations arises by defining

$$g_n(s) = 2\left(1+\left(\frac{\lambda_n}{ka}\right)^2\right)u_n(1,s), \qquad (1.8.25)$$

$$\omega_n(s) = 2A\left(1+\left(\frac{\lambda_n}{ka}\right)^2\right)^{-1/2}, \qquad (1.8.26)$$

and combining equations (1.8.23) and (1.8.24) to give the system

$$\left.\begin{aligned} \frac{d\delta_n}{ds} - \frac{\omega_n^2}{2A} g_n = 0 , \\ \frac{dg_n}{ds} + 2A\,\delta_n = 0 . \end{aligned}\right\} \qquad (1.8.27)$$

This system can be combined to form a single first order equation for δ_n,

$$\delta_n'' - 2(\varepsilon + \omega_n'/\omega_n)\delta_n' + \omega_n^2 \delta_n = 0 , \qquad (1.8.28)$$

where the primes indicate differentiation with respect to s.

The system of equations (1.8.27) and equation (1.8.28) determine the growth of disturbance waves on the filament core boundary. The limiting case of no compression should give Kelvin's solution for the stable waves on a vortex filament. The functions, ka, A, λ_n and ω_n become constants and $\varepsilon(s) = 0$. Under these conditions, equation (1.8.25) reduces to

$$\delta_n'' + \omega_n^2 \delta_n = 0 , \qquad (1.8.29)$$

where ω_n given by equations (1.8.26) and (1.8.29) is the frequency of the bounded periodic disturbance. In dimensional form, the core radius R(z,t) can be expressed as

$$R(z,t) = a(t)\left(1 + Re \sum_n b_n e^{in\theta + ikz}\right) , \qquad (1.8.30)$$

where the b_n are constants determined by the structure of the initial disturbance to the core velocities.

The effect of the compression on these stable waves will be examined in the next three sections.

1.9 Asymptotic Behavior for Uniform Core

As a first attempt to determine the stability of the compressed uniform core vortex, the asymptotic behavior can be examined. Disturbances which grow faster than the undisturbed core expansion are considered unstable, even though the time scale of the growth may be long compared with the physical mechanism being modelled.

For constant compression, equation (1.8.28) can be transformed into the standard form for applying the WKBJ method by defining a scaled displacement,

$$f(s) = \left(\omega_n e^{-\varepsilon s}\right)^{-1} \delta_n(s) . \tag{1.9.1}$$

The equation for f(s) is written

$$\frac{d^2 f}{ds^2} - \hat{q}(s) f(s) = 0 , \tag{1.9.2}$$

where

$$\hat{q}(s) = -\omega_n^2 + \varepsilon^2 - \omega_n''/\omega_n + 2\,\omega_n'/\omega_n \left(\varepsilon + \omega_n'/\omega_n\right) . \tag{1.9.3}$$

The function $\omega_n(s)$ is defined in equations (1.8.26) and (1.8.19), ε is the constant ratio of the compression to the initial rotation rate α/Ω_0, and s is the dimensionless time, $\Omega_0 t$.

For large s, q(s) can be expanded to give

$$\hat{q}(s) = \varepsilon^2 - 4e^{-4\varepsilon s} + O(e^{-10\varepsilon s}). \qquad (1.9.4)$$

This expression is bounded away from zero for s sufficiently large. Applying the WKBJ method to equation (1.9.2) gives

$$f(s) \sim \text{constant} \cdot \hat{q}_0^{-1/4} \exp\left[\int \hat{q}_0^{\frac{1}{2}} ds\right] \quad \text{as } s \to \infty. \qquad (1.9.5)$$

Equations (1.9.1) and (1.9.4) combine with the above to give the asymptotic expression for the deflection,

$$\delta_n(s) \sim \text{constant} \qquad \text{as} \quad s \to \infty. \qquad (1.9.6)$$

The dimensional or physical deflection grows at the same rate as the core radius, the neutrally stable growth rate.

For the time dependent compression, the asymptotic behavior of δ_n is determined using a form of equation (1.8.27). Define a time-like variable by

$$\xi = \frac{2s^{1-2\nu}}{1-2\nu}, \qquad (1.9.7)$$

where ν is the initial value of the compression. The restriction that ν be less than 1/2 is necessary in equation (1.9.7) in order that ξ tends to infinity for large s. Since the compression in the physical problem is small, this is an appropriate limitation on ν. Substituting into equation (1.8.27) gives

$$\left.\begin{aligned} \frac{d\delta}{d\xi} - \left(1 + \left(\frac{\lambda}{ka}\right)^2\right)^{-1} q &= 0, \\ \frac{dq}{d\xi} + \delta &= 0, \end{aligned}\right\} \qquad (1.9.8)$$

where the subscripts n referring to the mode of the internal structure have been dropped. The function $\lambda_n(\xi)$, defined in equation (1.8.19), is bounded above and below by the n^{th} root of the Bessel functions J_0 and J_1, according to the relation (1.8.20). Combining the equations to get a single second order equation in g gives

$$\frac{d^2g}{d\xi^2} + \left(1 + \left(\frac{\lambda}{ka}\right)^2\right)^{-1} g = 0, \qquad (1.9.9)$$

where the coefficient of g is bounded as ξ tends to infinity. Applying the WKBJ method to this equation gives the leading term for g,

$$g \sim \text{constant} \cdot \exp\left[\pm i \int \left(1 + \left(\frac{\lambda}{ka}\right)^2\right)^{-1/2} d\xi\right] \text{ as } \xi \to \infty, \qquad (1.9.10)$$

as bounded oscillations in ξ . The form of the deflection δ follows directly from equation (1.9.7) as

$$\delta \sim \text{constant} \cdot \exp\left[\pm i \int \omega_n ds\right] \quad \text{as} \quad s \to \infty. \qquad (1.9.11)$$

In the limit as ν tends to zero, this is the exact solution for the Kelvin waves. The introduction of the compression causes the waves to grow at a rate asymptotic to the core expansion rate.

The asymptotic behavior of the core displacement resolves neither the stability nor the model's validity. Part of the difficulty is that the unknown constant coefficient in the asymptotic expression can be large. The behavior of this constant with the initial parameters is examined in Section 1.11. The initial growth of the disturbances helps determine the feasibility of the model. This is examined for small constant compression in the next section.

1.10 Small Compression for Uniform Core

In Section 1.6 a two-timing technique was applied to the equation for the displacement of the stagnant core radius by introducing an averaged frequency. The same method can be used for the uniform core. Restricting the disturbances to be axisymmetric and the compression to be constant, the displacement of the core radius δ_n satisfies equation (1.8.28). For $\omega_n(s)$ written as a function $\omega(\varepsilon s)$ and the subscript dropped from δ_n, the equation becomes

$$\frac{d^2\delta}{ds^2} - 2\varepsilon\left(1+\frac{\omega'(\varepsilon s)}{\omega(\varepsilon s)}\right)\frac{d\delta}{ds} + \omega^2(\varepsilon s)\,\delta = 0. \tag{1.10.1}$$

When $\varepsilon = 0$, this reduces to the equation for a simple oscillation. The effect of the small, positive ε on this motion is to introduce a slow variation of the frequency and amplitude.

Define the fast time by the integral

$$\bar{s} = \int_0^s \omega(\varepsilon\xi)\,d\xi. \tag{1.10.2}$$

In terms of this variable, equation (1.10.1) can be rewritten as

$$\frac{d^2\delta}{d\bar{s}^2} - \frac{\varepsilon}{\omega}\left(2+\frac{\omega'}{\omega}\right)\frac{d\delta}{d\bar{s}} + \delta = 0. \tag{1.10.3}$$

If the function ω is considered a function of the slow time

$$\tilde{s} = \varepsilon s, \tag{1.10.4}$$

the displacement can be expressed as a regular series expansion in functions of the two times,

$$\delta = F_0(\bar{s},\tilde{s}) + \varepsilon F_1(\bar{s},\tilde{s}) + \cdots . \tag{1.10.5}$$

Substituting this form for δ into equation (1.10.3) and expanding the derivatives in the two variables, terms can be grouped according to powers of ε to give a hierarchy of equations,

$$\varepsilon^0: \quad \frac{\partial^2 F_0}{\partial \bar{s}^2} + F_0 = 0 , \tag{1.10.6}$$

$$\varepsilon^1: \quad \frac{\partial^2 F_1}{\partial \bar{s}^2} + F_1 = \frac{1}{\omega}\left(2+\frac{\omega'}{\omega}\right)\frac{\partial F_0}{\partial \bar{s}} - \frac{2}{\omega}\frac{\partial^2 F_0}{\partial \bar{s}\,\partial \tilde{s}} , \tag{1.10.7}$$

$$\varepsilon^2: \quad \frac{\partial^2 F_2}{\partial \bar{s}^2} + F_2 = \frac{1}{\omega}\left(2+\frac{\omega'}{\omega}\right)\left(\frac{\partial F_1}{\partial \bar{s}} + \frac{1}{\omega}\frac{\partial F_0}{\partial \tilde{s}}\right) - \frac{2}{\omega}\frac{\partial^2 F_1}{\partial \bar{s}\,\partial \tilde{s}} - \frac{1}{\omega^2}\left(\frac{\partial^2 F_0}{\partial \tilde{s}^2} - \frac{\omega'}{\omega}\frac{\partial F_0}{\partial \tilde{s}}\right). \tag{1.10.8}$$

The lowest order equation has the solution

$$F_0(\bar{s},\tilde{s}) = A_0(\tilde{s})\,\sin\left(\bar{s} + \Phi_0(\tilde{s})\right), \tag{1.10.9}$$

where $A_0(0)$ and $\Phi_0(0)$ are determined from the initial condition on δ . The functions of the slow time are determined by the requirement that F_1 is a bounded function of the fast time. When $F_0(\bar{s},\tilde{s})$ is substituted into equation (1.10.7), the equation for $F_1(\bar{s},\tilde{s})$ becomes

$$\begin{aligned}\frac{\partial^2 F_1}{\partial \bar{s}^2} + F_1 = {} & \frac{2}{\omega}\left(A_0' - A_0 - \frac{\omega'}{2\omega}A_0\right)\sin\left(\bar{s}+\Phi_0\right) \\ & + \frac{2}{\omega}A_0\Phi_0'\cos\left(\bar{s}+\Phi_0\right).\end{aligned} \tag{1.10.10}$$

In order that the solution for F_1 be bounded, the coefficients of the sine and cosine must vanish. These give that

$$A_0(\tilde{s}) = A_0(0)\left(\frac{\omega(\tilde{s})}{\omega(0)}\right)^{\frac{1}{2}} e^{\tilde{s}} , \tag{1.10.11}$$

$$\Phi_o(\tilde{s}) = \Phi_o(0). \tag{1.10.12}$$

Substituting the form of ω given in equation (1.8.26) into the expression for A_o, the behavior of δ_n for small compression is

$$\delta_n(s) = \delta_n(0) \left(\frac{1 + \left(\frac{\lambda_n(0)}{k_o a_o}\right)^2}{1 + \left(\frac{\lambda_n(s)}{ka}\right)^2} \right)^{\frac{1}{4}} \sin\left(\int_o^s \omega_n(\xi) d\xi + \Phi_o(\omega) \right), \tag{1.10.13}$$

where λ_n is given by equations (1.8.19) and (1.8.20).

The slowly varying amplitude needs to be examined over the range of $k_o a_o$ and n. Since the time behavior of $\lambda_n(s)$ is dependent solely on the function ka, the expression λ_n/ka, can be considered a function of ka. As ka increases from zero to infinity, λ_n increases from $j_{o,n}$ to $j_{1,n}$, the n^{th} roots of J_o and J_1. The ratio λ_n/ka behaves like $(ka)^{-1}$. For large values of λ_n/ka, corresponding to small ka or large n, the coefficient can be written

$$A_o(\tilde{s}) = A_o(0)\, e^{\frac{3}{2}\varepsilon s} + O\left(\left(\frac{\lambda_n}{ka}\right)^2\right). \tag{1.10.14}$$

This exponential behavior remains valid for values of εs sufficiently small that λ_n/ka remains large.

For small values of λ_n/ka corresponding to short waves and small n, the amplitude asymptotes a constant. This is the behavior predicted by the expansion for large εs in Section 1.9. Notice that for any initial condition, λ_n/ka and ω_n tend exponentially to zero for sufficiently large εs, forcing $\delta_n(s)$ to asymptote a constant.

If the bursting phenomenon is to be modelled by the compressed vortex, the growth given here must be responsible for some form of insta-

bility. The initially exponential amplification for large λ_n/ka seems a candidate. The time scale of the growth needs to be checked for Moore's estimated values of the physical parameters. This is done in the next section by numerically integrating the equation for δ_n. Care must be taken to insure that higher terms in the expansion are not misleading in the numerical calculation.

The next order correction to the small compression expansion is found by substituting $F_0(\bar{s},\tilde{s})$ and

$$F_1(\bar{s},\tilde{s}) = A_1(\tilde{s})\sin(\bar{s}+\Phi_1(\tilde{s})) \qquad (1.10.15)$$

into equation (1.10.8). The suppression of secular terms in F_2 requires the coefficients of the sine and cosine terms in the inhomogeneous term to vanish. The amplitude A_1 is of the same form as A_0. The phase Φ_1 satisfies the equation

$$\Phi_1' = -\frac{A_0''}{2\omega A_1'} + \frac{1}{\omega}\left(1+\frac{\omega'}{\omega}\right)\frac{A_0'}{A_1} \quad , \qquad (1.10.16)$$

where primes denote differentiation with respect to $\tilde{s}$. The time dependence of Φ_1 does not affect the actual growth of the disturbance. However, the analysis of the numerical calculations can be influenced by the modulations to the growth, especially when investigating the small compression behavior.

1.11 Numerical Results for Uniform Core

The effect of the initial parameters on the growth of the deflection can be examined by numerically integrating equation (1.8.27). The scheme described in Section 1.7 is used with the value of $\lambda_n(s)$

calculated using Newton's method on the implicit equation (1.8.19) at each time step.

The asymptotic behavior of the axisymmetric deflection is shown in Section 1.9 to be

$$\delta_n \sim C(k_o a_o, \varepsilon, n, \delta_n(0), \delta_n'(0)) \quad \text{as } n \to \infty \qquad (1.11.1)$$

for the initial conditions consisting of a single axial wave mode. The initial conditions are those for the Kelvin waves on the uncompressed filament. The phase ψ_o of the initial wave determines the initial condition as

$$\delta_n(0) = \cos(\psi_o), \qquad (1.11.2)$$

$$\delta_n'(0) = \omega_n(0) \sin(\psi_o), \qquad (1.11.3)$$

where ω_n is defined in equation (1.8.26). The initial amplitude is scaled out of the linearized problem.

The initial phase of $\pi/2$ results in the largest or close to the largest amplitude for small wave numbers. Limiting the study to curves with zero initial deflection allows the asymptote to be written

$$\delta_n(s) \sim \omega_n(0)\, C_1(k_o a_o, \varepsilon, n). \qquad (1.11.4)$$

The number of parameters can be reduced further by noticing that ka and λ_n appear only in the ratio λ_n/ka in equation (1.8.27). The $\lambda_n(s)$ vary slightly while ka increases exponentially with s. Hence the parameter n affects only the value of the initial ratio $\lambda_n(0)/ka$. The behavior

of the deflection for $n > 1$ should be close to that for $n = 1$ with $k_o a_o$ reduced by the ratio $\lambda(0)/\lambda_n(0)$. The numerical integration can be carried out for $n = 1$ and a range of $k_o a_o$.

The solution curves for $\varepsilon = .01$, $n=1$, $\psi_o = \pi/2$ and the wave numbers $k_o a_o = .00001, .0001, .001, .002, .005$ are given in Figure 1.3. As in the stagnant core results, decreasing $k_o a_o$ for long waves causes an increase in C_1. Shorter waves show an oscillatory behavior initially, and asymptote to a constant for sufficiently large s. The period of the Kelvin waves, written in parentheses in the figure, can be compared with the time for the asymptotic behavior to determine the nature of the solution. For decreasing values of ε the curves in Figure 1.3 keep the same shape with the horizontal and vertical scales increased and the values of $k_o a_o$ corresponding to the curves decreased by $1/\varepsilon$.

The largest values of C_1 are for the smallest wave numbers. Taking small initial wave numbers is equivalent to large values of n and moderate wave numbers as discussed earlier. Hence, the limit of the wavelength imposed by the physical parameters does not prevent large values of C_1. They result as the mode of the internal structure of the disturbance increases. Viscosity may provide a practical limit for large n, but the effective parameter $k_o a_o$ is smaller than for the stagnant core results. However, these values occur at later times than for solutions which asymptote smaller values. The rapid growth in the deflection may occur at times greater than the scale of the bursting phenomenon.

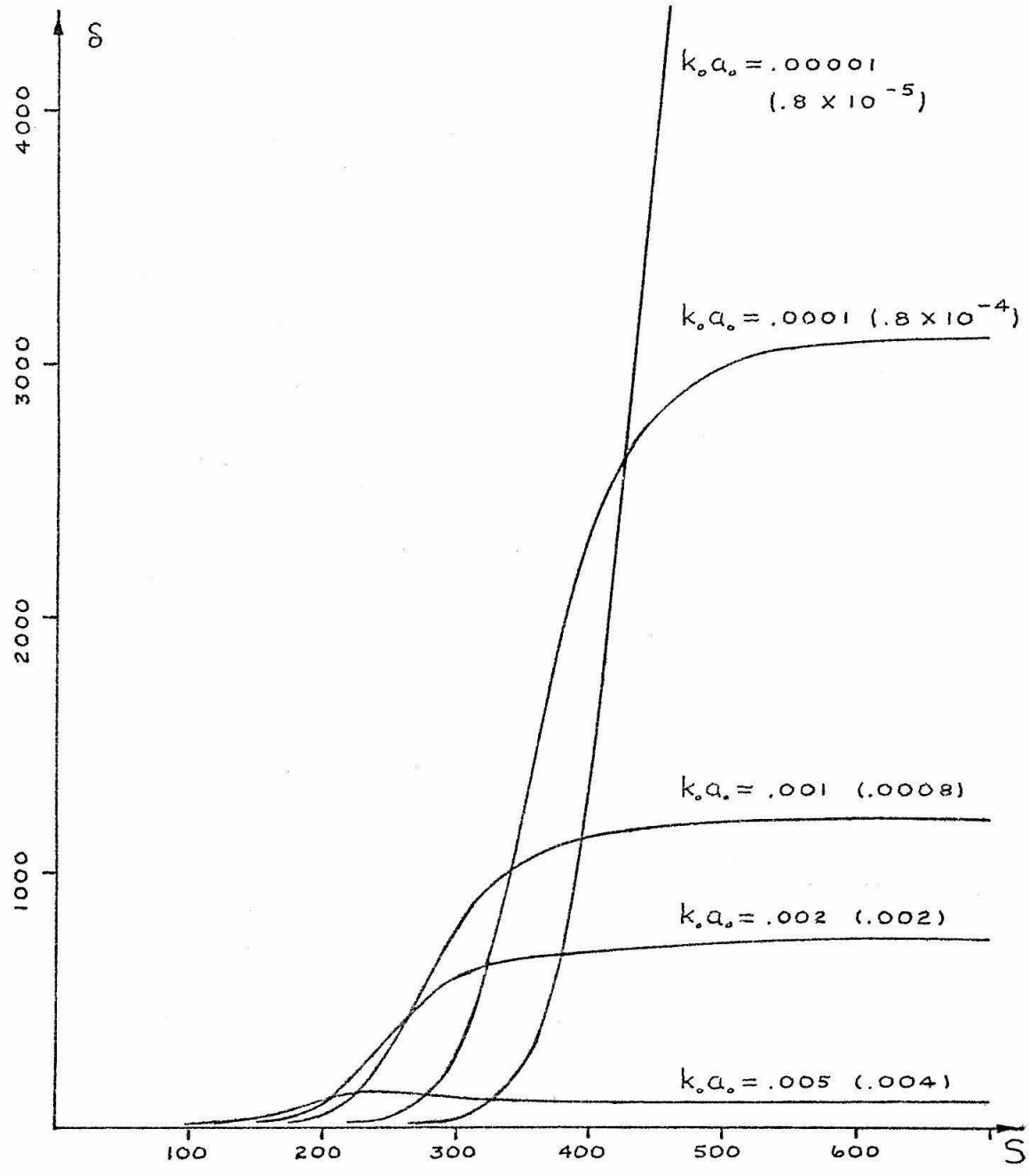

Figure 1.3 The uniform core vortex deflection graphed versus s for $\varepsilon = 0.01$ and several values of $k_0 a_0$. The curve for $k_0 a_0 = 10^{-5}$ asymptotes 6800. The periods of the corresponding Kelvin waves are given in parentheses.

In order to find the compression which could lead to bursting, the deflection is calculated for various values of ε. The solution curves for $k_o a_o = .01$, $n = 1$ and $\varepsilon = .01, .02, .03, .04, .05, .1$ and $.2$ are shown in Figure 1.4. The value of the compression leading to the maximum growth is about .03. The initial wave number is smaller than that for the physical problem. However, allowing higher modes in the internal structure of the disturbance yields similar curves with $k_o a_o = .06$ and $n = 3$, for example. This corresponds to about one-half of the Crow wavelength.

The time at which the rapid growth of the deflection occurs in the model can be compared with that of the physical problem. The time scale for the vortex pair is the time required to descend the separation distance. For vortices of strength κ separated by distance b, the descent time of the vortex system is $2\pi b^2/\kappa$. Moore and Saffman (1972) show the compression at the crest of the small amplitude waves to be

$$\alpha = \frac{\kappa}{2\pi b^2} (kb)^2 K_1(kb) \frac{\delta^*}{b} , \qquad (1.11.5)$$

where δ^* is the semi-amplitude of that component of the deflections above the plane of the vortex pair, k is the wave number and K_1 is a modified Bessel function of the second kind. The most unstable waves from Crow's analysis have

$$kb = .74 \qquad (1.11.6)$$

and δ^* of .71 times the wave amplitude. Combining these results with Moore's computed time for linking

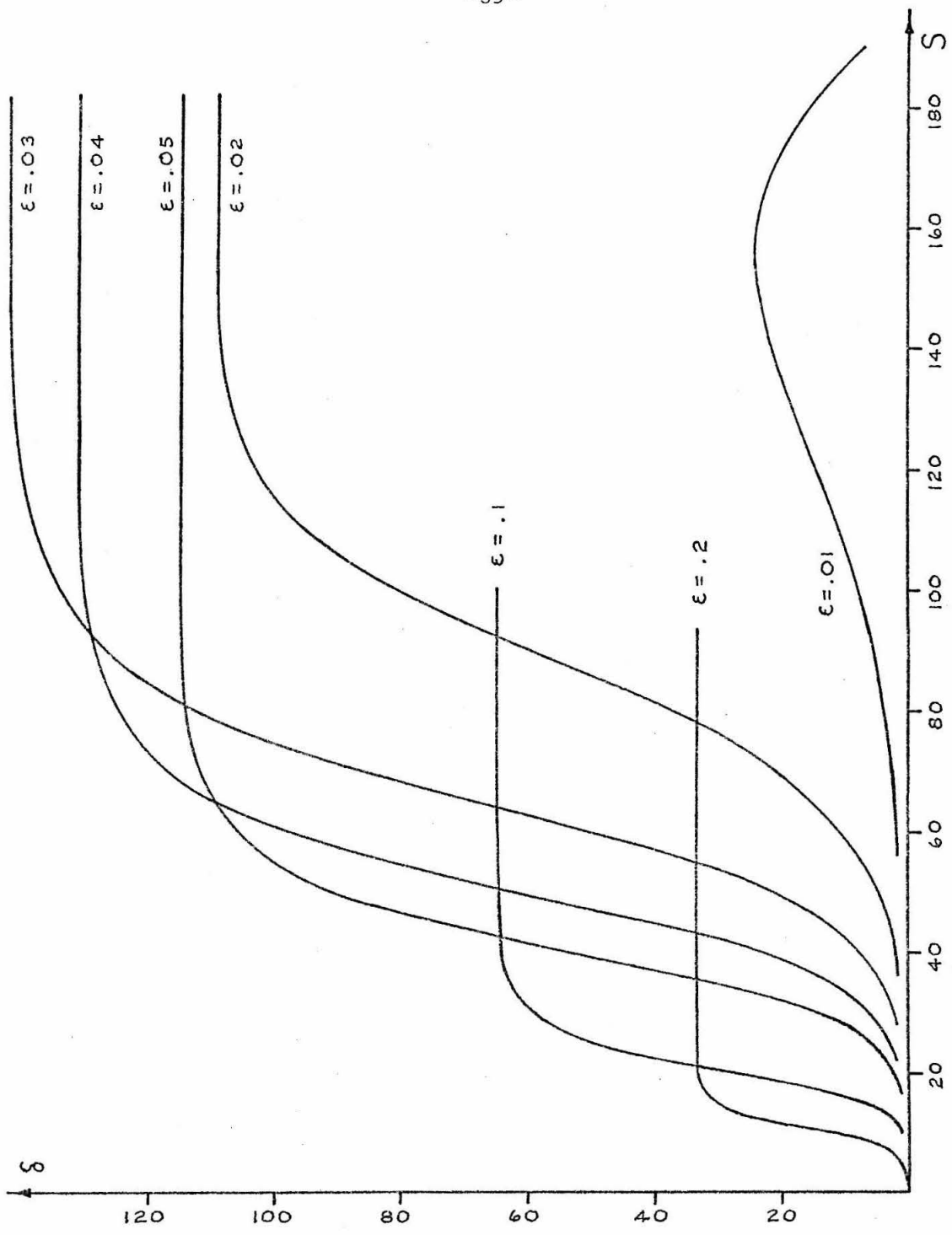

Figure 1.4 Uniform vortex deflection versus s for $k_o a_o = 0.01$ and several values of ε .

$$t_L = 2.5 \frac{2\pi b^2}{\kappa} , \tag{1.11.7}$$

gives a bound for the dimensionless time αt_L. If the approximation for α is assumed to hold for finite amplitudes and the vortex deflection to separation ratio is less than one, then the bound on αt_L becomes

$$\alpha t_L < .7 . \tag{1.11.8}$$

To compare the time in the model with this bound, denote by $s^*(\varepsilon, k_o a_o)$ the time for the deflection to reach one-half of its maximum amplitude. This is centered in the rapid rise of the curves in Figures 1.3 and 1.4. The scaled time εs^* is plotted against ε in Figure 1.5. The curves of constant $k_o a_o$ in this figure extend only to values of the parameters which lead to amplification of the deflection to at least ten times the Kelvin wave amplitude. When the value of ε is sufficiently small the dominant oscillatory nature of the solution gives an initially growing oscillation, similar to that shown for $k_o a_o$ in Figure 1.2. As ε is decreased for constant $k_o a_o$, a curve in Figure 1.5 drops off until the first maximum in the deflection curve is below 10. At this point the bursting time curve jumps to the time value corresponding to the next extremum of the deflection curve. A sawtooth curve is generated as ε is decreased further, but this is not included in Figure 1.5 as it does not represent a rapid growth in the deflection and occurs above the linking time anyway.

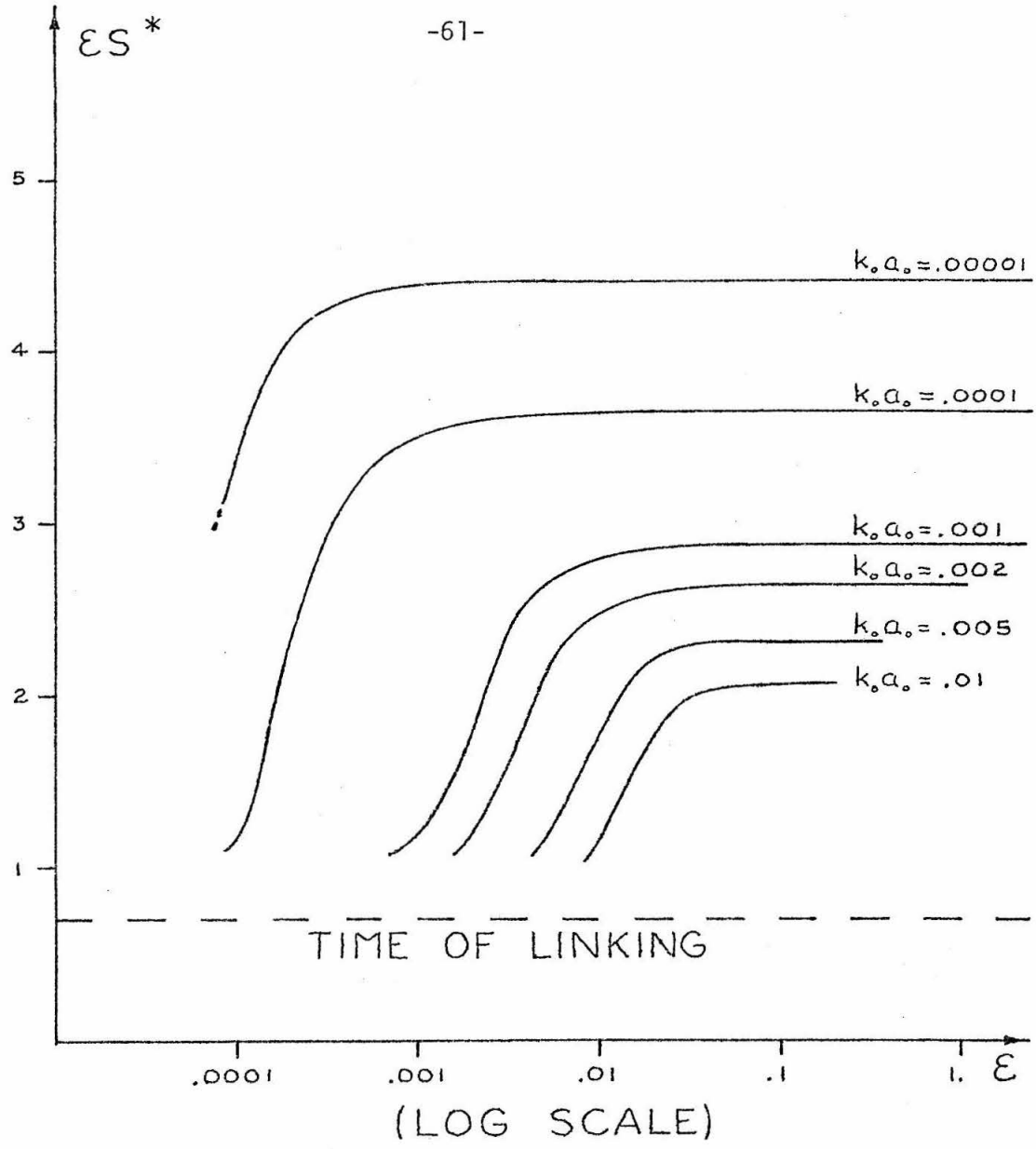

Figure 1.5 The scaled time of the rapid increase in the deflection versus the scaled compression. The maximum deflection must be greater than 10 and the curves are not continued to the left of $\varepsilon = 10^{-4}$.

The value of a_o/b used in Moore's calculation gives $\varepsilon = .003$, but since the cut-off method depends logarithmically on the core radius, the bound on the linking time given in equation (1.11.8) is expected to be adequate for the larger values of ε.

All the plotted values of εs^* lie above the linking time. As $k_o a_o$ is increased the value εs^* decreases, but the amplitude of the deflection decreases as well. No combination of the parameters $k_o a_o$ and ε give large amplitudes in sufficiently short time. The bursting phenomenon does not therefore appear to be adequately modeled by the effect of compression on the Kelvin waves.

CHAPTER 2

VORTEX IN A STRAIN FIELD

2.1 Introduction

The appearance and growth of waves around the circumference of a vortex ring is demonstrated experimentally by Krutzch (1939) and confirmed more recently by Widnall and Sullivan (1973) and others. An explanation for the appearance of this instability is offered by Widnall, Bliss and Tsai (1974). They argue that waves which displace the thin vortex core in the plane of the ring but do not propagate around the ring will be amplified by the local straining which results from the curvature of the ring. Moore and Saffman (1975) confirm this mechanism for the corresponding problem of a straight vortex filament in a small strain field. They give the form for the amplified waves when the vorticity is continuous. The wave numbers and growth rates associated with the unstable waves are calculated for the related special case of a uniform cored potential vortex by Tsai and Widnall (1976). The most unstable mode is shown to be for the vortex deformed by a superposition of the helical waves which do not propagate along the vortex. These calculations use an expansion in the small strain rate and find the correction to the helical Kelvin waves on the filament due to the strain. The wave numbers for the fastest growing waves on the strained vortex are those corresponding to the steady Kelvin waves.

Widnall and Tsai (1977) solve for the growth of waves on a uniform cored ring in an expansion in the ratio of the core radius to the ring radius. The leading order contribution to the growth in this expansion

gives behavior like the uniform cored straight vortex in a strain.

Saffman (1977) discusses the effect of considering realistic core profiles on the critical wave numbers and corresponding growth rates for the straight vortex in a strain field. The product of the wave number times the ring radius can be compared with the number of wave crests which appear on the observed rings. The relative growth rates for the first few critical wave numbers can be examined to predict the number of waves on the ring. It is the purpose of this chapter to demonstrate a method for calculating the growth rates for a general axi-symmetric distribution of vorticity in a straight vortex core of finite radius surrounded by potential flow.

2.2 The Steady Vortex Filament in a Straining Field

The fluid is assumed to be uniform, inviscid and incompressible with the constant density taken as unity. In a cylindrical coordinate system (r,θ,z) the undeformed vortex filament is aligned along the z axis with swirl velocity $V_0(r)$ in a core of radius a. The flow outside the core is that of a potential vortex. The strength of the filament is given by

$$\Gamma = 2\pi a V_0(r) . \tag{2.2.1}$$

The system is scaled by dividing the velocities by $V_0(a)$ and the radial coordinate by a. Define the new radial coordinate

$$X = r/a \tag{2.2.2}$$

and the core rotation rate by

$$\Omega(x) = \frac{1}{x}\,\frac{\bar{V}_0(ax)}{\bar{V}_0(a)} \qquad \text{for} \quad 0<x<1. \tag{2.2.3}$$

The rotation rate must be finite at the origin. The velocity field due to the vortex filament alone is denoted by $(0,\bar{v}_0,0)$, where

$$\bar{V}_0 = \begin{cases} x\Omega(x) & \text{for} \quad x<1, \\ 1/x & \text{for} \quad x>1. \end{cases} \tag{2.2.4}$$

The vorticity is non-zero only in the core where

$$\Delta = \frac{1}{x}\frac{d}{dx}(x^2\Omega). \tag{2.2.5}$$

The symbol Δ is used to denote the vorticity to eliminate confusion with the symbol for the frequency introduced later.

The corrections due to the external straining give the total velocity field, $(\bar{u},\bar{v}_0+\bar{v}_1,0)$. Far from the vortex filament, the velocities have the form

$$\left.\begin{aligned} \bar{u}_1 &\sim \varepsilon x \sin(2\theta) \\ \bar{v}_1 &\sim \varepsilon x \cos(2\theta) \end{aligned}\right\} \text{for } x \to \infty. \tag{2.2.6}$$

The parameter ε is the ratio of the rate of strain, e, to the dimensional rotation rate at the core edge,

$$\varepsilon = \frac{e}{\bar{V}_0(a)/a} = \frac{2\pi a^2 e}{\Gamma}. \tag{2.2.7}$$

The strain is assumed to be small, constraining $|\varepsilon| << 1$.

In order to evaluate the corrections to the flow field for a given axisymmetric distribution of vorticity in the core, it is convenient to introduce the stream functions, ψ_0 and ψ_1, defined by

$$u = -\frac{1}{x}\frac{\partial \psi}{\partial \theta} , \tag{2.2.8}$$

$$v = \frac{\partial \psi}{\partial x} , \tag{2.2.9}$$

where the subscripts 0 and 1 both apply. The stream function $\psi_0(x)$ due to the vortex alone is determined within an arbitrary constant by the swirl velocity $\bar{v}_0(x)$. Equations (2.2.6) give the asymptotic behavior of the correction due to the straining as

$$\psi_1(x,\theta) \sim \tfrac{1}{2}\varepsilon x^2 \cos(2\theta) \quad \text{as } x \to \infty. \tag{2.2.10}$$

In the region outside the vortex core the flow is irrotational, so that ψ_1 must satisfy Laplace's equation. The stream function can be written in the form

$$\psi_1 = \tfrac{1}{2}\varepsilon f(x)\cos(2\theta). \tag{2.2.11}$$

For the region of potential flow described by

$$x > X(\theta) \equiv 1 + \varepsilon A \cos(2\theta), \tag{2.2.12}$$

the function f(x) defining the stream function has the form

$$f(x) = x^2 + a_1/x^2, \tag{2.2.13}$$

where a_1 and A are constants to be determined.

In the filament core the vorticity is constant along the streamlines, giving

$$\Delta = F(\Psi_0). \tag{2.2.14}$$

If the same functional relation holds after imposing the external straining, the stream functions satisfy

$$\nabla^2(\Psi_0+\Psi_1) = F(\Psi_0+\Psi_1) \quad \text{for} \quad x < X(\theta). \tag{2.2.15}$$

Since ψ_1 is proportional to the small parameter ε, the approximate equation for the correction to the stream function can be written as

$$\nabla^2\Psi_1 = F'(\Psi_0)\Psi_1 . \tag{2.2.16}$$

Taking the derivative with respect to x in equation (2.2.14) and solving for $F'(\psi_0)$ gives

$$F'(\Psi_0) = \left(3\frac{d\Omega}{dx} + x\frac{d^2\Omega}{dx^2}\right)/x\Omega . \tag{2.2.17}$$

The form of ψ_1 given in equation (2.2.11) can be substituted into equation (2.2.16) along with the expression for F' above, to give the core equation,

$$\frac{d^2f}{dx^2} + \frac{1}{x}\frac{df}{dx} - \left[\frac{x\frac{d^2\Omega}{dx^2} + 3\frac{d\Omega}{dx}}{x\Omega} + \frac{4}{x^2}\right]f = 0 \quad \text{for } 0<x<X. \tag{2.2.18}$$

In terms of the unique bounded solution to the above satisfying

$$g(x) \sim x^2 \quad \text{as} \quad x \to 0, \tag{2.2.19}$$

any bounded solution can be written,

$$f(x) = a_0 g(x). \tag{2.2.20}$$

The constants a_0, a_1 and A are determined by the conditions on the interface between the regions of non-zero vorticity and potential flow. The arbitrary constant in the stream function allows the value on this streamline to be set equal to zero. This gives the two relations

$$\Psi_0(X) + \tfrac{1}{2}\varepsilon a_0 g(1)\cos(2\theta) = 0, \tag{2.2.21}$$

$$\log(X) + \tfrac{1}{2}\varepsilon(1+a_1)\cos(2\theta) = 0, \tag{2.2.22}$$

where only terms to $O(\varepsilon)$ have been retained. Expanding these expressions and simplifying gives the conditions

$$2A + a_0 g(1) = 0, \tag{2.2.23}$$

$$2A + a_1 = -1. \tag{2.2.24}$$

The continuity of the swirl velocity across the interface gives the relation

$$X\Omega(X) + \tfrac{1}{2}\varepsilon a_0 g'(1)\cos(2\theta) = X^{-1} + \varepsilon(1-a_1)\cos(2\theta), \tag{2.2.25}$$

where the prime denotes differentiation with respect to x. Substituting the form for X from equation (2.2.12) into the above and expanding gives the relation

$$(2+\Omega'(1))A + \tfrac{1}{2}g'(1)a_0 + a_1 = 1 . \tag{2.2.26}$$

The values of the constants a_0, a_1 and A are determined by the three linear equations (2.2.23), (2.2.24) and (2.2.26) to be

$$a_0 = 4\left(g'(1) - \Omega'(1)g(1)\right)^{-1}, \tag{2.2.27}$$

$$a_1 = a_0 g(1) - 1 , \tag{2.2.28}$$

$$A = -\tfrac{1}{2}a_0 g(1) , \tag{2.2.29}$$

and the correction to the vortex flow field due to the small external strain is uniquely determined to the leading order.

The case of uniform vorticity in the core gives

$$\Omega(x) = 1 , \quad g(x) = x^2 \tag{2.2.30}$$

and the stream function takes the form

$$\psi_0 + \psi_1 = \begin{cases} x^2\left(1 + \varepsilon\cos(2\theta)\right) & \text{for } x < 1-\varepsilon\cos(2\theta), \\ \log x + \tfrac{1}{2}\varepsilon\left(x^2+\tfrac{1}{x^2}\right)\cos(2\theta) & \text{for } x > 1-\varepsilon\cos(2\theta). \end{cases} \tag{2.2.31}$$

The steady velocity field $(\bar{u}_1, \bar{v}_0+\bar{v}_1, 0)$ follows directly from equations (2.2.31), (2.2.8) and (2.2.9).

2.3 The Equations for Stability

In order to investigate the stability of the steady flow field defined in the last section, the disturbance velocities $(\tilde{u},\tilde{v},\tilde{w})$ and pressure $\tilde{p}$ are added to the steady solutions. Substituting these into the Euler equations and retaining only terms linear in the disturbance quantities gives the governing equations

$$\frac{\partial\tilde{u}}{\partial t}+\bar{u}_1\frac{\partial\tilde{u}}{\partial x}+\tilde{u}\frac{\partial\bar{u}_1}{\partial x}+(\bar{v}_0+\bar{v}_1)\frac{\partial\tilde{u}}{\partial\theta}+\tilde{u}\frac{\partial\bar{v}_1}{\partial\theta}-\frac{2}{x}(v_0+v_1)\tilde{v}=-\frac{\partial\tilde{p}}{\partial x}\,, \tag{2.3.1a}$$

$$\frac{\partial\tilde{v}}{\partial t}+\bar{u}_1\frac{\partial\tilde{v}}{\partial x}+\tilde{u}\frac{\partial}{\partial x}(\bar{v}_0+\bar{v}_1)+\frac{1}{x}\left((\bar{v}_0+\bar{v}_1)\frac{\partial\tilde{v}}{\partial\theta}+\tilde{v}\frac{\partial\tilde{v}}{\partial\theta}\right)+\frac{1}{x}\left(\tilde{u}(\bar{v}_0+\bar{v}_1)+\tilde{v}\bar{u}_1\right)=\frac{-1}{x}\frac{\partial\tilde{p}}{\partial\theta}\,, \tag{2.3.1b}$$

$$\frac{\partial\tilde{w}}{\partial t}+\bar{u}_1\frac{\partial\tilde{w}}{\partial x}+\frac{1}{x}(\bar{v}_0+\bar{v}_1)\frac{\partial\tilde{w}}{\partial\theta}=-\frac{\partial\tilde{p}}{\partial z}\,, \tag{2.3.1c}$$

$$\frac{\partial\tilde{u}}{\partial x}+\frac{1}{x}\tilde{u}+\frac{1}{x}\frac{\partial\tilde{v}}{\partial\theta}+\frac{\partial\tilde{w}}{\partial z}=0\,. \tag{2.3.1d}$$

The position of the core interface changes due to the disturbance. Define the deflection $\tilde{\delta}$ such that the position of the core boundary is

$$x=X(\theta)+\tilde{\delta}(\theta,z,t)\,, \tag{2.3.2}$$

where X is defined in equation (2.2.12). The velocities $(\bar{u}_1+\tilde{u},\bar{v}_0+\bar{v}_1+\tilde{v},\tilde{w})$ must be continuous across the disturbed core boundary.

In order to simplify the notation, introduce the vector U, defined by

$$U=\begin{pmatrix}\tilde{u}\\ \tilde{v}\\ \tilde{w}\\ \tilde{p}\end{pmatrix}\,. \tag{2.3.3}$$

The system of equations (2.3.1) can then be written as

$$\frac{\partial}{\partial t}(LU) + MU = \frac{1}{2}\varepsilon\left(e^{2i\theta}N + e^{-2i\theta}\bar{N}\right)U, \tag{2.3.4}$$

where

$$L = \begin{pmatrix} 1 & 0 & 0 & 0 \\ 0 & 1 & 0 & 0 \\ 0 & 0 & 1 & 0 \\ 0 & 0 & 0 & 0 \end{pmatrix}, \tag{2.3.5}$$

$$M = \begin{pmatrix} \Omega\,\partial/\partial\theta & -2\Omega & 0 & \partial/\partial x \\ 2\Omega' + x\Omega' & \Omega\,\partial/\partial\theta & 0 & \frac{1}{x}\,\partial/\partial\theta \\ 0 & 0 & \Omega\,\partial/\partial\theta & \partial/\partial z \\ \frac{\partial}{\partial x} + \frac{1}{x} & \frac{1}{x}\,\partial/\partial\theta & \partial/\partial z & 0 \end{pmatrix}, \tag{2.3.6}$$

$$N = \begin{pmatrix} \left(\frac{i}{x}f' - \frac{i}{x^2}f + \frac{if}{x}\frac{\partial}{\partial x} - \frac{f'}{2x}\frac{\partial}{\partial\theta}\right) & \frac{1}{x}f' - \frac{2}{x^2}f & 0 & 0 \\ -\frac{1}{2}f'' - \frac{1}{2x}f' & \left(-\frac{i}{x}f' + \frac{if}{x^2} + \frac{i}{x}f\frac{\partial}{\partial x} - \frac{1}{2x}f'\frac{\partial}{\partial\theta}\right) & 0 & 0 \\ 0 & 0 & \left(\frac{i}{x}f\frac{\partial}{\partial x} - \frac{1}{2x}f'\frac{\partial}{\partial\theta}\right) & 0 \\ 0 & 0 & 0 & 0 \end{pmatrix}, \tag{2.3.7}$$

and $\bar{N}$ is the complex conjugate matrix of N. The definition of the core rotation $\Omega(x)$ is extended outside the core by

$$\Omega(x) = 1/x^2 \quad \text{for} \quad x > 1. \tag{2.3.8}$$

The notation used above is the same as that used by Moore and Saffman (1975).

The solution to the system (2.3.4) must satisfy conditions at the origin and infinity, as well as the condition of continuity of the velocities at the core boundary. The disturbance velocities and

pressure must tend to zero at infinity and be regular at the origin.

The disturbance solutions can be written as an expansion in the small parameter ε by defining

$$U = (\tilde{U}_0 + \varepsilon \tilde{U}_1 + \cdots) e^{ikz + i\omega t}, \tag{2.3.9}$$

$$\omega = \omega_0 + \varepsilon \omega_1 + \cdots, \tag{2.3.10}$$

$$k = k_0 + \varepsilon k_1 + \cdots . \tag{2.3.11}$$

Substituting this form into equation (2.3.4) and equating coefficients in powers of ε gives the hierarchy

$$(i\omega_0 L + M_0)\tilde{U}_0 = 0, \tag{2.3.12}$$

$$(i\omega_0 L + M_0)\tilde{U}_1 = \left(-i\omega_1 L - ik_1 P + \tfrac{1}{2}(e^{2i\theta} N + e^{-2i\theta} \bar{N})\right)\tilde{U}_0, \tag{2.3.13}$$

where

$$P = \begin{pmatrix} 0 & 0 & 0 & 0 \\ 0 & 0 & 0 & 0 \\ 0 & 0 & 0 & 1 \\ 0 & 0 & 1 & 0 \end{pmatrix} \tag{2.3.14}$$

and replacing the $\partial/\partial z$ in the matrix M by ik_0 gives the matrix M_0.

The conditions on the velocities at the core boundary are from a hierarchy of continuity conditions across the deformed boundary

$$\tilde{X}(\theta, z, t) = X(\theta) + (\delta_0 + \varepsilon \delta_1 + \cdots) e^{ikz + i\omega t}. \tag{2.3.15}$$

These constraints are calculated when needed in the next section.

2.4 Helical Standing Waves on the Cylindrical Vortex

The case modelling the vortex ring instability is for helical disturbances which do not propagate along the filament. To the lowest order in the small strain, these are the steady deflections corresponding to $\omega_0 = 0$ with angular dependence which can be separated by introducing two new vectors

$$\tilde{U}_0 = a_{+1} U_0(+1) e^{i\theta} + a_{-1} U_0(-1) e^{-i\theta}. \tag{2.4.1}$$

If the differentiation $\partial/\partial\theta$ in the matrix M_0 is replaced by the factor, in , to define a matrix $M_0(n)$, then the terms in equation (2.4.1) must satisfy

$$M_0(n)\, U_0(n) = 0 \quad \text{for} \quad n = \pm 1. \tag{2.4.2}$$

For clarity in the notation, whenever the argument represents the angular dependence, the sign is included. In this manner the value of a function $f(x)$ at $\lambda = 1$, $f(1)$, is not confused with the $n = 1$ mode of a function, say $g(+1)$.

The structure of the matrix operator $M_0(\pm 1)$ gives the relative form of the solutions as

$$U_0(+1) = \begin{pmatrix} iu \\ v \\ w \\ p \end{pmatrix} \; ; \; U_0(-1) = \begin{pmatrix} -iu \\ v \\ -w \\ p \end{pmatrix} . \tag{2.4.3}$$

Substituting the above into equation (2.4.2), the system can be reduced to two first order ordinary differential equations

$$\frac{du}{dx} = \frac{1}{x}\left(\frac{\Delta}{\Omega} - 1\right)u + \left(k_o^2 + \frac{1}{x^2}\right)\hat{P}\,, \tag{2.4.4}$$

$$\frac{d\hat{P}}{dx} = \left(1 - 2\frac{\Delta}{\Omega}\right)u - \frac{1}{x}\frac{\Delta}{\Omega}\hat{P}\,, \tag{2.4.5}$$

where

$$\hat{P} = P/\Omega\,, \tag{2.4.6}$$

and Δ is the dimensionless vorticity,

$$\Delta = 2\Omega + x\Omega'\,. \tag{2.4.7}$$

The remaining components of U_o are determined from the above by the relations

$$v = -\frac{\Delta}{\Omega}u - \frac{1}{x}\hat{P}\,, \tag{2.4.8}$$

$$w = -k_o\hat{P}\,. \tag{2.4.9}$$

The components above must be regular at the origin. This condition determines the solutions of equations (2.4.4) and (2.4.5) within an arbitrary constant amplitude. Without loss of generality, the solutions can be made unique by the conditions at the origin

$$u = 1 \qquad \text{at } x = 0\,, \tag{2.4.10}$$

$$\hat{P} \sim -x \qquad \text{as } x \to 0\,. \tag{2.4.11}$$

These determine the solutions in the core.

In the region outside the core the disturbance velocity field can be written in terms of a velocity potential. Using the form for the separation of the axial, azimuthal and time dependence given in equations (2.3.9) and (2.4.1), the velocity potential of mode n = 1 has the form

$$\tilde{\phi} = i C_o K_1(k_o x)\, e^{ikz + i\omega t + in\theta}. \tag{2.4.12}$$

The four vector $U_0(+1)$ follows from differentiation of the potential to give

$$U_o(+1) = C_o \begin{pmatrix} -i\left(k_o K_1(k_o x) + \frac{1}{x} K_1(k_o x)\right) \\ -\frac{1}{x} K_o(k_o x) \\ -k_o K_1(k_o x) \\ \frac{1}{x^2} K_1(k_o x) \end{pmatrix}, \tag{2.4.13}$$

where K_0 and K_1 are the modified Bessel functions of the second kind and C_0 is a constant to be determined from the conditions on the core boundary. The form of $U_0(-1)$ is given by equation (2.4.3) for the $U_0(+1)$ given above.

The velocity field for the undisturbed vortex is continuous across the core boundary. The velocities with the addition of the disturbances must also be continuous across the disturbed boundary. Introduce the notation,

$$\left[G(x)\right]_{x=H} = \lim_{h \to +0} \left(G(H+h) - G(H-h) \right), \tag{2.4.14}$$

that is, the brackets indicate the jump in the quantity across some curve. Then the continuity of the velocities and pressure gives

$$[\bar{u}_1 + \tilde{u}]_{x=\tilde{X}} = 0, \tag{2.4.15}$$

$$[\bar{v}_0 + \bar{v}_1 + \tilde{v}]_{x=\tilde{X}} = 0, \tag{2.4.16}$$

$$[\tilde{w}]_{x=\tilde{X}} = 0, \tag{2.4.17}$$

$$[\bar{p}_0 + \bar{p}_1 + \tilde{p}]_{x=\tilde{X}} = 0, \tag{2.4.18}$$

where $\tilde{X}$ is the disturbed boundary defined in equation (2.3.15). The parameter ε is set to zero to the lowest order in the strain, giving the conditions

$$[u]_{x=1} = [w]_{x=1} = [p]_{x=1} = 0, \tag{2.4.19}$$

where u, w and p are defined in equation (2.4.3). The continuity of the azimuthal velocity gives

$$[v]_{x=1} = -\left[\frac{d\bar{v}_0}{dx}\right]_{x=1} \delta_0, \tag{2.4.20}$$

where δ_0 is defined in equation (2.3.15) as the disturbance to the core radius.

The axial wave number k_0 can only take on certain values in order that the equations (2.4.19) hold. The continuity of pressure and axial velocity give a single constraint, that

$$\hat{p} = C_0 K_1(k_0) \qquad \text{on } x = 1. \tag{2.4.21}$$

Substituting the value of C_0 from the above into the continuity of radial

velocity gives the condition

$$u + \left(1 + k_o \frac{K_o(k_o)}{K_1(k_o)}\right)\hat{P} = 0 \quad \text{on} \quad x = 1. \tag{2.4.22}$$

The value of u and $\hat{p}$ at x = 1 depends on k_0 from the differential equation (2.4.4). The above gives a dispersion relation for the wave number. This is the result of taking $\omega_0 = 0$ at the start of the calculation.

2.5 Effect of Strain on the Disturbances

The angular dependence on the correction to the disturbance flow field is determined from equation (2.3.13). Substituting $\tilde{U}_0$ given by equation (2.4.1) into the inhomogeneous term in the equation for $\tilde{U}_1$ dictates the form in the forced modes as

$$\widetilde{U}_1 = U_1(-3)e^{-3i\theta} + U_1(-1)e^{-i\theta} + U_1(+1)e^{i\theta} + U_1(+3)e^{3i\theta}. \tag{2.5.1}$$

The angular dependence separates equation (2.3.13) into the four independent equations,

$$M_o(+3)U_1(+3) = \tfrac{1}{2}N(+1)a_{+1}U_o(+1), \tag{2.5.2}$$

$$M_o(+1)U_1(+1) = -i(\omega_1 L + k_1 P)a_{+1}U_o(+1) + \tfrac{1}{2}N(-1)a_{-1}U_o(-1), \tag{2.5.3}$$

$$M_o(-1)U_1(-1) = -i(\omega_1 L + k_1 P)a_{-1}U_o(-1) + \tfrac{1}{2}\bar{N}(+1)a_{+1}U_o(+1), \tag{2.5.4}$$

$$M_o(-3)U_1(-3) = \tfrac{1}{2}\bar{N}(-1)a_{-1}U_o(-1). \tag{2.5.5}$$

The +1 or -1 as the argument of the matrices N and $\bar{N}$ indicate that $\partial/\partial\theta$

has been replaced by +i or -i.

The homogeneous problems for the matrix operators $M_0(+3)$ and $M_0(-3)$ have only the trivial solution. Unique solutions for $U_1(-3)$ and $U_1(+3)$ can be determined from the equations and boundary conditions. The homogeneous problems associated with $M_0(+1)$ and $M_0(-1)$ have the non-zero solutions discussed in the previous section. Solutions to the inhomogeneous problem do not exist unless the forcing terms in equations (2.5.3) and (2.5.4) and the boundary conditions satisfy some constraints. Using this restriction the dispersion relation for the frequency correction ω_1 can be determined without having to determine the solutions $U_1(+1)$ and $U_1(-1)$. This is done in the next section. First the inhomogeneous terms in the boundary conditions must be determined.

The total velocities and pressure must be continuous across the disturbed boundary

$$x = \tilde{X} \equiv 1 + \varepsilon A \cos(2\theta) + (\delta_0 + \varepsilon \delta_1 + \cdots) e^{ikz + i\omega t} . \qquad (2.5.6)$$

The angular dependence of the deflection δ_0 can be separated by writing

$$\delta_0 = \sum_n \delta_0(n) e^{in\theta} . \qquad (2.5.7)$$

For helical waves only the modes n=+1 and n=-1 are considered. Denote the components of $U_1(n)$ by

$$U_1(n) = \begin{pmatrix} u_1(n) \\ v_1(n) \\ w_1(n) \\ p_1(n) \end{pmatrix} . \qquad (2.5.8)$$

The condition that the radial velocity be continuous across the core boundary becomes

$$\left[u_1(+1) + \tfrac{1}{2} A \tfrac{d}{dx}(-i a_{-1} u) - \tfrac{i}{2} \tfrac{df}{dx} \delta_0(-1) \right]_{x=1} = 0 , \qquad (2.5.9)$$

where the brackets indicate the jump across the surface x=1 as defined in equation (2.4.14). If the values for [du/dx] and [df/dx] are substituted from Sections 2.2 and 2.4, then

$$\left[u_1(+1) \right]_{x=1} = \tfrac{i}{2} A \left((3+\Omega') u + \left(1 + k_0 \tfrac{K_0(k_0)}{K_1(k_0)}\right) \hat{p} \right) a_{-1} \quad \text{at } x=1. \qquad (2.5.10)$$

The constants A and k_0 and the values of the functions u and $\hat{p}$ at x=1 depend on the form of $\Omega(x)$ in the vortex core.

The condition that the pressure be continuous across the core boundary gives

$$\left[-\tfrac{1}{2} A \tfrac{d}{dx}(x\Omega^2) \delta_0(-1) + \tfrac{1}{2}\left(\tfrac{df}{dx} - f\right) \delta_0(-1) + A a_{-1} \tfrac{dp}{dx} + p_1(+1) \right]_{x=1} = 0. \qquad (2.5.11)$$

Substituting for [dΩ/dx], [df/dx] and [dp/dx] in the above gives

$$\left[p_1(+1) \right]_{x=1} = -\tfrac{1}{2} A \left((2\Omega' + 3) u - \left(1 + k_0 \tfrac{K_0(k_0)}{K_1(k_0)}\right) \hat{p} \right) a_{-1} \quad \text{at } x=1, \qquad (2.5.12)$$

where $\Omega'(1)$ is the value from the core. The symmetry in the problem gives

$$\left[u_1(-1) \right]_{x=1} = - \left[u_1(+1) \right] a_{+1} / a_{-1} , \qquad (2.5.13)$$

$$\left[p_1(-1) \right]_{x=1} = \left[p_1(+1) \right] a_{+1} / a_{-1} . \qquad (2.5.14)$$

The conditions for the azimuthal and axial velocities are not necessary for calculating ω_1 or U_1. The matrix M_0 reduces to a second order differential operator, giving algebraic relations for v_1 and w_1 as in equations (2.4.8) and (2.4.9).

The homogeneous problem corresponding to equations (2.5.3) and (2.5.4) and the boundary conditions (2.5.13) and (2.5.14) for U_1 is the same as the lowest order problem solved in Section 2.4. The solution to the adjoint of the lowest order problem needs to be determined in order to apply the Fredholm alternative.

2.6 The Adjoint Solution

In order to define the adjoint problem introduce an inner product

$$\langle A, B\rangle = \int_0^\infty (\bar{a}_1 b_1 + \bar{a}_2 b_2 + \bar{a}_3 b_3 + \bar{a}_4 b_4)\,dx\,, \tag{2.6.1}$$

where the a_i and b_i are the components of the vectors A and B and the overbar indicates the complex conjugates. The adjoint solution $U_0^*(n)$, corresponding to the solution $U_0(n)$ must satisfy

$$M_0^*(n)\; U_0^*(n) = 0\,, \tag{2.6.2}$$

where

$$M_{0(n)}^* = \begin{pmatrix} -in\Omega & 2\Omega + x\Omega' & 0 & -d/dx + 1/x \\ -2\Omega & -in\Omega & 0 & -in/x \\ 0 & 0 & -in\Omega & -ik_0 \\ -d/dx & -in/x & -ik_0 & 0 \end{pmatrix}. \tag{2.6.3}$$

The boundary conditions for $U_0^*(n)$ are the same as those given in Section

2.4 for $U_o(+1)$. To calculate the form of the adjoint solution for the helical mode, denote

$$U_o^*(+1) = \begin{pmatrix} iu^* \\ v^* \\ w^* \\ p^* \end{pmatrix} \quad ; \quad U_o^*(-1) = \begin{pmatrix} -iu^* \\ v^* \\ -w^* \\ p^* \end{pmatrix} . \tag{2.6.4}$$

The form of the matrix operators $M_o^*(+1)$ and $M_o^*(-1)$ yield the relationship given above between $U_o^*(+1)$ and $U_o^*(-1)$ when they are appropriately normalized. Substituting the components into equation (2.6.2), the system can be written in terms of two ordinary differential equations,

$$\frac{du^*}{dx} = \frac{2}{x} u^* + (k_o^2 + 1/x^2)\, \hat{p}^* , \tag{2.6.5}$$

$$\frac{d\hat{p}^*}{dx} = (1 - 2\tfrac{\Delta}{\Omega})\, u^* + \tfrac{1}{x}(3 - 2\tfrac{\Delta}{\Omega})\, \hat{p}^* , \tag{2.6.6}$$

where

$$\hat{p}^* = p^*/\Omega . \tag{2.6.7}$$

The dimensionless vorticity Δ is defined in equation (2.4.7). The remaining components of U_o^* are determined from the algebraic relations

$$v^* = -2u^* - \tfrac{1}{x}\hat{p}^* , \tag{2.6.8}$$

$$w^* = -k_o \hat{p}^* . \tag{2.6.9}$$

The components of U_o^* must be regular at the origin. This constraint determines the solutions of equations (2.6.5) and (2.6.6) within an arbitrary normalization. The solutions are defined uniquely by the initial behavior

$$u^* \sim x \quad \text{as} \quad x \to 0, \tag{2.6.10}$$

$$\hat{p}^* \sim -x^2 \quad \text{as} \quad x \to 0, \tag{2.6.11}$$

for the range of x inside the core.

In the region outside the core, the vorticity is zero and the solution to equations (2.6.5) and (2.6.6) can be found in closed form. Applying the condition that the velocities and pressure must vanish at infinity gives

$$U_o^{*(+1)} = C_o^* \begin{pmatrix} -ix^2\left(k_o x K_o(k_o x) + K_1(k_o x)\right) \\ x^2\left(2k_o x K_o(k_o x) + K_1(k_o x)\right) \\ -k_o x^3 K_1(k_o x) \\ x K_1(k_o x) \end{pmatrix}. \tag{2.6.12}$$

The constant C_o^* is determined from the continuity of the velocities and pressure. If $\hat{p}^*(1)$ is the value of the function $\hat{p}^*(x)$ at x=1, then

$$C_o^* = \hat{P}^{*(1)} / K_1(k_o). \tag{2.6.13}$$

The adjoint operator was defined to satisfy

$$\langle M_o^* A, B \rangle = \langle A, M_o B \rangle \tag{2.6.14}$$

for any vectors A and B which satisfy the same boundary conditions and continuity conditions as U_o. If the vector A is replaced by the solution to the adjoint problem U_o^*, then the left side in equations (2.6.14) vanishes. For B the solution of the inhomogeneous problem

$$M_o B = F \tag{2.6.15}$$

with the same homogeneous boundary conditions as U_0, equation (2.6.14) gives the orthogonality relation

$$\langle U_o^*, F \rangle = 0 \tag{2.6.16}$$

as a requirement for the existence of a solution to (2.6.15).

To apply the above to the solutions $U_1(+1)$ and $U_1(-1)$, corrections must be made in equation (2.6.16) to take account of the inhomogeneous continuity conditions (2.5.10) and (2.5.12). If the components of the vector B in equation (2.6.14) are not continuous, then the equation becomes

$$\langle M_o^* A, B \rangle = \langle A, M_o B \rangle + \bar{a}_1 [b_4] + \bar{a}_4 [b_1], \tag{2.6.17}$$

where the brackets indicate the jump in the quantity across the discontinuity at x=1.

The solutions to the inhomogeneous equations (2.5.3) and (2.5.4) with jump conditions given by equations (2.5.10) and (2.5.12) exist only if

$$\langle U_o^*(+1), -i(\omega_1 L + k_1 P) a_{+1} U_o(+1) + \tfrac{1}{2} N(-1) a_{-1} U_o(-1) \rangle - i u^*(1)[p_1(+1)] + p^*(1)[u_1(+1)] = 0, \tag{2.6.18}$$

$$\langle U_o^*(-1), -i(\omega_1 L + k_1 P) a_{-1} U_o(-1) + \tfrac{1}{2} \bar{N}(+1) a_{+1} U_o(+1) \rangle + i u^*(1)[p_1(-1)] + p^*(1)[u_1(-1)] = 0. \tag{2.6.19}$$

Introduce the notation

$$L_{11} = \langle U_o^*(+1), L U_o(+1) \rangle, \tag{2.6.20}$$

$$P_{11} = \langle U_o^*(+1), P U_o(+1) \rangle, \tag{2.6.21}$$

$$i N_{-11} = \langle U_o^*(+1), N(-1) U_o(-1) \rangle, \tag{2.6.22}$$

$$i B_{-11} = \left(-i u^*(1) [p_1(+1)] + p^*(1) [u_1(+1)] \right) / a_{-1} . \tag{2.6.23}$$

Substituting the form for $[p_1(+1)]$ and $[u_1(+1)]$ given in equations (2.5.10) and (2.5.12) allows B_{-11} to be written

$$B_{-11} = \tfrac{1}{2} A \Big\{ \left(1 + k_o \tfrac{K_0(k_o)}{K_1(k_o)}\right)\left(p^*(1) - u^*(1)\right) p(1) + \left(3 + \Omega'(1)\right)\left(p^*(1) + u^*(1)\right) u(1) + \Omega'(1) u^*(1) u(1) \Big\}. \tag{2.6.24}$$

Equation (2.6.18) can be written in terms of the quantities defined above as

$$-i\left(\omega_1 L_{11} + k_1 P_{11}\right) a_{+1} + i\left(\tfrac{1}{2} N_{-11} + B_{-11}\right) a_{-1} = 0 . \tag{2.6.25}$$

The symmetries in the matrices are used to write equation (2.6.19) in terms of the quantities defined for equation (2.6.18). This gives

$$-i\left(\omega_1 L_{11} - k_1 P_{11}\right) a_{-1} - i\left(\tfrac{1}{2} N_{-11} + B_{-11}\right) a_{+1} = 0 . \tag{2.6.26}$$

Eliminating a_{+1} and a_{-1} in the above gives

$$\omega_1^2 = k_1^2 Q^2 - R^2, \tag{2.6.27}$$

where

$$Q = P_{11}/L_{11} \quad , \tag{2.6.28}$$

$$R = (\tfrac{1}{2}N_{-11} + B_{-11})/L_{-11} \, . \tag{2.6.29}$$

For continuous distributions of vorticity B_{-11} is zero and the coefficients above are those given by Moore and Saffman (1975).

The maximum growth rate is given by $\varepsilon|R|$ for helical waves with axial wave number k_0.

2.7 Uniform Core Result

For the vortex core with constant vorticity the velocity field $(\bar{u}_1, \bar{v}_0 + \bar{v}_1, 0)$ is described at the end of Section 2.2. Using this form for the undisturbed vortex, the disturbance velocities and adjoint solution can be evaluated in terms of Bessel functions, giving an implicit equation for the critical wave number k_0 and giving the frequency ω_1 in terms of integrals of these functions.

To determine the forms of $U_0(+1)$ for $x < 1$, the form of the rotation and vorticity, $\Omega(x) = 1$ and $\Delta(x) = 2$, are substituted into equations (2.4.4) and (2.4.5) and the equations combined to give

$$\frac{d^2\hat{p}}{dx^2} + \frac{1}{x}\frac{d\hat{p}}{dx} + \left(3k_0^2 - \frac{1}{x^2}\right)\hat{p} = 0 \, , \tag{2.7.1}$$

where $\hat{p}$ is the scaled pressure from equation (2.4.6). The constraint on the behavior of $\hat{p}$ at the origin given by equation (2.4.11) determines the solution to (2.7.1) to be

$$\hat{p}(x) = \frac{-2}{\sqrt{3}k_0} J_1(\sqrt{3}k_0 x) \, , \tag{2.7.2}$$

where J_1 is a Bessel function. The components of $U_0(+1)$ follow from $\hat{p}$ to give

$$U_{o(+1)} = \frac{2}{\sqrt{3}k_o}\begin{pmatrix} \frac{i}{3}(\sqrt{3}\,k_o J_o + \frac{1}{x}J_1) \\ -\frac{1}{3}(2\sqrt{3}k_o J_o - \frac{1}{x}J_1) \\ k_o J_1 \\ -J_1 \end{pmatrix}. \qquad (2.7.3)$$

The argument of the Bessel functions is $\sqrt{3}\,k_o x$ in the above. The form of $U_0(+1)$ for $x > 1$ is given by equations (2.4.13) and (2.4.21). The conditions of continuity for the radial velocity and pressure at the core boundary give the relation for the wave number k_o as

$$\frac{2}{k_o} + 3\frac{K_o(k_o)}{K_1(k_o)} - \sqrt{3}\,\frac{J_o(\sqrt{3}k_o)}{J_1(\sqrt{3}k_o)} = 0\ . \qquad (2.7.4)$$

The positive real roots of this equation $k_o^{(m)}$ lie in the intervals in which J_o/J_1 decrease from infinity to zero

$$j_{1,m}/\sqrt{3} < k_o^{(m)} < j_{0,m+1}/\sqrt{3} \quad ; \quad m = 1,2,\cdots\ , \qquad (2.7.5)$$

where $j_{0,m}$ and $j_{1,m}$ are the m^{th} largest positive roots of J_o and J_1. The larger roots correspond to more internal structure in the disturbances. The smallest five positive values for k_o are given in Table 2.1.

The solution to the adjoint problem is needed in order to find R and Q. The differential equations (2.6.5) and (2.6.6) can be combined to form the single equation

$$\frac{d^2}{dx^2}\left(\frac{1}{x}\hat{p}^*\right) + \frac{1}{x}\frac{d}{dx}\left(\frac{1}{x}\hat{p}^*\right) + \left(3k_o^2 - \frac{1}{x^2}\right)\frac{1}{x}\hat{p}^* = 0. \qquad (2.7.6)$$

The solution for $\hat{p}^*$ asymptotic to $-x^2$ as x tends to zero is

$$\hat{p}^*(x) = -\frac{2}{\sqrt{3}k_o} x J_1(\sqrt{3}k_o x). \tag{2.7.7}$$

The components of $U_0^*(+1)$ are determined from the relations given in Section 2.6. For the region $x < 1$, the adjoint solution can be written

$$U_o^*(+1) = x U_o(+1), \tag{2.7.8}$$

where $U_0(+1)$ is given in equation (2.7.3). Outside the core the solution $U_0^*(+1)$ is given by equations (2.6.12) and (2.6.13) and the relation given above does not hold.

To calculate the growth rates the integrals L_{11}, P_{11} and N_{-11} given by equations (2.6.20), (2.6.21) and (2.6.22) need to be evaluated. In terms of the components of $U_0(+1)$ and $U_0^*(+1)$, L_{11} and P_{11} can be written

$$L_{11} = \int_o^\infty (u^*u + v^*v + w^*w)\, dx, \tag{2.7.9}$$

$$P_{11} = \int_o^\infty (w^*p + p^*w)\, dx. \tag{2.7.10}$$

The integrands can be written as combinations of Bessel functions by substituting the explicit forms of the components given by equations (2.4.13), (2.6.12), (2.7.3) and (2.7.8). Then the integrals become

$$L_{11} = \frac{4}{27k_o^2}\left\{ \int_o^1 (15k_o^2 x J_o^2 + 2\sqrt{3}k_o J_o J_1 + x\left(\frac{2}{x^2} + 9k_o^2\right) J_1^2)\, dx + \left(\frac{k_o J_1(\sqrt{3}k_o)}{K_1(k_o)}\right)^2 \int_1^\infty x^3 (K_o^2 + K_1^2)\, dx \right\}, \tag{2.7.11}$$

$$P_{11} = -\frac{8}{2k_o^2}\left\{ \int_o^1 x J_1^2\, dx + \left(\frac{J_1(\sqrt{3}k_o)}{K_1(k_o)}\right)^2 \int_1^\infty x K_1^2\, dx \right\}, \tag{2.7.12}$$

where the argument of J_0 and J_1 is $\sqrt{3}\, k_0 x$, and of K_0 and K_1 is $k_0 x$.

The form of the integral N_{-11} in terms of the vector components is

$$\begin{aligned} N_{-11} = \int_0^1 & \left(-u^*(4u + 2xu') + v^*(4u + 2xv') - w^*(2w + 2xw')\right) dx \\ & + \int_1^\infty \Big\{ -u^*\left(2(1 - 3/x^4)u + (1 - 1/x^4)xu' - 4v/x^4\right) \\ & \quad + v^*\left(2(1 + 1/x^4)u + 2v/x^4 + (1 + 1/x^4)xv'\right) \\ & \quad + w^*\left((1 - 1/x^4)w + (1 + 1/x^4)xw'\right) \Big\} dx . \end{aligned} \tag{2.7.13}$$

Instead of substituting the forms of $U_0(+1)$ and $U_0^*(+1)$ into the above and attempting to simplify the resulting expression for the numerical integration, the components and derivatives are computed and the algebra is done numerically in the integration scheme.

The integration on $0 < x < 1$ is carried out using Simpson's rule, subdividing the interval until the error estimate is less than 5×10^{-5}. Since the modified Bessel functions decrease exponentially to zero for large arguments, the value of the integral for x from one to infinity depends strongly on the contribution of the integrand near x=1. The integration is done on intervals of length 5 until the correction is not significant.

The resulting values of R and Q for the first five wave numbers are given in Table 2.1:

k_0	R	Q
2.505	1.142	.266
4.35	1.139	.162
6.17	1.136	.116
7.99	1.134	.091
9.81	1.133	.074

Table 2.1 Values of R and Q for the first five critical wave numbers for the uniform core vortex

For very large wave numbers the integrals defining R and Q can be approximated to check the numerical results. For large m the asymptotic form of equations (2.7.5) and (2.7.4) defining $k_o^{(m)}$ give

$$J_o(\sqrt{3}\,k_o)/J_1(\sqrt{3}\,k_o) = \sqrt{3}\,. \tag{2.7.14}$$

Substituting the asymptotic behavior for J_0 and J_1 into the above gives

$$k_o^{(m)} \sim \frac{\pi}{\sqrt{3}}\left(m+\tfrac{5}{12}\right) \qquad \text{for large } m. \tag{2.7.15}$$

For these values of k_0 the asymptotic form for the integrals in equations (2.7.11), (2.7.12) and (2.7.13) can be evaluated to give

$$L_{11} \sim \frac{32}{9\sqrt{3}\,\pi\,k_o} \qquad \text{as } k_o \to \infty, \tag{2.7.16}$$

$$P_{11} \sim -\frac{8}{3\sqrt{3}\,\pi\,k_o^2} \qquad \text{as } k_o \to \infty, \tag{2.7.17}$$

$$N_{-11} \sim -\frac{16}{3\sqrt{3}\,\pi\,k_o} \qquad \text{as } k_o \to \infty. \tag{2.7.18}$$

The asymptotic form of B_{-11} is determined from equation (2.6.24) and the components of $U_0(+1)$ and $U_0^*(+1)$ to be

$$B_{-11} \sim \frac{-4}{3\sqrt{3}\,\pi\,k_o} \qquad \text{as } k_o \to \infty. \tag{2.7.19}$$

The values of Q and R for large wave numbers, found by substituting the above into equations (2.6.28) and (2.6.29) are

$$Q \sim 3/4k_o \qquad \text{as } k_o \to \infty, \tag{2.7.20}$$

$$R \sim 9/8 = 1.125 \quad \text{as } k_o \to \infty. \tag{2.7.21}$$

These values can be compared with those given in Table 2.1 with good agreement. Also, they indicate that even though the growth rate is largest for the smallest positive wave number, it decreases by only two percent over the range of critical wave numbers.

2.8 General Distribution of Vorticity in the Core

The analysis in Sections 2.2 through 2.6 is for an axisymmetric distribution of vorticity in the core, given by

$$\Delta(x) = \frac{1}{x}\frac{d}{dx}\left(x^2\Omega(x)\right), \tag{2.2.5}$$

which is bounded at the origin and decreasing outwards. A numerical algorithm for evaluating the wave number k_0 and the corresponding factors R and Q in the expression for the frequency follows from this analysis once $\Omega(x)$ is given. The numerical eigenvalue problem for k_0 reduces to finding the roots of equation (2.4.22), where the values of u and $\hat{p}$ at x=1 are determined by integrating the differential equations (2.4.4) and (2.4.5).

The values for R and Q depend on integrals over both the core and outer regions. The contribution to these integrals in the core can be evaluated by solving the initial value problem defined by the system

$$\frac{dq}{dx} = h, \tag{2.8.1}$$

$$\frac{dh}{dx} = -\frac{1}{x}h + \left(\frac{1}{x\Omega}(3\Omega' + x\Omega'') + 4/x^2\right)q, \tag{2.8.2}$$

$$\frac{du}{dx} = \frac{1}{x}\left(\frac{\Delta}{\Omega} - 1\right)u + \left(k_0^2 + 1/x^2\right)\hat{p}, \tag{2.8.3}$$

$$\frac{d\hat{p}}{dx} = \left(1 - 2\frac{\Delta}{\Omega}\right)u - \frac{1}{x}\frac{\Delta}{\Omega}\hat{p}, \tag{2.8.4}$$

$$\frac{du^*}{dx} = \frac{2}{x}u^* + (k_o^2 + 1/x^2)\hat{P}^*, \tag{2.8.5}$$

$$\frac{d\hat{P}^*}{dx} = (1-2\frac{\Delta}{\Omega})u^* + \frac{1}{x}(3-2\frac{\Delta}{\Omega})\hat{P}^*, \tag{2.8.6}$$

$$\frac{d\hat{L}}{dx} = u^*u + (2u^* + \frac{1}{x}\hat{P}^*)(\frac{\Delta}{\Omega}u + \frac{1}{x}\hat{P}) + k_o^2\hat{P}^*\hat{P}, \tag{2.8.7}$$

$$\frac{d\hat{P}}{dx} = -2k_o\Omega\hat{P}^*\hat{P}, \tag{2.8.8}$$

$$\frac{d\hat{N}}{dx} = -u^*((3xg'-2g)u/2x^2 + \frac{1}{x}gu' + (xg'-2g)v/x^2) + v^*((xg''+g')u/2x - (xg'-2g)v/2x^2 + \frac{1}{x}gv') + k_o^2\hat{P}^*(g'\hat{P} + 2g\hat{P}')/2x, \tag{2.8.9}$$

where v and v* are given by equations (2.4.8) and (2.6.8). The initial values come from the behavior of the functions near x=0. A small value of x is used as the initial value and the integration carried to x=1. The exact form of the initial values is discussed in greater detail in the next section.

The value of the constant a_0 is determined from g(1) and g'(1) according to equation (2.2.27). The contribution of the core region to the integrals L_{11}, P_{11} and N_{-11} are given by $\hat{L}(1)$, $\hat{P}(1)$ and $a_0\hat{N}(1)$.

The contribution to the integrals from x > 1 can be written explicitly in terms of the matrices and vectors from Section 2.6, giving definite integrals of Bessel functions. If these are denoted as L_{11}^o, P_{11}^o and N_{-11}^o, then they have the form

$$L_{11}^o = \frac{\hat{P}^{(1)}\hat{P}^{*(1)}}{k_o^2 K_1^2(k_o)} F(k_o), \tag{2.8.10}$$

$$P_{11}^o = -2\frac{\hat{P}^{(1)}\hat{P}^{*(1)}}{k_o K_1^2(k_o)} G(k_o), \tag{2.8.11}$$

$$N_{-11}^o = \frac{\hat{P}^{(1)}\hat{P}^{*(1)}}{K_1^2(k_o)}\left(\frac{1}{k_o^2}H_1(k_o) + a_1 k_o^2 H_2(k_o)\right), \tag{2.8.12}$$

where a_1, $\hat{p}(1)$ and $\hat{p}^*(1)$ are determined from the core solution. The constant a_1 is given in equation (2.2.28). The functions of the wave number have the form

$$F(k_o) = \int_{k_o}^{\infty} x^3 \left(K_o^2(x) + K_1^2(x) \right) dx \,, \tag{2.8.13}$$

$$G(k_o) = \int_{k_o}^{\infty} x\, K_1^2(x)\, dx \,, \tag{2.8.14}$$

$$H_1(k_o) = \int_{k_o}^{\infty} \left(3x K_o^2 + 2(1-x^2) K_o K_1 - x K_1^2 \right) x^2 dx \,, \tag{2.8.15}$$

$$H_2(k_o) = \int_{k_o}^{\infty} \left(3x^2 K_o^2 + 2x(5+x^2) K_o K_1 + (8+3x^2) K_1^2 \right) \frac{dx}{x^2} \,. \tag{2.8.16}$$

These integrals can be evaluated using the same methods as in the uniform core problem.

The factors R and Q are determined by the combination of the integrals,

$$L_{11} = \hat{L}(1) + L_{11}^{o} \,, \tag{2.8.17}$$

$$P_{11} = \hat{P}(1) + P_{11}^{o} \,, \tag{2.8.18}$$

$$N_{-11} = \hat{N}_{-11}(1) + N_{-11}^{o} \,, \tag{2.8.19}$$

and the boundary terms B_{-11} defined by equation (2.6.24). The numerical problem is straightforward and a relevant example is discussed in the next section.

2.9 Viscous Core Model

Saffman (1977) demonstrates that the rotation profile for the core of vortex rings can be approximated under certain conditions by

$$\Omega(x) = M(3/4; 2; -x^2/\varepsilon_1^2) \,/\, M(3/4; 2; -1/\varepsilon_1^2), \qquad (2.9.1)$$

where M is the confluent hypergeometric function. Since the parameter ε_1^2 is proportional to the inverse of the Reynolds number, this profile may give some insight to the effect of Reynolds number on the vortex ring instability.

The properties of the confluent hypergeometric function are taken from Abramowitz and Stegun (1965). For large ε_1 the core profile approaches the uniform profile discussed in Section 2.7. For small ε_1 the swirl velocity, $\bar{v}_o = x\Omega(x)$, increases from zero to a maximum of $\bar{v}_o = .69\varepsilon_1^{-1/2}$ at $x = 1.45\varepsilon_o$, then decreases to $\bar{v}_o = 1$ at $x=1$. This behavior for small ε_1 must be considered in the numerical scheme to maintain accuracy as ε_1 is decreased. The step size and starting point in the integration of equations (2.8.1) through (2.8.9) must be adjusted as ε_1 is varied. The initial values are defined earlier by using the behavior of the solutions for small x as an approximate at some small starting point x_o. If x_o is taken too small, roundoff errors will be large. More terms in the expansions of the solutions near the origin can be calculated to allow for larger values of x_o.

The behavior of $\Omega(x)$ and $\Delta(x)$ near the origin follows from the series expansion of the confluent hypergeometric function

$$M(3/4; 2; -x^2/\varepsilon_1^2) = 1 - \frac{3x^2}{8\varepsilon_1^2} + O\left(\left(\frac{x}{\varepsilon_1}\right)^4\right). \qquad (2.9.2)$$

Substituting into equations (2.9.1) and (2.2.5), the expansion for Ω and

the ratio Δ/Ω can be written

$$\Omega(x) = \Omega(0)\left(1 - \frac{3x^2}{8\varepsilon_1^2} + O\left(\left(\frac{x}{\varepsilon_1}\right)^4\right)\right), \tag{2.9.3}$$

$$\frac{\Delta(x)}{\Omega(x)} = 2 - \frac{3x^2}{4\varepsilon_1^2} + O\left(\left(\frac{x}{\varepsilon_1}\right)^4\right). \tag{2.9.4}$$

The second term in the initial behavior of each of the unknowns in the system of equations (2.8.1) through (2.8.9) follows directly once given the form above for the rotation. The resulting two-term expansions near the origin are

$$g(x) \sim x^2\left(1 - x^2/4\varepsilon_1^2\right), \tag{2.9.5}$$

$$h(x) \equiv g'(x) \sim x\left(2 - x^2/\varepsilon_1^2\right), \tag{2.9.6}$$

$$u(x) \sim 1 - \left(\frac{5k_0^2}{8} + \frac{3}{8\varepsilon_1^2}\right)x^2, \tag{2.9.7}$$

$$\hat{p}(x) \sim x\left(-1 + \left(3k_0^2/8 + 3/8\varepsilon_1^2\right)x^2\right), \tag{2.9.8}$$

$$u^*(x) \sim x\left(1 - \frac{5k_0^2}{8}x^2\right), \tag{2.9.9}$$

$$\hat{p}^*(x) \sim x^2\left(-1 + \frac{3k_0^2}{8}x^2\right), \tag{2.9.10}$$

$$\hat{L}(x) \sim x^2\left(1 - \left(k_0^2/2 + 3/16\varepsilon_1^2\right)x^2\right), \tag{2.9.11}$$

$$\hat{P}(x) \sim -k_0^2/2\,\Omega(0)\,x^4\left(1 - \left(k_0^2/2 + 1/4\varepsilon_1^2\right)x^2\right), \tag{2.9.12}$$

$$\hat{N}(x) \sim x\left(-2 + \left(k_0^2/8 + 3/4\varepsilon_1^2\right)x^2\right). \tag{2.9.13}$$

At the starting point x_0 the relative error in the initial values above is $O((x_0/\varepsilon_1)^4)$. This estimate can help in the choice of the starting point.

The chord method is used to determine the first few critical wave numbers, the roots of equation (2.4.22). For each iterate the values of $\hat{p}(1)$ and $u(1)$ are determined by integrating equations (2.8.3) and (2.8.4)

from the initial values given by equations (2.9.7) and (2.9.8) at the point x_0. The value of x_0 is set at 1/128 for larger ε_1 and decreased by powers of 1/2 to maintain the ratio x_0/ε_1 at less than .04 . The predictor-corrector scheme described in Section 1.7 is used with the step size set at the value for x_0. For small ε_1 the step size is increased outside the region in which $x\Omega(x)$ varies rapidly. The resulting values of the first three critical wave numbers are given in Table 2.2.

The procedure for calculating the contribution to the corresponding values of R and Q from the core is the same as described above for finding $\hat{p}(1)$ and $u(1)$ except that the system has 9 equations instead of 2. The values $\hat{L}(1)$, $\hat{P}(1)$, $\hat{N}(1)$, $\hat{p}(1)$ and $\hat{p}^*(1)$, along with the constants a_0, a_1 and A determined by $g(1)$ and $g'(1)$, are used in the expressions for L_{11}, P_{11} and N_{-11}. The remaining contributions to R and Q are given by the functions F, G, H_1 and H_2 defined by equations (2.8.13) through (2.8.16). These depend only on the value of the critical wave number. The resulting computed values of R and Q are given in Table 2.2.

Notice that the values for R and Q for large ε_1 are identical to those in the uniform core calculation, as expected.

ε_1	$k_o^{(1)}$	R_1	Q_1	$k_o^{(2)}$	R_2	Q_2	$k_o^{(3)}$	R_3	Q_3
100	2.51	1.142	.266	4.35	1.139	.162	6.17	1.136	.116
5.0	2.51	1.145	.267	4.36	1.143	.162	6.20	1.140	.117
1.0	2.73	1.220	.270	4.76	1.217	.169	6.75	1.213	.123
0.9	2.79	1.234	.269	4.86	1.231	.170	6.89	1.227	.124
0.8	2.88	1.252	.268	5.01	1.248	.169	7.10	1.245	.124
0.7	3.01	1.274	.264	5.23	1.271	.168	7.40	1.267	.123
0.6	3.21	1.303	.257	5.57	1.300	.163	7.86	1.297	.119
0.5	3.53	1.341	.249	6.12	1.340	.152	8.62	1.338	.111
0.4	4.08	1.392	.223	7.05	1.397	.130	9.91	1.396	.092
0.3	5.04	1.465	.183	8.69	1.475	.194	12.16	1.476	.061
0.2	6.96	1.563	.116	11.91	1.566	.045	16.47	1.558	.026
0.1	12.48	1.670	.034	20.49	1.646	.0087	18.03	1.623	.0057
.075	15.99	1.695	.0181	25.65	1.664	.0045	35.35	1.638	.0031
0.05	22.72	1.718	.0070	35.40	1.684	.0018	49.47	1.653	.0012

Table 2.2 The values of the first three critical wave numbers k_o denoted as $k_o^{(1)}$, $k_o^{(2)}$ and $k_o^{(3)}$ and the values of R and Q subscripted corresponding to the wave numbers.

CHAPTER 3

UNIFORM VORTEX IN A UNIFORM SIMPLE SHEAR FLOW

3.1 Introduction

The mathematical method described in Chapter 2 for the strained vortex allows easy examination of a range of problems involving small, two-dimensional deformations of a vortex filament. Only the matrices on the right side of equation (2.3.4) and the interface conditions need be changed. The form of these matrices and conditions depend on the deformation to that flow field due to the straight vortex filament alone.

The external deformation examined in this chapter is that due to a simple shear. This flow may give insight into the behavior of short waves on the trailing vortices behind aircraft near the ground, where the crosswinds approximate a pure shear flow. Also, since the shear flow is rotational, the form of the corrected frequency is expected to show some differences from that for the straining field.

Moore and Saffman (1971) calculate the shape of the uniform vortex filament in a simple shear and find that a solution exists for the vortex cross-section of an ellipse when the shear σ is sufficiently small. They also investigate the stability to two-dimensional disturbances. The three-dimensional stability can be examined by expanding the exact solution in the ratio of the shear σ to the constant vorticity in the filament to give the corrections to the vortex flow due to the shear. In this case it is easier to calculate the corrections to the velocity field of the vortex due to the shear flow from the governing equations.

3.2 Steady Deformation of the Vortex Filament

For the vortex filament along the z axis in the cylindrical coordinate system (r,θ,z), the steady flow field does not vary in the axial direction. The magnitude of the uniform vorticity is taken to be 2 and the core radius to be 1, and the stream function of the vortex filament without the imposed shear then has the form

$$\psi_0 = \begin{cases} -\frac{1}{2}r^2 & \text{for } r<1, \\ -\log r & \text{for } r>1, \end{cases} \tag{3.2.1}$$

where the stream function is defined in the usual sense by

$$u = \frac{1}{r}\frac{\partial \psi}{\partial \theta}, \tag{3.2.2}$$

$$v = -\frac{\partial \psi}{\partial r}, \tag{3.2.3}$$

and u and v are the radial and azimuthal velocities.

The correction to the stream function due to the shear is denoted $\varepsilon\psi_1$, where the magnitude of ε is the ratio of the shear to the vorticity in the uniform core and the sign is chosen to have positive ε correspond to the shear rotation in a positive sense. Far from the vortex the total stream function has the form

$$\psi_0 + \varepsilon\psi_1 \sim -\frac{\varepsilon}{2}r^2(1-\cos(2\theta)) - \log r \quad \text{as } r\to\infty. \tag{3.2.4}$$

The angular dependence shows that the appropriate form for the steady deformation to the interface between the vortex core and surrounding fluid is

$$r = R(\theta) \equiv 1 + \varepsilon A \cos(2\theta),$$

where A is determined by the conditions at the interface, and only $O(\varepsilon)$ corrections are retained.

In the core the total stream function must satisfy

$$\nabla^2 (\psi_0 + \varepsilon \psi_1) = -2 \qquad \text{for} \quad r < R(\theta), \tag{3.2.5}$$

$$\psi_0 + \varepsilon \psi_1 = 0 \qquad \text{on} \quad r = R(\theta) \tag{3.2.6}$$

and $\psi_0 + \varepsilon\psi_1$ must be regular at the origin. The solution with the appropriate angular dependence can be written

$$\psi_0 + \varepsilon \psi_1 = -\tfrac{1}{2} \left(r^2 - a^2 - 2\varepsilon r^2 A \cos(2\theta) \right) \quad \text{for } r < R. \tag{3.2.7}$$

Outside the core the stream function must satisfy

$$\nabla^2 (\psi_0 + \varepsilon \psi_1) = -2\varepsilon \qquad \text{for} \quad r < R(\theta) \tag{3.2.8}$$

and the boundary conditions given by equations (3.2.4) and (3.2.6). The tangential velocities must be continuous across the surface $r = R(\theta)$ giving an additional constraint that

$$\frac{\partial}{\partial r} (\psi_0 + \varepsilon \psi_1) = -1 + \varepsilon A \cos(2\theta) \qquad \text{on } r = R(\theta). \tag{3.2.9}$$

The right hand side of this equation follows from the form of the stream function in the core given by equation (3.2.7). The solution to equation (3.2.8) satisfying the asymptotic condition (3.2.4) and the continuity

condition (3.2.9) can be written

$$\psi_0 + \varepsilon\psi_1 = -(1-\varepsilon)\log r - \tfrac{1}{2}\varepsilon\left[r^2 - 1 - (r^2 + \tfrac{1}{r^2})\cos(2\theta)\right] \quad \text{for } r > R. \tag{3.2.10}$$

The constraint (3.2.6) that $\psi_0 + \varepsilon\psi_1$ be zero on $r = R$ forces the constant A to be 1, so that

$$R(\theta) = 1 + \varepsilon\cos(2\theta). \tag{3.2.11}$$

The steady velocity field determined by the stream function from equation (3.2.2) and (3.2.3) is of the form $(\varepsilon\bar{u}_1, \bar{v}_0 + \varepsilon\bar{v}_1, 0)$, where

$$V_0 = \begin{cases} r & \text{for } r < R(\theta), \\ 1/r & \text{for } r > R(\theta), \end{cases} \tag{3.2.12}$$

$$u_1 = \begin{cases} -2r\sin(2\theta) & \text{for } r < R(\theta), \\ -\frac{1}{r}(r^2 + 1/r^2)\sin(2\theta) & \text{for } r > R(\theta), \end{cases} \tag{3.2.13}$$

$$V_1 = \begin{cases} -2r\cos(2\theta) & \text{for } r < R(\theta), \\ \frac{1}{r}(r^2 - 1 - (r^2 - 1/r^2)\cos(2\theta) & \text{for } r > R(\theta). \end{cases} \tag{3.2.14}$$

The stability of this steady flow field is examined in the next section.

3.3 Stability Equations

The same notation as in Section 2.3 is employed. The disturbance velocities $(\tilde{u},\tilde{v},\tilde{w})$ and pressure $\tilde{p}$ are added to the steady solutions and the resulting disturbed velocity and pressure field is required to satisfy the Euler equations, linearized in the disturbance quantities. These equations are then written concisely by defining the vector

$$U = \begin{pmatrix} \tilde{u} \\ \tilde{v} \\ \tilde{w} \\ \tilde{p} \end{pmatrix} \tag{3.3.1}$$

to give the equation,

$$\frac{\partial}{\partial t}(LU) + MU = \epsilon\left(T + \tfrac{1}{2}e^{2i\theta}N + \tfrac{1}{2}e^{-2i\theta}\bar{N}\right)U, \tag{3.3.2}$$

where L, M, T, N and $\bar{N}$ are matrices defined by

$$L = \begin{pmatrix} 1 & 0 & 0 & 0 \\ 0 & 1 & 0 & 0 \\ 0 & 0 & 1 & 0 \\ 0 & 0 & 0 & 0 \end{pmatrix}, \tag{3.3.3}$$

$$M = \begin{pmatrix} \frac{1}{r}\bar{V}_o\frac{\partial}{\partial\theta} & -\frac{2}{r}\bar{V}_o & 0 & \partial/\partial r \\ \frac{d\bar{V}_o}{dr} + \frac{1}{r}\bar{V}_o & \frac{1}{r}\bar{V}_o\frac{\partial}{\partial\theta} & 0 & \frac{1}{r}\partial/\partial\theta \\ 0 & 0 & \frac{1}{r}\bar{V}_o\frac{\partial}{\partial\theta} & \partial/\partial z \\ \frac{\partial}{\partial r} + \frac{1}{r} & \frac{1}{r}\partial/\partial\theta & \partial/\partial z & 0 \end{pmatrix}, \tag{3.3.4}$$

$$T = \begin{cases} (0) & \text{for } r < R(\theta), \\ \begin{pmatrix} -(1-1/r^2)\frac{\partial}{\partial\theta} & 2(1-1/r^2) & 0 & 0 \\ -2 & -(1-1/r^2)\partial/\partial\theta & 0 & 0 \\ 0 & 0 & -(1-1/r^2)\partial/\partial\theta & 0 \\ 0 & 0 & 0 & 0 \end{pmatrix} & \text{for } r > R(\theta), \end{cases} \tag{3.3.5}$$

$$N=\begin{cases}\begin{pmatrix} -2i\left(1+r\frac{\partial}{\partial r}\right)+2\frac{\partial}{\partial\theta} & 0 & 0 & 0 \\ 4 & 2i\left(1-r\frac{\partial}{\partial r}\right)+2\frac{\partial}{\partial\theta} & 0 & 0 \\ 0 & 0 & -2ir\frac{\partial}{\partial r}+2\frac{\partial}{\partial\theta} & 0 \\ 0 & 0 & 0 & 0 \end{pmatrix} \\ \qquad\qquad \text{for} \quad r<R(\theta), \\ \begin{pmatrix} -i\left(1-\frac{3}{r^4}+\left(1+\frac{1}{r^4}\right)r\frac{\partial}{\partial r}+\left(1-\frac{1}{r^4}\right)\frac{\partial}{\partial\theta}\right. & 0 & 0 & 0 \\ 2\left(1+\frac{1}{r^4}\right) & i\left(1-\frac{3}{r^4}-\left(1+\frac{1}{r^4}\right)r\frac{\partial}{\partial r}+\left(1-\frac{1}{r^4}\right)\frac{\partial}{\partial\theta}\right. & 0 & 0 \\ 0 & 0 & \left(-i\left(1+\frac{1}{r^4}\right)r\frac{\partial}{\partial r}\right. & 0 \\ 0 & 0 & \left.+\left(1-\frac{1}{r^4}\right)\frac{\partial}{\partial\theta}\right) & 0 \end{pmatrix} \\ \qquad\qquad \text{for} \quad r>R(\theta), \end{cases} \tag{3.3.6}$$

and $\overline{N}$ is the complex conjugate of N. Notice that the matrices M and L are identical to those in Chapter 2. The components of U must be regular at the origin and tend to zero at infinity. The total velocities, $(\overline{u}_1+\tilde{u},\ \overline{v}_0+\overline{v}_1+\tilde{v},\tilde{w})$, must be continuous across the disturbed core boundary at

$$r = R(\theta) + \tilde{\delta}. \tag{3.3.7}$$

The axial and time dependence can be separated in equation (3.3.2) and the solution written in terms of an expansion in the small parameter ε by taking the form of the solution as

$$U = (\tilde{U}_0 + \varepsilon\tilde{U}_1 + \cdots)\, e^{ikz+i\omega t}, \tag{3.3.8}$$

where

$$\omega = \omega_0 + \varepsilon\omega_1 + \cdots , \tag{3.3.9}$$

$$k = k_0 + \varepsilon k_1 + \cdots . \tag{3.3.10}$$

When these expressions are substituted into equation (2.3.2), the result can be split into a hierarchy of equations in powers of the parameter ε. The first two equations in the hierarchy are

$$(i\omega_0 L + M_0)\tilde{U}_0 = 0 , \tag{3.3.11}$$

$$(i\omega_0 L + M_0)\tilde{U}_1 = (-i\omega_1 L - ik_1 P + T + \tfrac{1}{2}(e^{2i\theta}N + e^{-2i\theta}\bar{N}))\tilde{U}_0 , \tag{3.3.12}$$

where

$$P = \begin{pmatrix} 0 & 0 & 0 & 0 \\ 0 & 0 & 0 & 0 \\ 0 & 0 & 0 & 1 \\ 0 & 0 & 1 & 0 \end{pmatrix} \tag{3.3.13}$$

and M_0 is the matrix M with $\partial/\partial z$ replaced by ik_0.

The disturbed core boundary can be expressed in a form consistent with the velocities by writing the interface position as

$$r = R(\theta) + (\delta_0 + \varepsilon\delta_1 + \cdots)e^{ikz + i\omega t} . \tag{3.3.14}$$

The deflections δ_0 and δ_1 are functions only of θ.

The condition that the total velocities and pressure be continuous across the core boundary gives constraints on the jumps in the values of the disturbance quantities across that surface. To lowest

order in ε, the radial and axial disturbance velocities and the disturbance pressure are continuous across the interface. This condition on the components of U_0, along with equation (3.3.11), gives the same lowest order problem as in Chapter 2. The solutions in the normal azimuthal modes are the stable Kelvin waves on a uniform cylindrical vortex, given by Kelvin (1880). The frequency ω_0 is determined by the axial wave number n. (The expression for ω_0 was derived for n = 0 in Section 1.8 using a different notation.) The Kelvin wave frequencies are the roots of the equation

$$\frac{K_n'(k_0)}{K_n(k_0)} + \frac{1}{\lambda}\frac{J_n'(\lambda k_0)}{J_n(\lambda k_0)} + \frac{2n}{k_0\lambda^2(\omega_0+n)} = 0, \qquad (3.3.15)$$

where

$$\lambda^2 = \frac{4}{(\omega_0+n)^2} - 1 \qquad (3.3.16)$$

and primes indicate differentiation with respect to the argument. Denote the solution to the above for a given k_0 and n as $\omega(k_0,n)$ and the corresponding solution for the velocities and pressure by $U_0(n)e^{in\theta}$, then the expression for $U_0(n)$ within an arbitrary multiplicative constant is

$$U_0(n) = \begin{cases} \begin{pmatrix} i\left(\frac{1}{\lambda} J_n'(\lambda k_0 r) + \frac{2n}{\lambda^2 k_0(\omega_0+n)r} J_n(\lambda k_0 r)\right) \\ -\frac{2}{\lambda(\omega_0+n)} J_n'(\lambda k_0 r) - \frac{n}{\lambda^2 k_0 r} J_n(\lambda k_0 r) \\ J_n(\lambda k_0 r) \\ -\frac{1}{k_0}(\omega_0+n) J_n(\lambda k_0 r) \end{pmatrix} & \text{for } r<1, \\ \frac{J_n(\lambda k_0)}{K_n(k_0)} \begin{pmatrix} -i K_n'(k_0 r) \\ \frac{n}{k_0 r} K_n(k_0 r) \\ K_n(k_0 r) \\ -\frac{1}{n}(\omega_0 + \frac{n}{r^2}) K_n(k_0 r) \end{pmatrix} & \text{for } r>1. \end{cases} \tag{3.3.17}$$

3.4 Effect of the Shear

For the lowest order solution consisting of a single azimuthal mode, the correction due to the shear has the form

$$\tilde{U}_1 = \left(e^{2i\theta} U_{1(n+2)} + U_{1(n)} + e^{-2i\theta} U_{1(n-2)}\right) e^{in\theta} \tag{3.4.1}$$

and satisfies the equations

$$\left(i\omega_0 L + M_{0(n+2)}\right) U_{1(n+2)} = \tfrac{1}{2} N_{(n)} U_{0(n)}, \tag{3.4.2}$$

$$\left(i\omega_0 L + M_{0(n)}\right) U_{1(n)} = \left(-i\omega_1 L - ik_1 P + T\right) U_{0(n)}, \tag{3.4.3}$$

$$\left(i\omega_0 L + M_{0(n-2)}\right) U_{1(n-2)} = \tfrac{1}{2} \bar{N}_{(n)} U_{0(n)}, \tag{3.4.4}$$

where $M_0(n)$ and $N(n)$ are the matrices M_0 and N with the $\partial/\partial\theta$ replaced by in. Equations (3.4.2) and (3.4.4) with the appropriate boundary conditions have unique solutions when ω_0 does not also satisfy the dispersion relation for the n+2 or n-2 azimuthal mode. Equation (3.4.3) has a solution only when the right hand side of the equation satisfies the constraint discussed in Section 2.6; that is, the Fredholm alternative is applied. This gives ω_1 directly as

$$\omega_1 = -i \frac{\langle U_0^{*(n)}, T U_0^{(n)} \rangle}{\langle U_0^{*(n)}, L U_0^{(n)} \rangle} , \tag{3.4.5}$$

where k_1 has been taken to be zero and no boundary terms appear. From the form of U_0, U_0^* and T, it can be shown that equation (3.4.5) is real. Thus shear does not destabilize in this case.

The argument fails when ω_0 takes values which yield homogeneous solutions for both n and n±2. In the last chapter steady helical waves were shown to exist as superpositions of the n=+1 and n=-1 modes. These correspond to the critical wave numbers $k_0^{(m)}$ for which $\omega_0 = 0$. In this case it is necessary to take $\tilde{U}_0$ of the form

$$\tilde{U}_0 = a_{+1} U_0^{(+1)} e^{i\theta} + a_{-1} U_0^{(-1)} e^{-i\theta} \tag{3.4.6}$$

and examine the solutions for the correction $\tilde{U}_1$ of the form

$$\tilde{U}_1 = U_1^{(+3)} e^{3i\theta} + U_1^{(+1)} e^{i\theta} + U_1^{(-1)} e^{-i\theta} + U_1^{(-3)} e^{-3i\theta} . \tag{3.4.7}$$

Substituting these into equation (3.3.12) and separating in the angular dependence, the two equations for which nontrivial solutions of the

homogeneous equations exist are

$$M_0(+1)U_1(+1) = a_{+1}(-i\omega_1 L - ik_1 P + T)U_0(+1) + \tfrac{1}{2}N(-1)\,a_{-1}U_0(-1), \quad (3.4.8)$$

$$M_0(-1)U_1(-1) = a_{-1}(-i\omega_1 L - ik_1 P + T)U_0(-1) + \tfrac{1}{2}\bar{N}(-1)\,a_{+1}U_0(+1). \quad (3.4.9)$$

The forms for $U_0(+1)$, $U_0(-1)$ and the adjoint solutions $U_0^*(+1)$ and $U_0^*(-1)$ are given in Section 2.7. The orthogonality requirements given by equations (2.6.18) and (2.6.19) need a term due to the matrix T added in order to apply to the system above. Define T_{11} by

$$iT_{11} = \langle U_0(+1), TU_0(+1)\rangle \quad (3.4.10)$$

and L_{11}, P_{11}, N_{-11} and B_{-11} as in Section 2.6, then the orthogonality conditions become

$$(\omega_1 L_{11} + k_1 P_{11} - T_{11})a_{+1} - (\tfrac{1}{2}N_{-11} + B_{11})a_{-1} = 0, \quad (3.4.11)$$

$$(\omega_1 L_{11} - k_1 P_{11} + T_{11})a_{-1} + (\tfrac{1}{2}N_{-11} + B_{-11})a_{+1} = 0, \quad (3.4.12)$$

where the form of B_{-11} has to be determined. Section 2.6 gives

$$iB_{11} = \left(-iu^*(1)[p_1(+1)] + p^*(1)[u_1(+1)]\right)/a_{-1}, \quad (3.4.13)$$

where the brackets indicate the jump in the enclosed quantity across the interface. The continuity conditions give

$$[u_1(+1)] = 2i\delta_0(-1) + \tfrac{i}{2}\left[\frac{du}{dr}\right], \quad (3.4.14)$$

$$[p_1(+1)] = -\tfrac{1}{2}\left[\frac{dp}{dr}\right] , \tag{3.4.15}$$

where -iu and p are components of $U_0(-1)$, given in equations (3.3.17).

Eliminating a_{+1} and a_{-1} in the real equations (3.4.11) and (3.4.12) gives

$$\omega_1^2 = \left((T_{11} - k_1 P_{11})^2 - (\tfrac{1}{2} N_{-11} + B_{-11})^2 \right) / L_{11}^2 . \tag{3.4.16}$$

Notice that the wave number corresponding to the fastest growing wave is not exactly the one for steady waves, but slightly different. If $k_0^{(m)}$ is the critical wave number for the strained vortex, then the fastest growing waves have

$$k = k_0^{(m)} + \varepsilon \frac{T_{11}}{P_{11}} . \tag{3.4.17}$$

Hence the effect of the rotational deformation differs from the potential deformation of the strain in the shift in the wave number. The values of N_{-11} and B_{-11} are changed as well, but the shortwave instability exists in a similar fashion to the strained vortex.

CHAPTER 4

FLOW OVER A WING WITH AN ATTACHED FREE VORTEX

4.1 Introduction

It was claimed several years ago by W. Kasper that the lift on a large aspect ratio wing could be significantly increased, so that controlled flight at extremely low forward speed would be possible, by designing the wing so that there would be an extensive region of vortex flow over the upper surface. Films demonstrating the possibility were shown in 1973 by O. Sviden and W. Kasper (see Riley 1973) and a popular description of the wing has been given by Cox (1973). Sink rates were reported of 200 fpm at 30 mph and 100 fpm at 20 mph, corresponding to lift/drag ratios of L/D = 13.2 and L/D = 17.6, respectively. There is nothing unusual about such values at high speeds, but at 20-30 mph they appear remarkable, and are presumably concomitant with significant increases in the lift coefficient without corresponding change in the drag coefficient.

The fact that the vortices produced by separation at sharp leading edges can increase the lift on an airfoil is well known for delta wings and similar low aspect ratio airfoils, and there is a fairly extensive literature on vortex lift for slender wings (see, for example, Polhamus 1971). The concept of using the vortices for control has also been discussed (Landahl and Widnall 1971).

However, to the best of present knowledge there have been no calculations of a similar nature carried out for high aspect ratio wings,

to determine if a free vortex could stand over the wing and increase the lift. There have been studies of two-dimensional flow past cylinders and flat plates with a pair of counter rotating line vortices lying downstream symmetrically and at rest relative to the body. (For references and corrections of earlier errors, see Smith and Clark 1975). These calculations are relevant to the slender body theory of flow over delta wings. But although it is obvious that, particularly at high angles of attack, leading edge separation will produce vortices and increase lift on a wing of large aspect ratio, it has not been possible to find references to flow past such shapes with attached free vortices. Perhaps this obvious idea has not been explored theoretically (or work has been forgotten) because of the assumption that such flows would in practice always be associated with large values of the drag, as the flow around the vortex would not reattach to the body but form an extensive wake. It should be noted in this connection that a prototype "Kasper airfoil" was tested in a wind tunnel as a student project (Walton 1974) with discouraging results; the lift increased at high angles of attack but so did the drag. Nevertheless, the claims of Kasper suggest that it may be possible to gain the advantages of increased lift by creating a vortex over the wing, without necessarily paying the price of increased drag, and the purpose of the present chapter is to present a simple idealized solution describing such a flow.

Considered here is the two-dimensional flow of an incompressible inviscid fluid over a two-dimensional airfoil at angle of attack.

For simplicity, the calculation is first done for a flat plate. A method to extend the investigation to the general Joukowski airfoil is demonstrated in Section 5.6. The flow is assumed to be steady, and it is supposed that there is a line vortex in the flow at rest relative to the airfoil. The existence of such a solution and the resulting effects on the lift are investigated in this chapter.

4.2 Equilibrium of the Free Vortex

The flow picture is sketched in Figure 4.1. Dimensionless variables will be used exclusively. The airfoil of length 2 lies along the x-axis from -1 to 1. The flow of unit velocity is at angle of attack α. There is a line vortex of strength κ at rest at the point (x_0,y_0). In addition, there is a circulation Γ about the airfoil. We use complex variables, $z = x + iy$, and $w = \Phi + i\Psi$ is the complex potential. Then w is an analytic function of z, with Ψ = constant on the airfoil and

$$w \sim e^{-i\alpha} z + \frac{i}{2\pi}(K+\Gamma) \log z \quad \text{as } z \to \infty. \qquad (4.2.1)$$

Note that for convenience the circulation is taken positive when in the clockwise sense. At this stage, κ, Γ, $z_0 = x_0 + iy_0$, are unknowns. There is no loss of generality in supposing $0 \leq \alpha \leq \pi/2$.

The circulation about the airfoil is referred to as being due to a bound vortex. A force must be applied to the wing to maintain the flow; this is the Kutta lift and it is perpendicular to the direction of flow at infinity. The vortex at z_0 is free, i.e., it is not

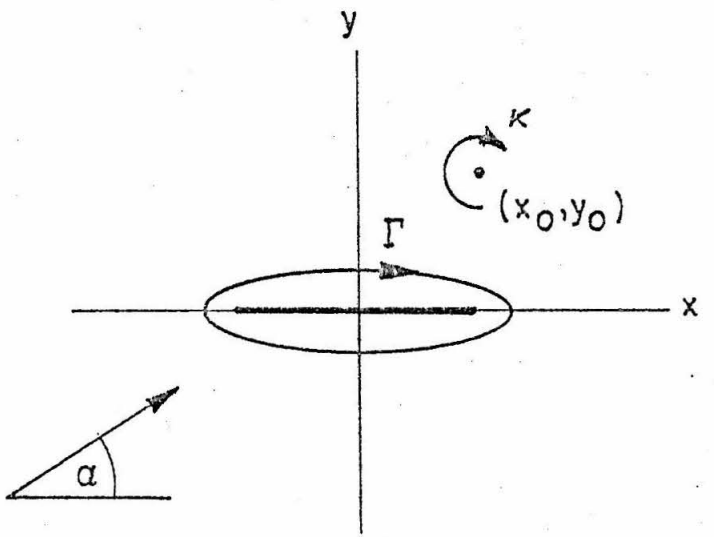

(a) Physical Plane $z = x + iy$

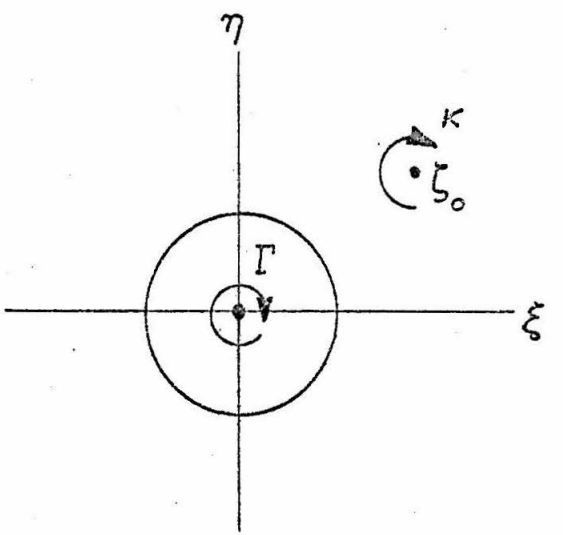

(b) Transform Plane $\zeta = \xi + i\eta$

Figure 4.1

subjected to any force, and is not produced by inserting a small wing at z_0. The Helmholtz laws require for steady motion that the free vortex be at a stagnation point, i.e.,

$$\lim_{z \to z_0} \left(\frac{dw}{dz} - \frac{i\kappa}{2\pi} \frac{1}{z - z_0} \right) = 0 . \tag{4.2.2}$$

However, the presence of the free vortex will affect the force on the body, and it follows readily from considerations of the momentum flux at infinity or directly from the Blasius formulas that the Kutta lift on the wing is

$$L = \kappa + \Gamma . \tag{4.2.3}$$

(In dimensional units, multiply by ρU, where ρ = density, U = velocity of free stream.)

If $\kappa = 0$, the indeterminacy of the picture is removed by imposing the Kutta condition at the trailing edge that the velocity be finite there. The result is

$$\Gamma = 2\pi \sin \alpha . \tag{4.2.4}$$

If $\kappa \neq 0$, three further equations can be obtained, giving four in all for the four real unknowns, by also imposing a Kutta condition on the leading edge and using equation (4.2.2). However, it will be shown in Section 4.3 that these equations have no solution and that it is not possible to impose a Kutta condition at both the leading and trailing edges, even though in principle there are sufficient degrees of freedom (cf. Smith and Clark 1975).

The velocity potential is obtained by mapping the airfoil into the unit circle by the transformation

$$z = \tfrac{1}{2}\left(\zeta + 1/\zeta\right), \quad \zeta = z + (z^2-1)^{1/2}, \tag{4.2.5}$$

where $(z^2-1)^{1/2} = |z^2-1|^{1/2}$ when $z > 1$, and the z-plane is cut from -1 to +1. Then,

$$w = \tfrac{1}{2}e^{-i\alpha}\left(\zeta + e^{2i\alpha}/\zeta\right) + \frac{iK}{2\pi}\left(\log(\zeta-\zeta_0) - \log(\zeta - 1/\bar{\zeta}_0)\right) + \frac{i}{2\pi}(K+\Gamma)\log\zeta \tag{4.2.6}$$

is an analytic function with the appropriate singularities and satisfying the boundary conditions, where ζ_0 is the image of z_0.

The condition (2.2) that the free vortex be at rest gives, after some algebra

$$e^{-i\alpha}\left(\zeta_0^2 - e^{2i\alpha}\right) + \frac{i\Gamma}{\pi}\zeta_0 + \frac{iK}{\pi}\zeta_0\frac{2-\zeta_0^2-|\zeta_0|^2}{(\zeta_0^2-1)(|\zeta_0|^2-1)} = 0. \tag{4.2.7}$$

Put $\zeta_0 = \rho e^{i\phi}$, and break into real and imaginary parts to obtain

$$\cos(\phi-\alpha) = \frac{K}{\pi}\,\frac{\rho^3\sin(2\phi)}{(\rho^2-1)(\rho^4-2\rho^2\cos(2\phi)+1)}, \tag{4.2.8}$$

$$\sin(\phi-\alpha) = \frac{K\rho}{\pi}\,\frac{\rho^4(1+\cos(2\phi))-\rho^2(1+3\cos(2\phi))+2}{(\rho^4-1)(\rho^4-2\rho^2\cos(2\phi)+1)} - \frac{\Gamma\rho}{\pi(\rho^2-1)}. \tag{4.2.9}$$

4.3 The Kutta Condition

In order that the inviscid flow be compatible with thin boundary layers on the airfoil surface, the velocity is assumed to be finite at

the trailing edge z = 1. This Kutta condition requires that $dw/d\zeta = 0$ at $\zeta = 1$, because of the singularity of the transformation. One real equation then results:

$$\sin\alpha = \frac{K+\Gamma}{2\pi} - \frac{K}{2\pi}\frac{\rho^2-1}{\rho^2-2\rho\cos\phi+1} \quad . \tag{4.3.1}$$

The velocity at the trailing edge is

$$V = \cos\alpha - \frac{K}{\pi}\frac{\rho(\rho^2-1)\sin\phi}{(\rho^2+1-2\rho\cos\phi)^2} \quad . \tag{4.3.2}$$

The physical considerations which led to the Kutta condition will only be applicable if $V > 0$, which is a necessary condition for (3.1) to apply.

A Kutta condition at the leading edge $\zeta = -1$ gives the real equation:

$$\sin\alpha = -\frac{K+\Gamma}{2\pi} + \frac{K}{2\pi}\frac{\rho^2-1}{\rho^2+2\rho\cos\phi+1} \quad . \tag{4.3.3}$$

It is now not hard to verify that equations (4.2.8), (4.2.9), (4.3.1) and (4.3.3) have no solution in common. Equations (4.3.1) and (4.3.3) are solved for K and Γ and substituted into (4.2.8) and (4.2.9) to obtain

$$\frac{(\rho^2-1)^2}{2\rho^2} = -\frac{\sin\alpha\sin\phi}{\cos(\phi-\alpha)} = -\frac{\sin\alpha\sin^2\phi}{\cos\phi\sin(\phi-\alpha)} \quad . \tag{4.3.4}$$

This equation obviously has no nontrivial solutions. Hence, there is no nontrivial flow field of the type being considered in which a Kutta condition is satisfied at both leading and trailing edges.

4.4 The Free Vortex Locus

The Kutta condition at the trailing edge and the two equations for equilibrium of the free vortex provide three equations for the four unknowns κ, Γ, ρ, ϕ. A locus of positions is therefore expected. From equations (4.2.8), (4.2.9) and (4.3.1) we obtain

$$\kappa = \frac{\pi}{\rho^3 \sin 2\phi} \cos(\phi-\alpha)(\rho^2-1)(\rho^4 - 2\rho^2 \cos 2\phi + 1), \tag{4.4.1}$$

$$\kappa+\Gamma = \frac{\pi(\rho^2+1)}{\rho^3 \sin 2\phi}\left[(\rho^2-1)^2 \cos\phi \cos\alpha + (\rho^4+1)\sin\phi \sin\alpha\right], \tag{4.4.2}$$

$$F(\rho,\phi) \equiv \left[(\rho+1/\rho)^2-4\right]\cos\phi\cos(\phi-\alpha) - (\rho+1/\rho)\sin\alpha\sin\phi + 2\sin\alpha\sin\phi\cos\phi = 0. \tag{4.4.3}$$

This last equation determines for given angle of attack α the locus of possible positions of the free vortex. Only real roots of the quadratic for $\rho + 1/\rho$ which are greater than 2 are relevant, as ρ must be real and $\rho > 1$. In addition, the condition $V > 0$ is equivalent to

$$\tfrac{1}{2}\left[(\rho+1/\rho)^2-4\right](1+\tan\alpha\tan\phi) < \frac{\rho+1/\rho-2\cos\phi}{\rho+1/\rho+2\cos\phi}. \tag{4.4.4}$$

By inspection, one sees that (4.4.3) has one positive root for $\rho + 1/\rho$ greater than 2 if $0 < \phi < \pi/2$ or $\pi/2 + \alpha < \phi < \pi$. Using $x_0 = \frac{1}{2}(\rho + 1/\rho)\cos\phi$ and $y_0 = \frac{1}{2}(\rho - 1/\rho)\sin\phi$, the closed form expression for z_0, κ, Γ can be written in terms of ϕ. The resulting formulas are sufficiently complicated to prohibit their use other than for numerical calculations.

For small ϕ or $\pi - \phi$, when the vortex is close to the trailing or leading edge, the leading terms in the expansions give

$$\left.\begin{aligned} \rho + 1/\rho &= 2 + \tfrac{1}{4}\phi^3 \tan\alpha\ , \quad x_0 = 1 - \tfrac{1}{2}\phi^2\ , \quad y_0 = \tfrac{1}{2}(\phi^5 \tan\alpha)^{1/2}\ , \\ K &= 2\pi\,(\phi^5 \sin\alpha \cos\alpha)^{1/2}\ , \quad K+\Gamma = 2\pi \sin\alpha\ (1+\phi^2) \end{aligned}\right\} \tag{4.4.5}$$

and ($\tilde{\phi} = \pi - \phi$)

$$\left.\begin{aligned} \rho + 1/\rho &= 2 + \tilde{\phi} \tan\alpha\ , \quad x_0 = -1 - \tfrac{1}{2}\tilde{\phi} \tan\alpha\ , \quad y_0 = (\tilde{\phi}^3 \tan\alpha)^{1/2}\ , \\ K &= 4\pi \sin\alpha\,(\tilde{\phi} \tan\alpha)^{1/2}\ , \quad K+\Gamma = 2\pi \sin\alpha\ (1+\tilde{\phi} \tan\alpha)\ . \end{aligned}\right\} \tag{4.4.6}$$

When the free vortex is near the trailing edge ($\phi << 1$) there are in addition to the stagnation point on the lower surface near $x = -\cos 2\alpha$ two more stagnation points on the upper surface near the trailing edge. Thus the solution describes flow with a small separation bubble near the trailing edge. When the free vortex is close to the leading edge ($\tilde{\phi} << 1$), there are also two additional stagnation points, but one is on the upper surface and the other is now on the lower surface. The flow is going backwards over the leading edge, and serves as a model of the small leading edge separation bubble which can occur, except that the oncoming flow is separating before the leading edge. One can ask if extra line vortices could be added to satisfy a Kutta condition at the leading edge as well as the trailing edge, but the algebra quickly becomes unmanageable.

The stagnation points are at $x = \cos\theta$ where

$$\sin(\theta-\alpha) + \sin\alpha = \frac{K}{2\pi}(\rho - 1/\rho)\left[\frac{1}{\rho + 1/\rho - 2\cos(\theta-\phi)} - \frac{1}{\rho + 1/\rho - 2\cos\phi}\right] \tag{4.4.7}$$

and the root $\theta = 0$ is spurious (it is the Kutta condition). For ϕ close to π, the additional stagnation points are at $\theta = \pi \pm (\tilde{\phi} \tan \alpha)^{1/2}$. When ϕ is close to zero, they are at $\theta = \phi \pm \frac{1}{2}(3\phi^3 \tan \alpha)^{1/2}$.

4.5 Results for the Flat Plate

In Figure 4.2 the free vortex locations (x_0, y_0) are shown for $\alpha = .1$ and $\alpha = \pi/6$. The lift, $\kappa + \Gamma$, is shown in Figure 4.3 as a function of y_0 for the same angles of attack. The maximum lift occurs when the trailing edge is a stagnation point and the condition (4.4.4) is violated. Figure 4.4 shows the maximum lift plotted against the angle of attack. A finite lift is obtained at zero angle of attack. Also shown on this figure is the lift without the free vortex ($2\pi \sin \alpha$), and it is clear that large increases in the lift can be obtained.

The streamline patterns depend on whether the vortex is on the locus emanating from the trailing edge or on the locus coming from the leading edge. In the former case, as the free vortex gets stronger and moves away from the wing, the angle of attack being constant, the rearward stagnation point on the upper surface moves backward, the forward stagnation point on the upper surface moves forward, giving an increasing region of reverse flow, and the stagnation point on the lower surface moves rearward. In Figure 4.5 the streamlines for this case are shown near the limiting flow. This flow pattern is qualitatively similar to that reported by Kasper and Walton, who notice by means of tufts that there is forward flow over the rear part of the wing.

In the case when the free vortex is on the locus coming from the leading edge, the stagnation point on the upper surface moves rearward

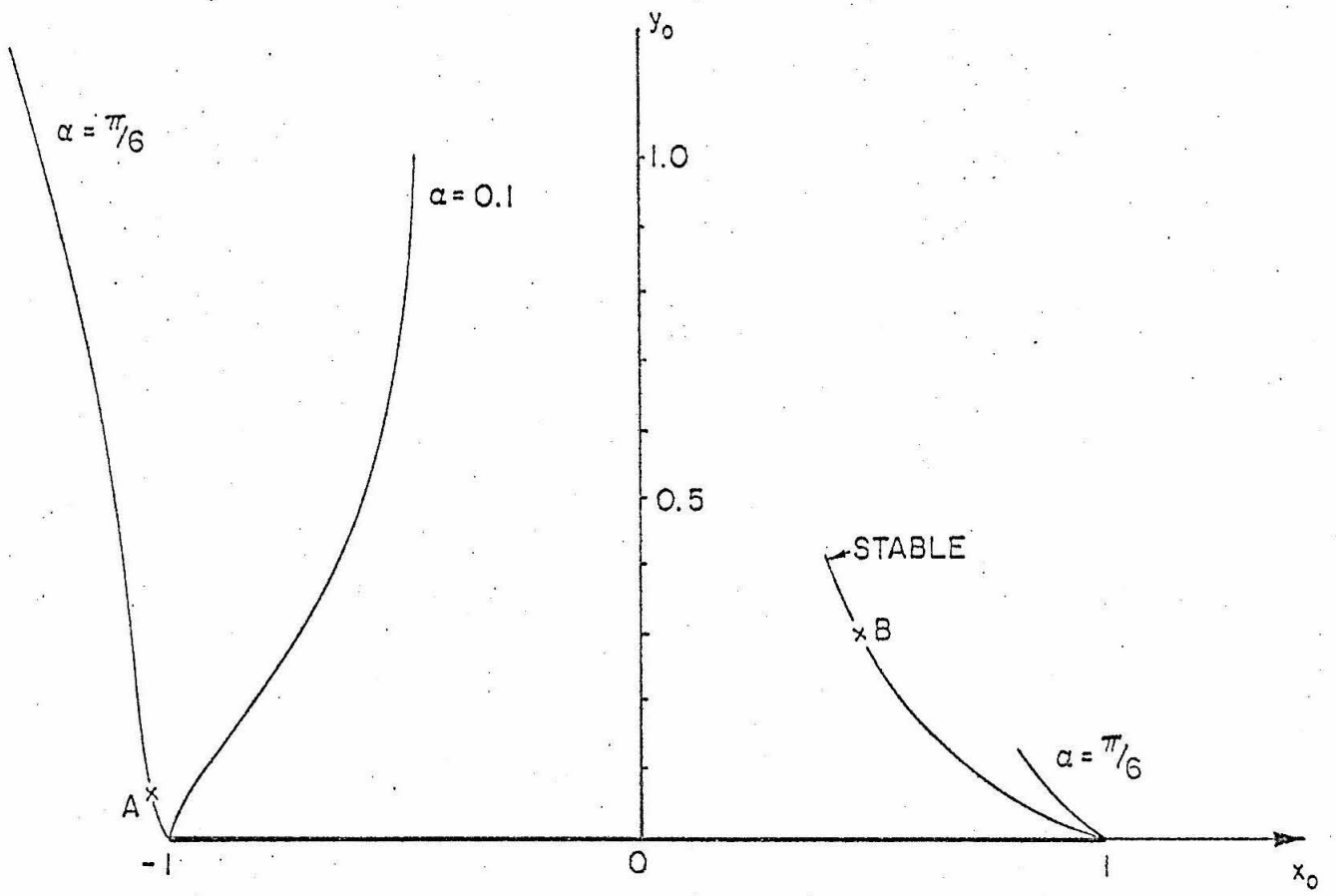

Figure 4.2 Loci of free vortex for $\alpha = .1$ (5.1°) and $\alpha = \pi/6$ (30°). Point A marks position where leading edge bubble lifts off (see Figure 4.6). For $\alpha = .1$ this happens too close to leading edge to be marked on the figure. Point B marks transition from instability to stability according to criterion of equation (4.5.5).

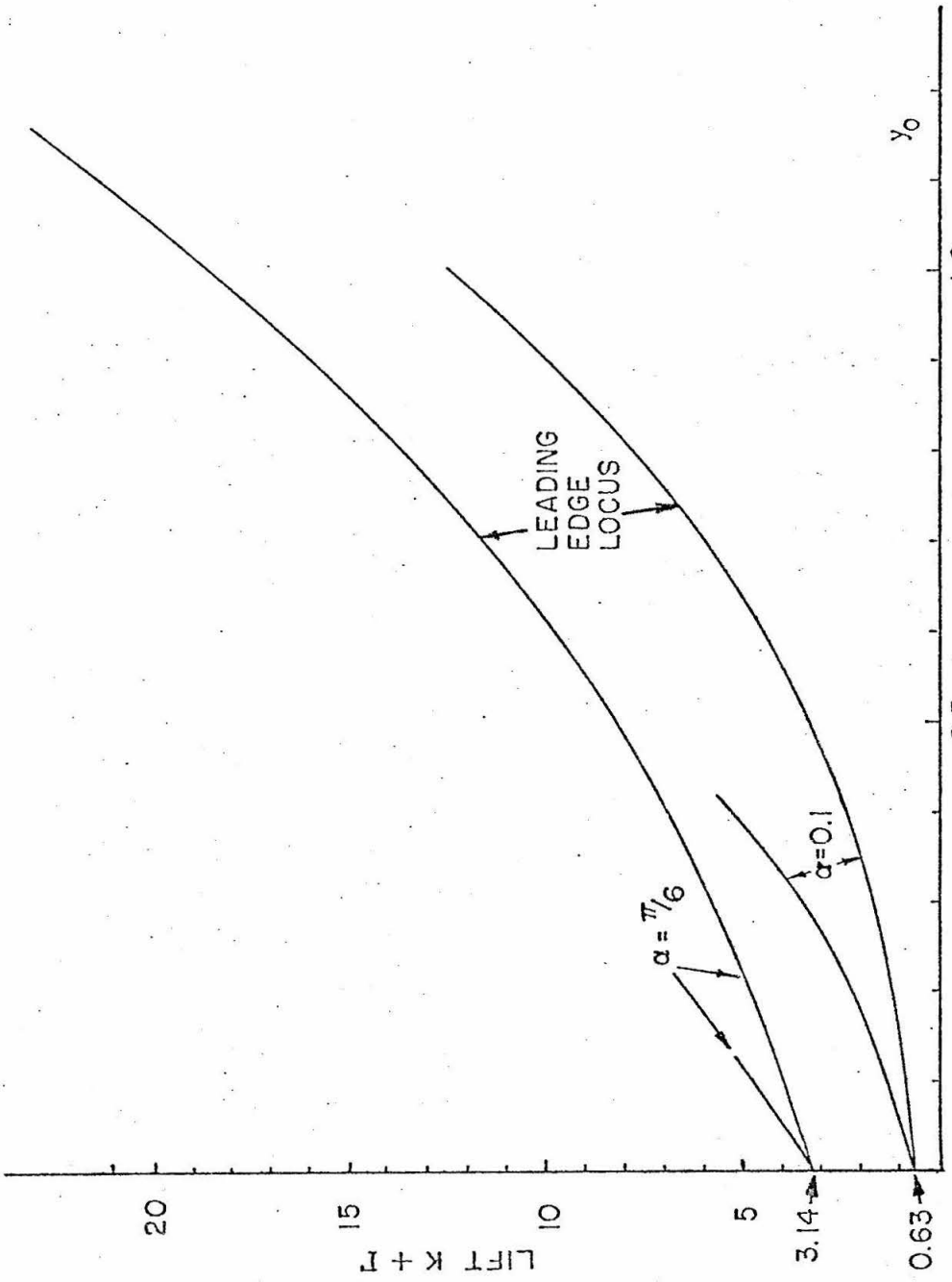

Figure 4.3 Lift on wing as a function of height y_0 of free vortex above wing for $\alpha = .1$ and $\alpha = \pi/6$. Ordinate intercepts are $2\pi \sin \alpha$.

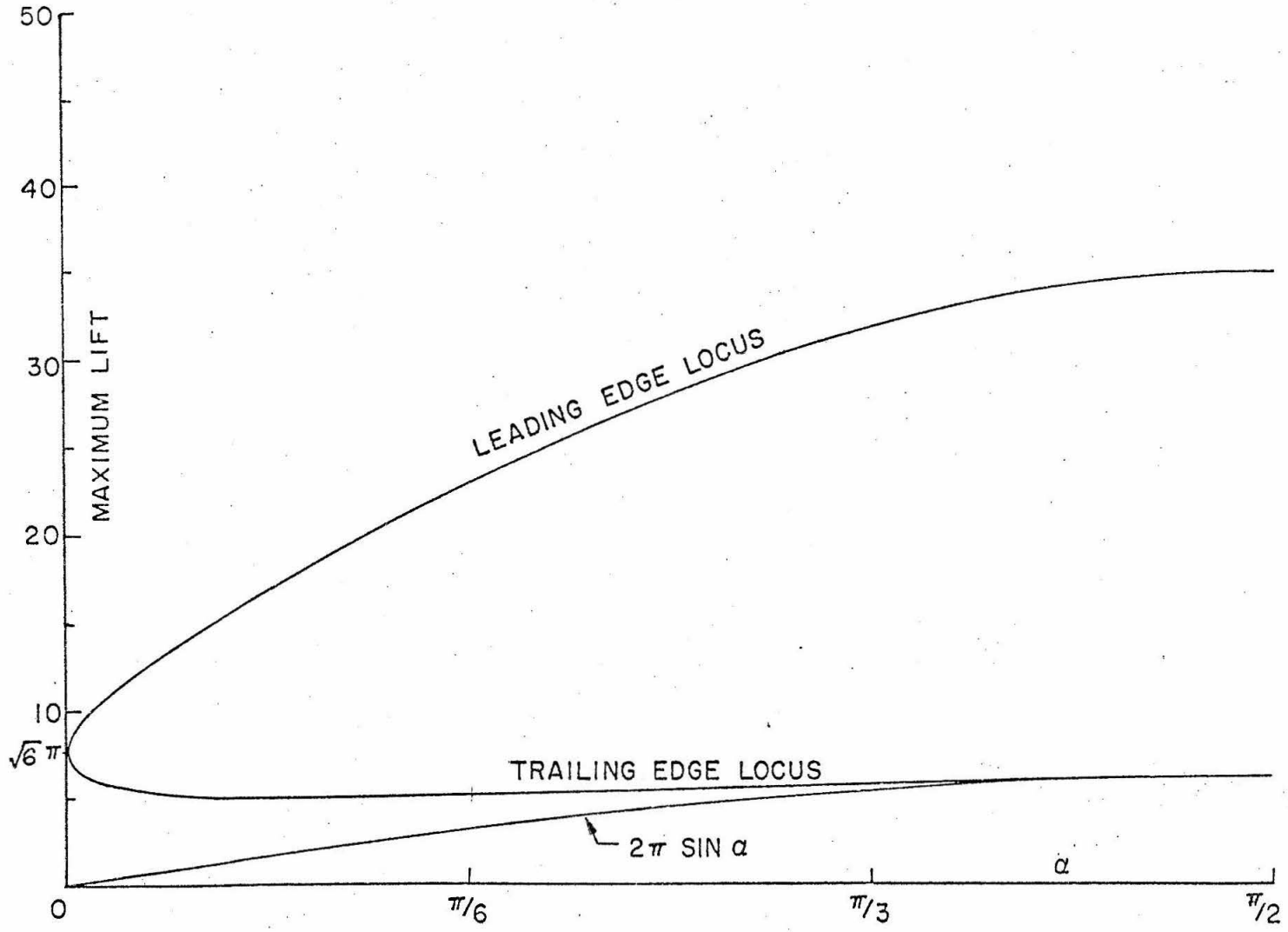

Figure 4.4 Maximum lift as function of angle of attack for leading edge and trailing edge loci. Also shown is the Kutta lift.

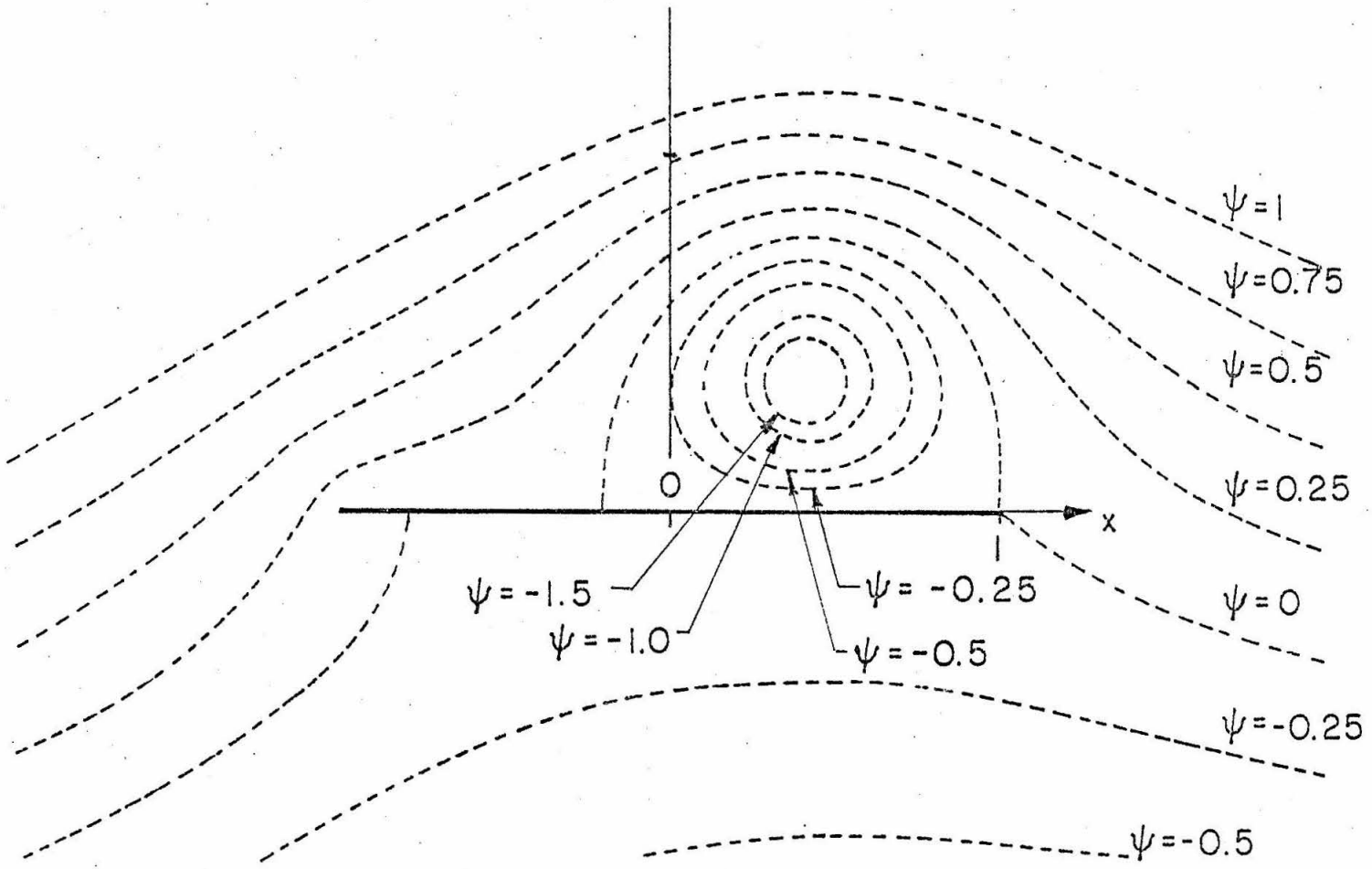

Figure 4.5 Streamline pattern for vortex on trailing edge locus for $\alpha = 0.1$ and maximum lift. There is a close correspondence between this figure and 3.83 of Prandtl (1952) showing a stalled airfoil.

and those on the lower surface approach one another, as the free vortex gets stronger and moves away from the wing with α kept constant. Eventually, the stagnation points below the wing merge and move off the wing, there being subsequently a stagnation point in the flow. Examples of these two cases are shown in Figure 4.6. This happens before the upper stagnation point reaches the trailing edge.

Figure 4.7 gives a typical plot of $q^2 (= -2p)$ on the airfoil. The case shown is for $\alpha = \pi/6$ and maximum lift on the trailing edge locus. The increased lift is due to additional suction under the vortex and near the leading edge.

Finally, a partial investigation of the stability of the flow is presented. Even if the disturbances are restricted to be two-dimensional, the stability of the configuration is a nontrivial problem as the Kutta condition requires that in unsteady flow a vortex sheet of variable strength exists downstream of the wing. However, if the Kutta condition is ignored for unsteady flow, and it is supposed that the free vortex and bound vortex have the strength κ and Γ, respectively, of the steady state, then the calculation is completely straightforward. The analysis is now described briefly. From the complex potential given by (4.2.6), it follows after some algebra that the complex velocity of the free vortex, u - iv, is given by

$$\begin{aligned} u - iv &= \left[e^{-i\alpha}\zeta^2 - e^{i\alpha} - \frac{\kappa}{\pi}\frac{\zeta^2}{\zeta - 1/\bar{\zeta}} + \frac{i(\kappa+\Gamma)}{\pi}\zeta - \frac{i\kappa}{\pi}\frac{\zeta}{\zeta^2-1} \right] / (\zeta^2-1) \\ &= Q(\zeta, \bar{\zeta}), \quad \text{say}, \end{aligned} \tag{4.5.1}$$

where ζ is the position of the vortex. In the equilibrium position, $\zeta = \zeta_0$ and $Q(\zeta_0, \bar{\zeta}_0) = 0$ gives equation (4.2.7).

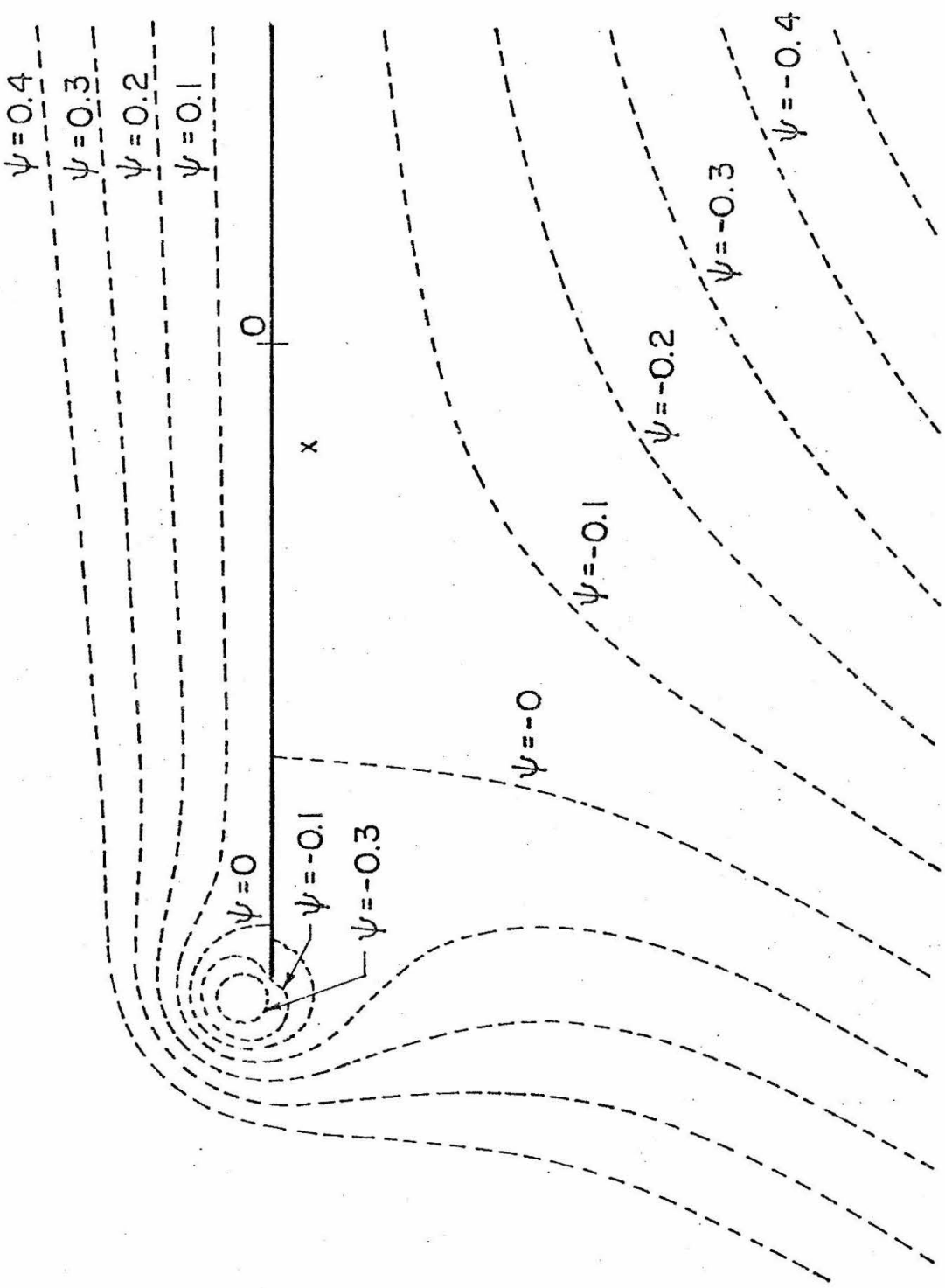

Figure 4.6a Streamline pattern for vortex on leading edge bubble. $\alpha = \pi/6$. $\phi = 3.0$, separation bubble is attached.

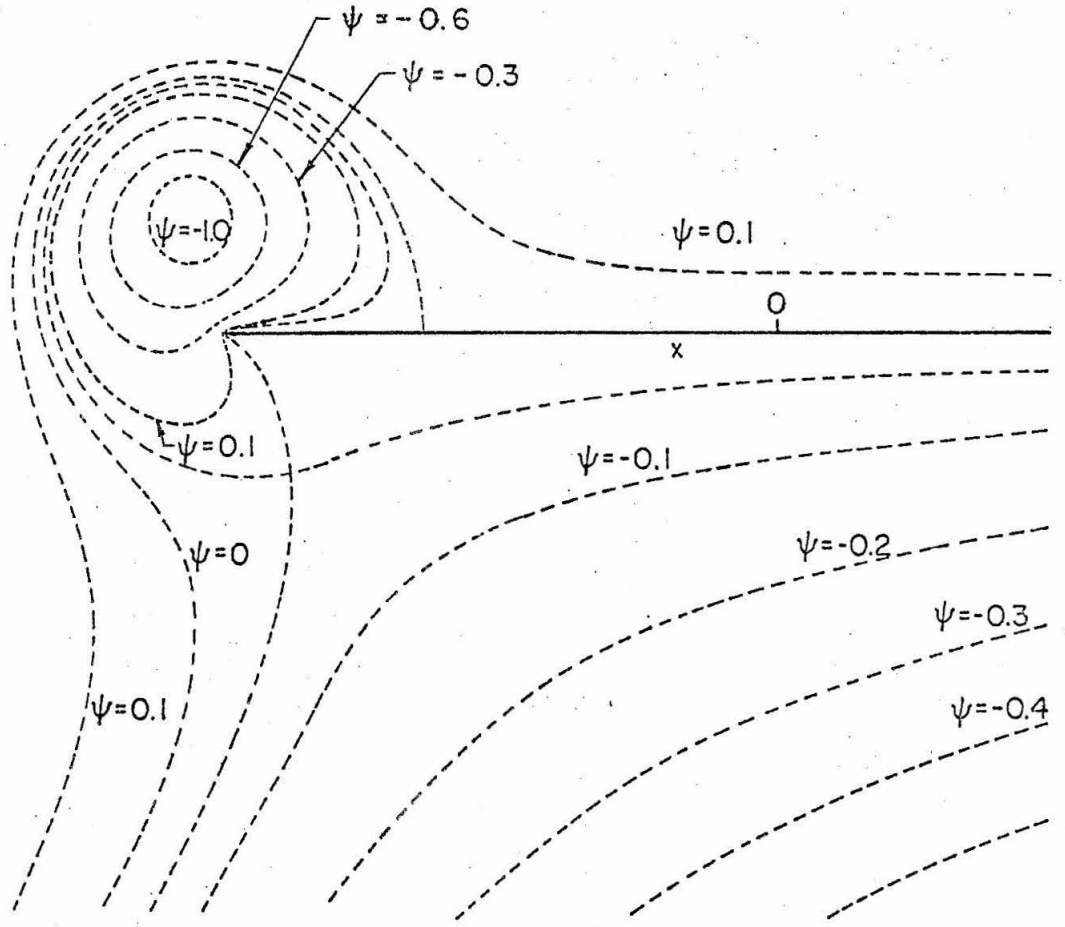

Figure 4.6b Streamline pattern for vortex on leading edge bubble $\alpha = \pi/6$. $\phi = 2.8$, separation bubble has lifted off.

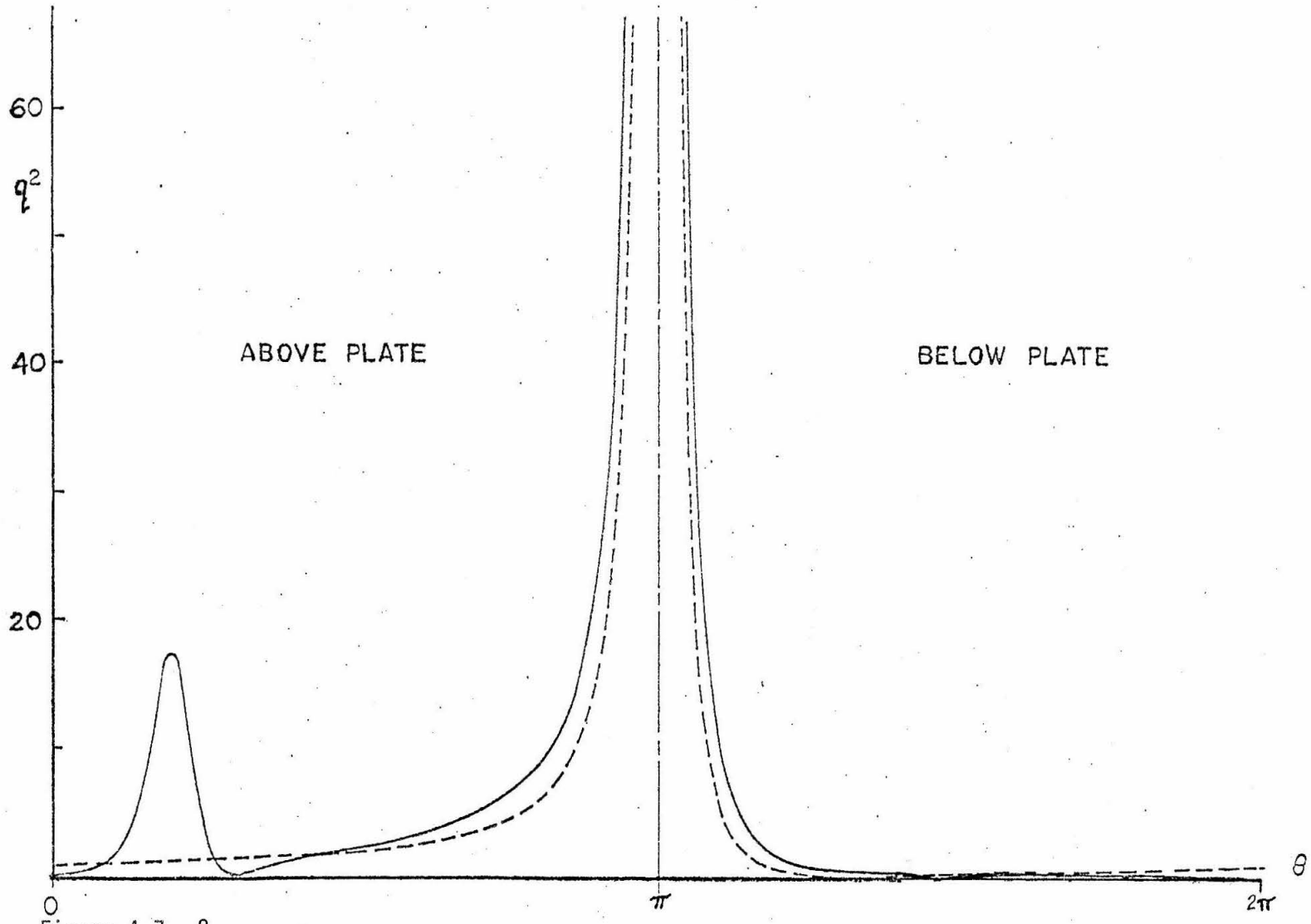

Figure 4.7 q^2 (= -2p) versus θ on the airfoil for $\alpha = \pi/6$ and maximum lift position on trailing locus. Trailing edge locus ——. No free vortex ----.

If now the vortex is displaced to the point $\zeta_0 + \zeta'$ in the transform plane, it can be shown that

$$\frac{d\bar{\zeta}'}{dt} = a\zeta' + b\bar{\zeta}', \tag{4.5.2}$$

where

$$a = \left(\frac{\partial Q}{\partial \zeta}\frac{d\bar{\zeta}}{d\bar{z}}\right)_0 \quad , \quad b = \left(\frac{\partial Q}{\partial \bar{\zeta}}\frac{d\bar{\zeta}}{d\bar{z}}\right)_0 ; \tag{4.5.3}$$

the subscript 0 denotes evaluation at $\zeta = \zeta_0$. Equation (4.5.2) has solutions proportional to $e^{\sigma t}$, where

$$\sigma^2 - (b+\bar{b})\sigma + b\bar{b} - a\bar{a} = 0 . \tag{4.5.4}$$

It is found that $b + \bar{b} = 0$. Hence, there is instability if

$$a\bar{a} > b\bar{b} . \tag{4.5.5}$$

If (4.5.5) is not satisfied, linear theory predicts stability, but nonlinear effects may destabilize.

It is found that there is a range of values of α and ϕ or y_0 for which (4.5.5) is violated. The angle of attack α must be less than 0.137 ($\simeq 8°$), the vortex must be on the trailing edge locus, and the values of ϕ lie in a range depending on α which includes, however, the value for maximum lift. The possible positions for $\alpha = 0.1$ are shown on Figure 4.2. There are no stable positions on the leading edge locus. It is emphasized that this conclusion of stability is tentative, and the problem needs to be analyzed using the methods developed for unsteady wing flow.

4.6 Vortex above a Joukowski Airfoil

The locus of possible positions and strengths for a vortex stationary in the flow field above an airfoil can also be calculated when the airfoil is the image of the unit circle under some conformal map. For the airfoil profile in the z=x+iy plane and the unit circle in the $\zeta = \xi + i\eta$ plane a class of conformal maps which generate the Joukowski airfoils are defined by the map $z = f(\zeta)$ where

$$f(\zeta) = \tfrac{1}{2}\left(\zeta + (\zeta-1)(T-ic) + \frac{1}{\zeta+(\zeta-1)(T-ic)}\right). \qquad (4.6.1)$$

The parameters T and c give the airfoil thickness and camber. When T and c are both zero the map generates the flat plate as shown in Figure 4.1. When they are nonzero, the flat plate is replaced by an airfoil profile with its cusp at z=1.

The form of $f(\zeta)$ given by equation (4.6.1) is not essential in the following analysis, but it is a convenient one in the numerical work as it generates a range of shapes by varying the two parameters. In general $f(\zeta)$ is assumed to satisfy several conditions so that the shape has some resemblance to an airfoil. The airfoil is directed to the left with the cusp placed at z=1. The condition that z=1 correspond to $\zeta = 1$ on the unit circle requires $f(1) = 1$ and $f'(1) = 0$. The asymptotic behavior of f is required in order to determine the complex potential. For the class given by (4.6.1),

$$f(\zeta) \sim \tfrac{1}{2} A e^{-i\chi}\zeta \qquad \text{as } |\zeta| \to \infty, \qquad (4.6.2)$$

where A and χ are real.

The complex potential for the flow outside the airfoil with a stream of unit velocity at angle α at infinity and a point vortex of strength κ at $z_0 = f(\zeta_0)$ has the form

$$W(\zeta) = \tfrac{1}{2} A e^{-i\alpha'}\left(\zeta + e^{2i\alpha'}/\zeta\right) + \frac{i}{2\pi}(\kappa+\Gamma)\log\zeta + \frac{i\kappa}{2\pi}\left(\log(\zeta-\zeta_0) - \log(\zeta - 1/\bar{\zeta}_0)\right), \tag{4.6.3}$$

where

$$\alpha' = \alpha + \chi \tag{4.6.4}$$

and Γ is the circulation around the wing. The circulation is taken as positive in the clockwise direction.

The free vortex must be located at a stagnation point in the flow field. In terms of the complex potential and map given by equations (4.6.1) and (4.6.3) the condition that $z_0 = f(\zeta_0)$ is a stagnation point can be written

$$\lim_{\zeta\to\zeta_0}\left(\frac{dw}{d\zeta}\frac{d\zeta}{dz} - \frac{i\kappa}{2\pi}\frac{1}{f(\zeta)-f(\zeta_0)}\right) = 0 . \tag{4.6.5}$$

Since the function $f(\zeta)$ is analytic at ζ_0, the equation above can be reduced by substituting the form for $w(\zeta)$ to give

$$\tfrac{1}{2} A e^{-i\alpha'}\left(\zeta_0 - \frac{1}{\bar{\zeta}_0}e^{2i\alpha'}\right) + \frac{i}{2\pi}(\Gamma+\kappa) - \frac{i\kappa}{2\pi}\left(\frac{\zeta_0\bar{\zeta}_0}{\zeta_0\bar{\zeta}_0 - 1} + \tfrac{1}{2}\zeta_0\frac{f''(\zeta_0)}{f'(\zeta_0)}\right) = 0 . \tag{4.6.6}$$

The primes on f indicate differentiation with respect to its argument.

At the trailing edge of the body the flow must go smoothly past the cusp. In order to have bounded velocities, the velocity potential must

satisfy w'(1) = 0. This gives the expression for the Kutta condition as

$$A\sin\alpha' - \frac{K+\Gamma}{2\pi} + \frac{K}{2\pi}\left(\frac{\zeta_0\bar{\zeta}_0 - 1}{(\zeta_0-1)(\bar{\zeta}_0-1)}\right) = 0. \qquad (4.6.7)$$

The velocity at the trailing edge must be positive, giving the constraint

$$V = \frac{1}{A^2}\left[A\cos\alpha' + \frac{iK}{2\pi}\left(\frac{(\zeta_0\bar{\zeta}_0-1)(\zeta_0-\bar{\zeta}_0)}{(\zeta_0-1)^2(\bar{\zeta}_0-1)^2}\right)\right] > 0. \qquad (4.6.8)$$

The complex equation (4.6.6) and the real equation (4.6.7) give three real equations for the four unknowns κ, Γ, ζ_0 and η_0, where $\zeta_0 = \xi_0 + i\eta_0$. A locus of solutions satisfying (4.6.8) may exist, depending on the choice of $f(\zeta)$. In order to devise a general scheme to determine the locus, equation (4.6.7) can be solved for Γ and the result substituted into equation (4.6.6). The resulting equation can be written in terms of a complex valued function $G(\zeta_0, \bar{\zeta}_0; \kappa)$ as

$$G(\zeta_0, \bar{\zeta}_0; \kappa) = 0, \qquad (4.6.9)$$

where

$$G = \tfrac{1}{2}Ae^{-i\alpha'}\left(\zeta_0 - \frac{1}{\bar{\zeta}_0}e^{2i\alpha'}\right) + iA\sin\alpha' + \frac{iK}{2\pi}\left(\frac{\zeta_0\bar{\zeta}_0 - 1}{(\zeta_0-1)(\bar{\zeta}_0-1)} - \frac{\zeta_0\bar{\zeta}_0}{\zeta_0\bar{\zeta}_0-1} - \tfrac{1}{2}\zeta_0\frac{f''(\zeta_0)}{f'(\zeta_0)}\right). \qquad (4.6.10)$$

The value of ζ_0 satisfying $G = 0$ for a given κ will give a solution if (4.6.8) is satisfied.

The classical wing solution is realized for $\kappa = 0$ as this requires $\zeta_0 = 1$ and $\Gamma = 2\pi A \sin(\alpha')$. For values of κ greater than zero, Newton's method can be applied to the complex equation (4.6.9) to find the complex roots which must then satisfy (4.6.8). Applying Newton's method to the complex equation is equivalent to solving the real second order system

$$g_1(\xi,\eta) = 0, \tag{4.6.11a}$$

$$g_2(\xi,\eta) = 0, \tag{4.6.11b}$$

where $G = g_1 + i g_2$ and the root is $\zeta_0 = \xi_0 + i\eta_0$. The elements of the Jacobian matrix can be evaluated by using the identities:

$$\frac{\partial g_1}{\partial \xi} + i\frac{\partial g_2}{\partial \xi} = \frac{\partial G}{\partial \xi} + \frac{\partial G}{\partial \bar{\xi}}, \tag{4.6.12}$$

$$\frac{\partial g_1}{\partial \eta} + i\frac{\partial g_2}{\partial \eta} = i\left(\frac{\partial G}{\partial \xi} - \frac{\partial G}{\partial \bar{\xi}}\right). \tag{4.6.13}$$

The initial guess for ζ_0 is important as there are possibly several solutions in the ζ plane. For the flat plate there are the two loci of solutions for sufficiently small κ, as well as possible roots of G inside the unit circle. Only those roots $|\zeta_0| > 1$ are of interest.

A systematic approach to generate the roots begins with κ small and the initial guess for ζ_0 near 1. The solution curve can be evaluated by increasing κ in small increments. From the results for the flat plate, the leading edge of the airfoil also needs to be examined for a second locus of solutions.

Notice that this method provides a means for investigating the possible positions for the free vortex, but it does not prove that other

possible positions do not exist.

4.7 Airfoil Results

Two example profiles are presented here in order to demonstrate some of the similarities and differences between the possible positions of a free vortex above a flat plate and an airfoil profile with nonzero thickness and camber.

For the first example the map parameters are taken as T = .05 and c = .07. The resulting profile and loci of possible vortex positions are shown in Figure 4.8 for the airfoil at angles of attack of .1 and $\pi/6$. In each case the lift increases for positions along the curves moving away from the airfoil. The maximum values of the lift, $\kappa+\Gamma$, and the lift for the airfoil with no free vortex are given in Table 4.1 along with those values for the flat plate.

	No Free Vortex		Trailing Locus		Leading Locus	
(T,c)	α=0.1	$\alpha=\pi/6$	α=0.1	$\alpha=\pi/6$	α=0.1	$\alpha=\pi/6$
Plate (0,0)	0.6	3.1	5.5	5.2	12.5	23.3
(.05,.07)	1.1	3.7	4.2	4.6	13.5	24.4
(.13,.14)	1.6	4.3	3.4	-	15.1	26.1

Table 4.1 Maximum value of the lift, $\kappa+\Gamma$, for the flat plate and the two example airfoil profiles

Notice that the values of the maximum lift on the trailing loci have decreased from the values for the flat plate, even though the values of the lift without the free vortex are larger. On the leading loci the maximum lifts are slightly larger for the airfoil.

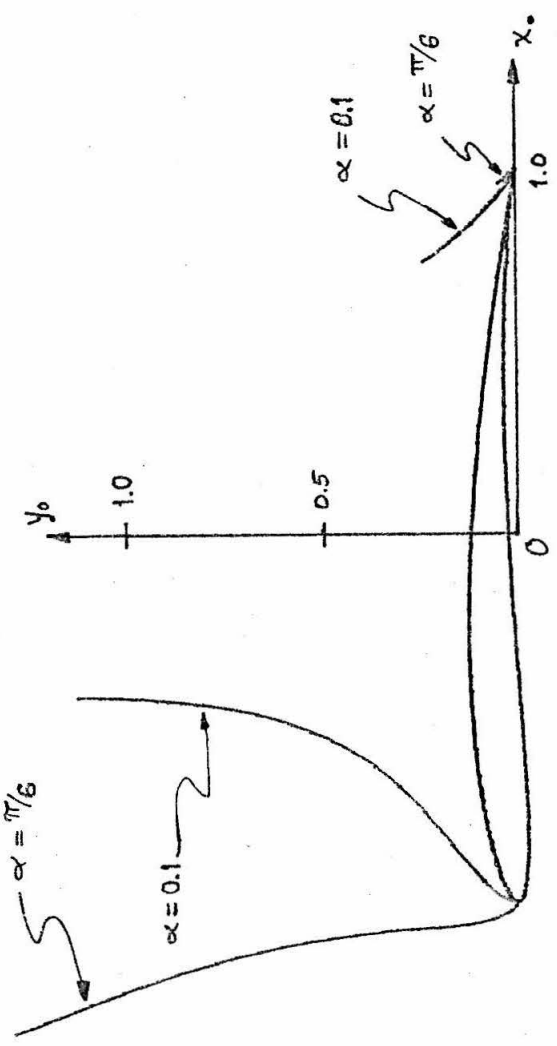

Figure 4.8 Loci of free vortex for $\alpha = 0.1$ and $\alpha = \pi/6$ with wing parameters $T = .05$ and $c = .07$.

The two trailing loci do not extend to the trailing edge. As the free vortex strength κ is decreased to zero from the value for the vortex farthest from the airfoil, the trailing edge velocity first increases, then decreases to negative values as the vortex is moved close to the point z=1. The velocity V does not approach the value of the trailing velocity for the airfoil in the absence of the free vortex as κ tends to zero. This behavior differs from the flat plate, where the trailing edge velocity is well behaved and increases to the limiting value for the plate without the vortex as κ tends to zero. The lower limit on the trailing edge locus for α=.1 is not apparent in Figure 4.8 because it lies very close to the trailing edge. For α=.1 the closest point to the trailing edge has x = .9996 and y = .0004 and for $\alpha = \pi/6$ the closest point has x = .987 and y = .013.

The second example uses the map parameters T=.13 and c=.14. The airfoil profile and loci of positions for the free vortex are shown in Figure 4.9 for angles of attack of .1 and $\pi/6$. As in the first example the trailing edge velocity is negative when the free vortex is near the trailing edge. For α=.1 the trailing locus gives a curve segment disjoint from the airfoil and for $\alpha = \pi/6$ there are no points on the curve extending from the trailing edge which give a positive velocity V. Hence for $\alpha=\pi/6$ there is only the leading locus of solutions. The maximum values of the lift corresponding to these solutions are given in Table 4.1, along with the lift in the absence of the free vortex. When a trailing locus exists, the lift is increased as a result of the free vortex, but the maximum lift is less than that corresponding to the flat

plate. On the leading loci the maximum lift increases as the Kutta lift for the airfoil without the free vortex increases.

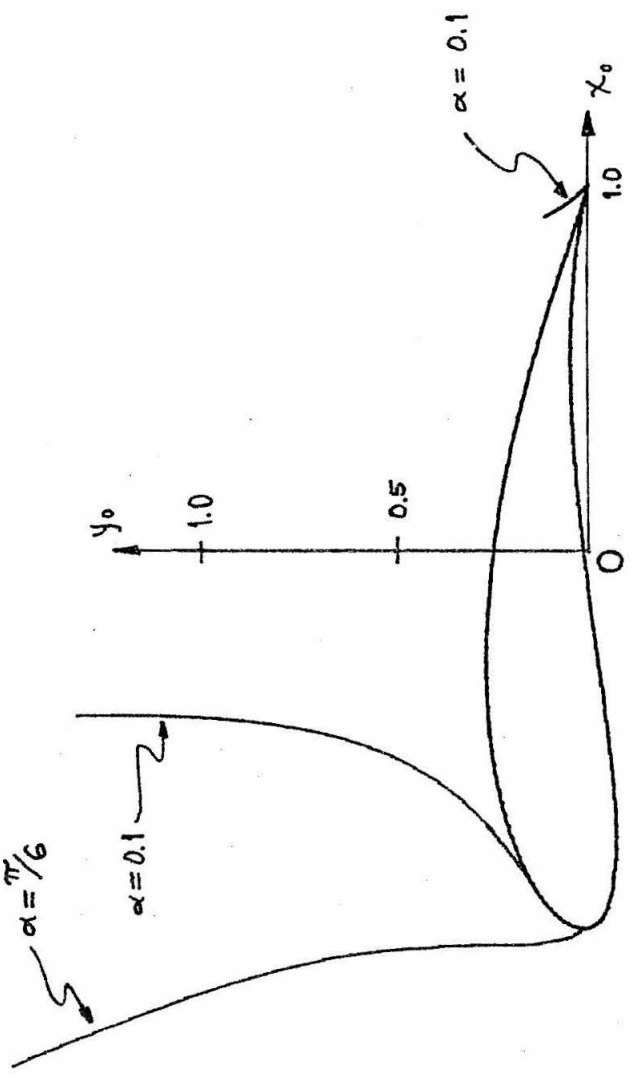

Figure 4.9 Loci of free vortex for $\alpha = 0.1$ and $\alpha = \pi/6$ with wing parameters T = .13 and c = .14. Notice there is no trailing locus for $\alpha = \pi/6$.

CHAPTER 5

TRAJECTORIES OF AN IDEAL VORTEX PAIR NEAR AN ORIFICE

5.1 Introduction

Experimental work with vortex pairs, such as that by Barker and Crow (1977) and others, raises questions about the effect of the geometric shape of the apparatus on the trajectories of the line vortices, since the initial motion of the vortex pair depends on the proximity of the walls. To provide some information on this matter, the idealized case of two-dimensional potential flow produced by a pair of point vortices in the presence of boundaries is calculated. A qualitative estimate of the effects of geometry on the trajectories of the vortices is obtained in this way.

In addition, the calculation of the vortex pair gives a rough approximation of the behavior of a vortex ring formed near solid boundaries, the solution of this problem for even an idealized axisymmetric ring being a much more difficult calculation.

The trajectory of a single vortex has been calculated by Paul (1934), Routh (1881), and others in various geometries, using the "Routh Streamfunction". Although the symmetry of the vortex pair reduces our problem to one with a single vortex, the resulting geometries are more complicated than those handled by the above.

The method introduced by Routh, and later generalized by Lin (1943), calculates the equation for the trajectory of a vortex in a simple geometry, and using a conformal map and the "velocity of transformation" evaluates the trajectory in the mapped geometry.

The present work covers two wall geometries in detail and comments on the more general geometry that includes the first two as limiting cases (see Figure 5.1). The first case is a semi-infinite horizontal channel of width 2L cut into an infinite vertical wall. In the second case the channel walls are of negliglble thickness and are represented by two semi-infinite parallel plates, separated by distance 2L. These two geometries are the extremes of the more general case of the parallel channel cut into a wall which angles away from the opening. The similar geometry consisting of a gap of width 2L in an infinite vertical wall is considered by Karweit (1975), and his results are quoted in Section 5.4. In all cases the line vortices are parallel to the channel opening and placed symmetrically about the centerline through the opening. The vortices are directed as if they were formed by the roll up of vortex sheets formed when fluid passes impulsively through the opening; hence the lower vortex has positive (counterclockwise) vorticity and the upper one negative (clockwise) vorticity. Reversal of the strengths just reverses the direction of motion. In the absence of any boundaries the vortex pair would travel to the left at a constant velocity.

5.2 Calculation of the Velocity and Trajectory

From symmetry, the line passing between the vortices and bisecting the channel is a streamline and can be replaced by a wall, reducing the problem to one with a single vortex. Fix a coordinate axis by placing the origin at the lower edge of the opening in a Cartesian (x,y) coordinate system and taking the centerline (streamline) wall to be the line $y = L$. The channel wall is the $x > 0$ axis.

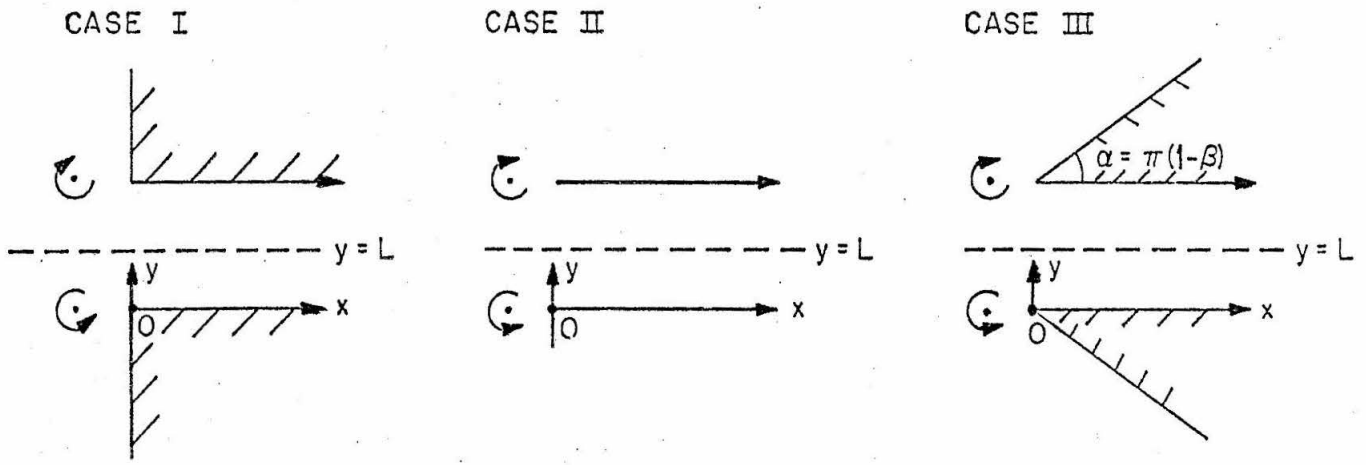

Figure 5.1 The wall geometries considered with a possible position for the vortex pair.

In each case, the Schwarz-Christoffel mapping theorem gives a map taking the walls in the complex z plane ($z = x + iy$) to the ξ axis in the complex ζ plane ($\zeta = \xi + i\eta$), with the interior region in the z plane mapped into the region $\eta > 0$. Denote such a map by $z = f(\zeta)$; then f is analytic for $\mathrm{Im}(\zeta) > 0$.

The vortex trajectory is the curve on which the "Routh Streamfunction" or trajectory function is a constant. For the motion of the vortex of strength κ in the ζ plane, the trajectory function is given by

$$\chi = \frac{\kappa}{4\pi} \log \eta \,. \tag{5.2.1}$$

Routh's result is that the trajectory function for motion of the vortex in the z plane is

$$\tilde{\chi} = \chi + \frac{\kappa}{4\pi} \log |f'(\zeta)| \,. \tag{5.2.2}$$

The trajectory curves in the z plane are then the images of the curves

$$\eta^2 |f'(\zeta)|^2 = \text{constant} \tag{5.2.3}$$

under the map $z = f(\zeta)$.

In order to evaluate the time development of a trajectory it is necessary to determine the velocity along the path. The velocity components (u,v) of the vortex can be calculated from the trajectory function by the relationships

$$u = \frac{\partial \tilde{\chi}}{\partial y} \quad , \quad v = -\frac{\partial \tilde{\chi}}{\partial x} \,. \tag{5.2.4}$$

Combining the velocity components to form the conjugate of the complex velocity simplifies the calculation. The velocity components for a vortex at the position $z_0 = f(\zeta_0)$ are given by

$$u - iv = \frac{iK}{2\pi}\left(\frac{1}{(\zeta_0 - \bar{\zeta}_0) f'(\zeta_0)} + \frac{f''(\zeta_0)}{2(f'(\zeta_0))^2}\right). \qquad (5.2.5)$$

The images of the trajectories in the ζ plane are given by the solution curves $\zeta_0(t)$ of the equation

$$\frac{d\zeta_0}{dt} = (u+iv)/f'(\zeta_0). \qquad (5.2.6)$$

This differential equation can be integrated numerically (and for some simple cases analytically) as an initial value problem, along with $z = f(\zeta)$, to give the vortex trajectories. Note that the parameter L acts as a length scale and K/L scales the velocities, hence L and K do not affect the shapes of the trajectories.

5.3 Results

CASE I: In the z plane the lower channel wall lies on $y = 0$, $x > 0$, the vertical wall on $y < 0$, $x = 0$, and the centerline wall on $y = L$. The Schwarz-Christoffel transformation yields the map from the ζ plane

$$z = f(\zeta) = \frac{-L}{\pi}\left(\log(\sqrt{\zeta}-1) - \log(\sqrt{\zeta}+1) + 2\sqrt{\zeta}\right) + iL \qquad (5.3.1)$$

and the image of the vortex trajectories in the mapped ζ plane is described by

$$\frac{\eta^2(\xi^2+\eta^2)^{1/2}}{(\xi-1)^2+\eta^2} = C, \quad \text{for constant } C, \qquad (5.3.2)$$

or the solutions of

$$\frac{d\zeta}{dt} = \frac{i\pi K}{L}\left(\frac{\bar{\zeta}+1}{4\bar{\zeta}} + \frac{\bar{\zeta}-1}{\zeta-\bar{\zeta}}\right)\frac{\zeta-1}{|\zeta|} \quad . \tag{5.3.3}$$

Some of the possible vortex paths are shown in Figure 5.2. The differential equation is used to generate the trajectories in order to give the time increments. An Adam-Moulton predictor-corrector scheme using the Runge-Kutta-Gill method as a start and restart scheme is used to carry out the numerical integration. We set $\kappa = L = 1$, and the integration step length was varied to maintain the local relative error at less than 0.5×10^{-4}.

If the vortex pair starts too close to the vertical wall, then it will not travel away from the wall, but into the channel. In some trajectories the vortices pass through the opening, but then turn back out of the channel. The dividing trajectory, corresponding to the curve with $C = 1$ in the ζ plane, originally asymptotes $x = -L/\pi$ and finally asymptotes $y = L/2$ in the channel. It crosses the x axis at $x = -0.28L$.

CASE II: In the z plane the lower channel wall is a plate on $y = 0$ for $x > 0$. The centerline wall is on $y = L$. The map from the ζ plane is defined by

$$z = f(\zeta) = -\frac{L}{\pi}\left[\zeta + \log(\zeta-1)\right] + iL. \tag{5.3.4}$$

In the ζ plane the images of the trajectories are the curves

$$\frac{\eta^2(\xi^2+\eta^2)}{(\xi-1)^2+\eta^2} = C, \tag{5.3.5}$$

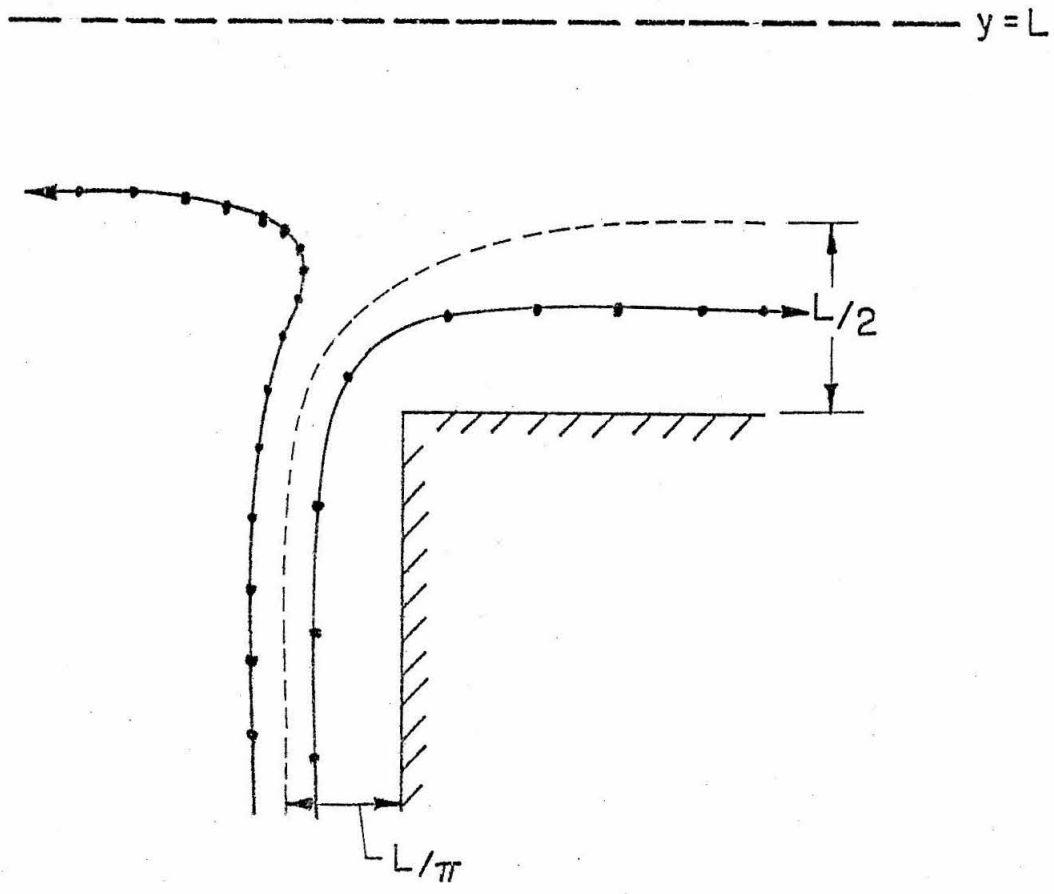

Figure 5.2 The dashed curve is the limiting trajectory for vortices traveling down the channel in the geometry of case I. Some other possible trajectories are drawn along with time marks. The dots placed along the trajectory represent a time increment of L^2/κ. The curves are the trajectories of one of the vortices of the pair.

for constant C, or the solutions of

$$\frac{d\zeta}{dt} = \frac{i\pi}{L} K \frac{(\zeta-1)}{|\zeta|^2}\left(\frac{1}{\zeta} + \frac{2(\bar{\zeta}-1)}{\zeta-\bar{\zeta}}\right). \tag{5.3.6}$$

Some of the trajectories are shown in Figure 5.3.

The trajectories are similar to those in Case I. For some initial positions the vortices will travel into the channel and then turn back out. The dividing trajectory for vortices traveling down the channel originally asymptotes $y = -L/\pi$ and finally asymptotes $y = L/2$ in the channel. The distances from the walls to the asymptotes are the same as in Case I. The dividing trajectory crosses the x axis at $x = -0.20L$.

CASE III: In the z plane, the lower channel wall lies on $y = 0$, $x > 0$ and the centerline wall on $y = L$. The angling wall lies on $z = r\exp(i\pi(1+\beta))$ for $r > 0$ and fixed β. The range of β considered here is $\frac{1}{2} \le \beta \le 1$. Case I is for $\beta = \frac{1}{2}$ and Case II for $\beta = 1$. The Schwarz-Christoffel transformation yields the map from the ζ plane

$$z = -\frac{L}{\pi}\int_0^{\zeta} \frac{s^{\beta}}{s-1}\, ds\,. \tag{5.3.7}$$

The image of the vortex trajectories in the mapped ζ plane are the curves

$$\frac{\eta^2(\xi^2+\eta^2)^{\beta}}{(\xi-1)^2+\eta^2} = C\,, \tag{5.3.8}$$

for some constant C.

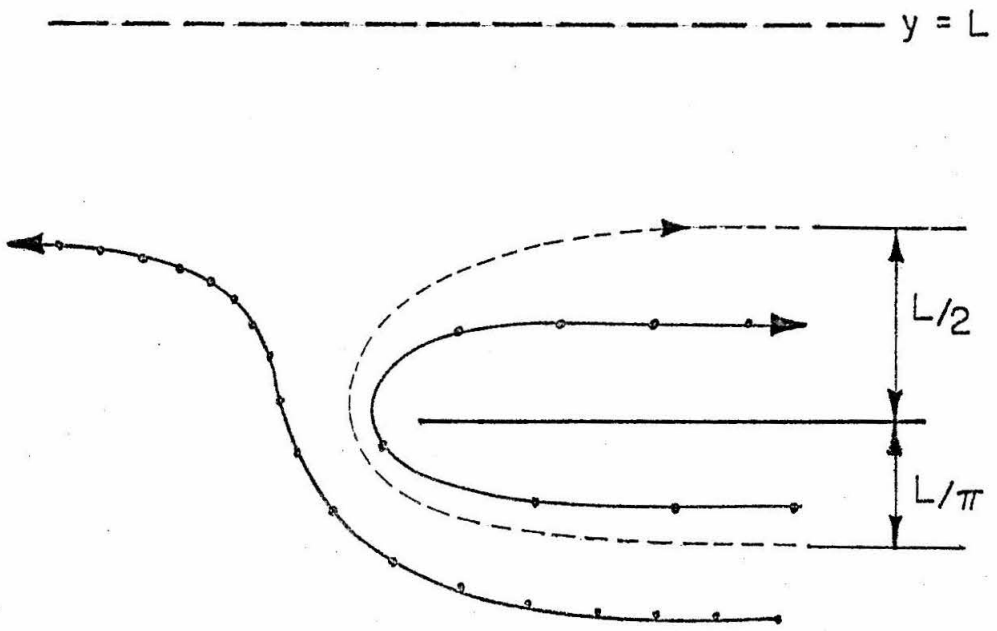

Figure 5.3 The limiting trajectory and typical trajectories for case II. The dots along the trajectory are placed at time increments of L^2/κ. The curves are the trajectories of one of the vortices of the pair.

The nature of the trajectories are the same as in the first two cases, and although the map cannot be explicitly integrated in elementary terms, the asymptotes of the dividing streamline can be determined. Since a single vortex in an infinite channel will travel in the direction opposite when placed in the top half rather than in the bottom half of the channel, the limiting trajectory will asymptote to L/2. In the ζ plane this corresponds to a curve on which $\zeta \to 1$ with the restriction $\frac{1-\xi}{\eta} \to +0$. Substituting this into the equation for the trajectory above and taking the limit gives the image of the limiting trajectory as the curve with C = 1. Taking the limit as $\eta \to -\infty$ and mapping the resulting asymptotic value of ζ to the z plane, it is found that the curve originally asymptotes to the line traced by $z = (r - iL/\pi)\exp i\pi(1+\beta)$ for $r \to +\infty$. This line is parallel to the angling wall and separated by a distance L/π, which is therefore independent of the wall angle.

5.4 Comments on Applications

For vortex rings generated by pushing fluid out of a tube with a piston, the initial position of the vortex ring can be varied by changing the piston stroke length. In the experiments of Didden (1977), using a thin walled tube enclosing the piston, the vortex ring formed by a short stroke length shrinks down to a diameter of less than the tube opening. For longer stroke the ring propagates away with close to a constant diameter and if the stroke is sufficiently long, more than a single ring is formed.

When attempting to generate single rings with a small ratio of the core radius to the ring radius, the initial position of the ring

must be far enough from the apparatus that the ring travels without the shrinking. An estimate of the effect of the apparatus shape on the ring diameter can be obtained from the results of the previous section and Karweit (1975). For the first two geometries in Figure 5.1 and the gap in the vertical wall considered by Karweit, the critical trajectories divide the possible initial positions of the vortex ring into two regions. On the apparatus side of these curves the vortex ring is not expected to propagate away. The possible initial positions for the vortex ring form a curve extending outward from the edge of the apparatus and curving away from the center line. The smaller the distance at which the initial curve crosses the dividing trajectory, the better the geometry for producing rings which travel away from the apparatus with little change in the diameter. In the case of Karweit and the second case in Section 5.3, that distance is greater than .28L. For the first case in Section 5.3, the thin walled tube, the distance is less than .20L, making it the preferable geometry.

CHAPTER 6

Structure of a linear array of hollow vortices of finite cross-section

By G. R. BAKER, P. G. SAFFMAN AND J. S. SHEFFIELD
Applied Mathematics, California Institute of Technology, Pasadena

Free-streamline theory is employed to construct an exact steady solution for a linear array of hollow, or stagnant cored, vortices in an inviscid incompressible fluid. If each vortex has area A and the separation is L, there are two possible shapes if $A^{\frac{1}{2}}/L$ is less than a critical value 0·38 and none if it is larger. The stability of the shapes to two-dimensional, periodic and symmetric disturbances is considered for hollow vortices. The more deformed of the two possible shapes is found to be unstable while the less deformed shape is stable.

1. Introduction

The recent observations by Brown & Roshko (1974) of organized vortex structures in the turbulent mixing layer have rekindled interest in the hydrodynamics of arrays of parallel line vortices. Moore & Saffman (1975) argued that the spacing of the vortex structures was controlled by the fact that there is an upper limit on the line density of a linear array of vortices of finite cross-section in non-viscous incompressible flow. When the vortices come too close, the induced straining fields are too intense for the individual vortices to exist in a steady state. However, they restricted their analysis to uniform vortices with constant vorticity in the cores, and the critical density or spacing was determined by an approximate argument (which was however supported by numerical work) because exact analysis was too hard.

It turns out that if the vortex cores are hollow or stagnant, so that the vorticity is concentrated into vortex sheets on the surfaces of the vortices, then the problem can be solved exactly by the free-streamline theory of inviscid, incompressible, two-dimensional flow, and the purpose of this paper is to present the calculation as a contribution to the theory of vortices. We see no direct physical application of the results, but similar calculations for two-dimensional arrays may be of interest in the theory of uniformly rotating superfluid helium, and the exact results provide a means of checking the approximate argument of Moore & Saffman. A similar calculation was carried out (before the present work was done) by Hill (1975) for a single hollow vortex in a uniform straining field.

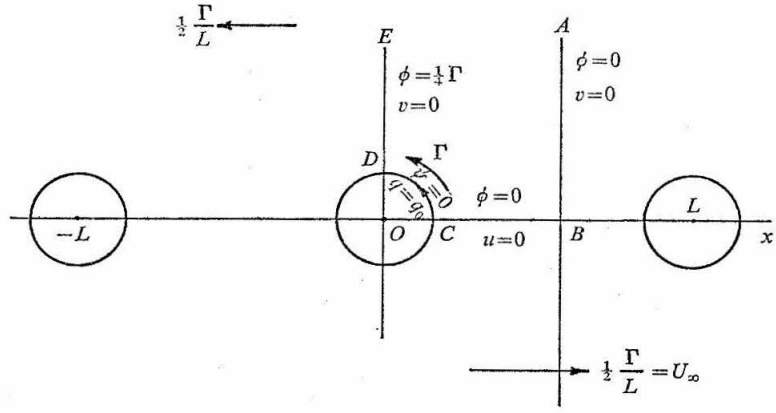

FIGURE 1. The physical plane for a regular array of vortices with fore-and-aft symmetry.

2. The physical plane

We consider an infinite linear array of identical vortices lying on the x axis with centres at nL, $n = 0, \pm 1, \pm 2, \ldots$. Each vortex is hollow or has a stagnant core. In steady flow, constant pressure inside the cores requires that the fluid speed has a constant value, q_0 say, on the boundary of each vortex. The circulation Γ about each vortex is related to q_0 by

$$\Gamma = Pq_0, \tag{2.1}$$

where P is the perimeter of each vortex.

At large distances, the array looks like a vortex sheet of strength $2U_\infty$, where

$$U_\infty = \tfrac{1}{2}\Gamma/L. \tag{2.2}$$

The array is characterized by the dimensionless ratio

$$R = U_\infty/q_0 = \tfrac{1}{2}P/L. \tag{2.3}$$

We shall calculate a unique steady solution for $0 < R < 1$ in which each vortex has fore-and-aft symmetry, i.e. is symmetrical about the x axis and the line parallel to the y axis through its centre. It can be shown (see appendix) that no solutions with this symmetry exist for $R > 1$ and that reflexional symmetry about the centre implies fore-and-aft symmetry.

The limit $R = 0$ corresponds to an array of point vortices or a single vortex in unbounded fluid, according as the limit is reached by $P \to 0$ or $L \to \infty$. $R = 1$ gives a vortex sheet in which each vortex is pulled out longitudinally and squeezed sideways to lie along a length L of the x axis. Notice that in the limit $R = 1$ and the limit $P = 0$ the area A of each vortex is zero.

The deformation of the cores is conveniently measured by $P/A^{\frac{1}{2}}$, which has the minimum value of $2\pi^{\frac{1}{2}}$ for a circle and becomes large with the eccentricity. We are interested in how the deformation depends upon the spacing for vortices of given size and strength. The area A is a more basic measure of the size than the peri-

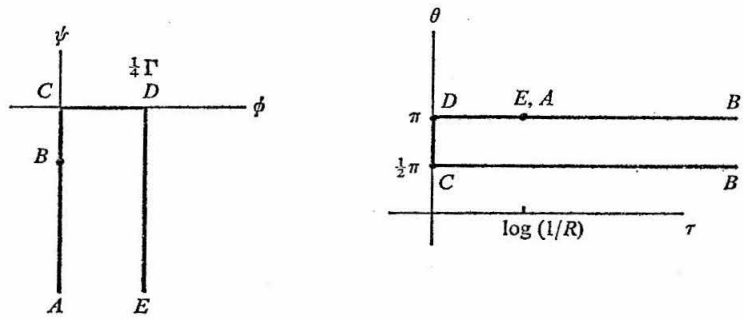

FIGURE 2. The mappings of the contour $ABCDE$ in the physical plane into the potential (ϕ, ψ) plane and hodograph (τ, θ) plane.

meter and $A^{\frac{1}{2}}/L$ is a dimensionless quantity that specifies the relative spacing of the array. The procedure is to calculate $P/A^{\frac{1}{2}}$ and $A^{\frac{1}{2}}/L$ as functions of R, and by eliminating R obtain the deformation in terms of the spacing.

The physical plane is shown in figure 1. Because of the symmetry it suffices to calculate the flow inside the contour $ABCDE$. Either the direction or magnitude of the velocity is known on the contour, and the methods of free-streamline theory can therefore be applied by mapping the potential plane into the hodograph plane.

3. The mappings

We introduce the complex variable $z = x + iy$, the complex potential $w = \phi + i\psi$, the complex velocity

$$u - iv = dw/dz = q\, e^{-i\theta}, \tag{3.1}$$

and the hodograph variable

$$\Omega = \log(q_0/q) + i\theta = \tau + i\theta, \quad \text{say.} \tag{3.2}$$

The potential and hodograph planes are shown in figure 2. B is a stagnation point because of the symmetry. The Schwarz–Christoffel transformations

$$w = \frac{i\Gamma}{2\pi}\log[(\zeta+1)^{\frac{1}{2}} - (\zeta-1)^{\frac{1}{2}}] - \frac{i\Gamma}{4\pi}\log 2, \tag{3.3}$$

$$\Omega = -\log[\{(b-1)(\zeta+1)\}^{\frac{1}{2}} - \{(b+1)(\zeta-1)\}^{\frac{1}{2}}] + \tfrac{1}{2}\log(\zeta-b) + \tfrac{1}{2}\log 2 \tag{3.4}$$

transform the interiors of the contours into the upper half of the $\zeta = \xi + i\eta$ plane, with $E \to \xi = -\infty$, $D \to \xi = -1$, $C \to \xi = 1$, $B \to \xi = b$, and $A \to \xi = \infty$, where

$$b = (1 + R^4)/2R^2. \tag{3.5}$$

The physical plane follows from integrating

$$\frac{dz}{d\zeta} = \frac{1}{q_0}\frac{dw}{d\zeta}e^{\Omega} = -\frac{iRL}{2^{\frac{1}{2}}\pi}\frac{(\zeta-b)^{\frac{1}{2}}}{(\zeta^2-1)^{\frac{1}{2}}}[\{(b-1)(\zeta+1)\}^{\frac{1}{2}} - \{(b+1)(\zeta-1)\}^{\frac{1}{2}}]^{-1}. \tag{3.6}$$

The quadrant of the vortex surface from D to C is mapped into the part of

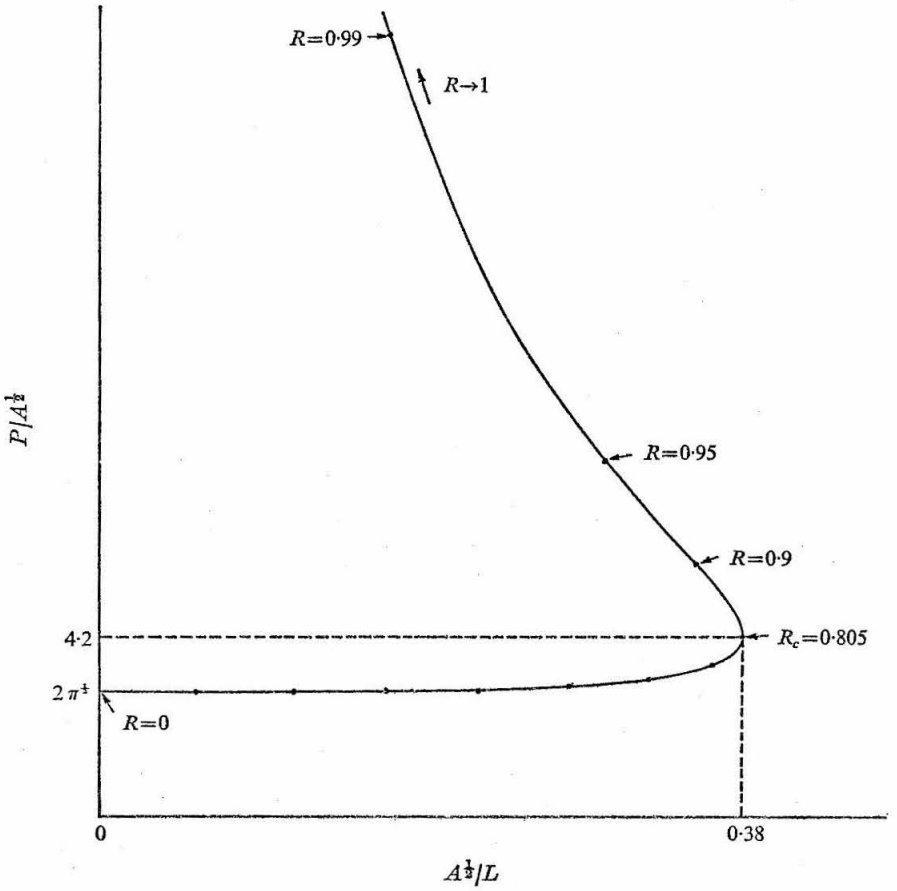

FIGURE 3. Perimeter length as a function of inverse distance between the cores. Variables are normalized with $A^{\frac{1}{2}}$. The seven dots on the bottom half of the curve are the values for $R = 0{\cdot}1\ (0{\cdot}1)\ 0{\cdot}7$.

the real ζ axis from $\xi = -1$ to $\xi = 1$. Making the substitution $\xi = -\cos 2\lambda$, we find for the parametric equation $z = Z(\lambda) = X(\lambda) + iY(\lambda)$ of the vortex with centre at the origin

$$X = \frac{L}{2\pi}(1+R^2)\sin^{-1}\left(\frac{2R\sin\lambda}{1+R^2}\right), \quad Y = \frac{L}{2\pi}(1-R^2)\sinh^{-1}\left(\frac{2R\cos\lambda}{1-R^2}\right), \quad (3.7)$$

where $0 \leqslant \lambda < 2\pi$ gives the complete perimeter.

The vortex is obviously circular as $R \to 0$, and flattens to the slit

$$-\tfrac{1}{2}L < x < \tfrac{1}{2}L \quad \text{as} \quad R \to 1.$$

The perimeter P is $2RL$. The area A is found by numerical integration, which gives A/L^2 as a function of R. Figure 3 shows a plot of $P/A^{\frac{1}{2}}$ against $A^{\frac{1}{2}}/L$. Note the maximum value of $A^{\frac{1}{2}}/L$ for a value $R = R_c \doteq 0{\cdot}805$.

4. Discussion

For a given value of $A^{\frac{1}{2}}/L$, there are either two or no possible steady states. If hollow or stagnant-cored vortices of given size are placed in an array such that their separation is too small, there is no possible steady state and the vortices presumably disintegrate. For the vortex of largest area for given L, the length of the major axis is $0{\cdot}71L$ and that of the minor axis is $0{\cdot}25L$.

A similar, although not identical, behaviour holds for a single hollow vortex of area A and circulation Γ in a uniform irrotational deformation with strain rate ϵ. Hill (1975) has shown that there are either one, two or no steady states according as $\epsilon A/\Gamma < 0{\cdot}03$, $0{\cdot}03 < \epsilon A/\Gamma < 0{\cdot}1$ or $0{\cdot}1 < \epsilon A/\Gamma$. Following Moore & Saffman (1975), we can estimate the critical value of $A^{\frac{1}{2}}/L$ for an array from the result for a single vortex by putting $\epsilon = \pi\Gamma/6L^2$ in the critical value for the single vortex. This gives an estimate of $0{\cdot}43$ for the critical value of $A^{\frac{1}{2}}/L$. The exact value is $0{\cdot}38$, so that the approximate argument of Moore & Saffman (1975) appears to be reasonable. The exact value of $P/A^{\frac{1}{2}}$ for the critical vortex is $4{\cdot}2$ for the array and $4{\cdot}5$ for the single vortex.

The existence of two possible configurations of the array suggests that at least one of them is unstable, and this should be the most deformed. We shall now verify this idea, by investigating the linear stability to infinitesimal perturbations of an array of hollow vortices, and demonstrate the existence of a class of disturbances to which the array is unstable for $R > R_c$ and stable for $R < R_c$.

5. Stability of an array of hollow vortices

We shall restrict attention here to infinitesimal periodic disturbances with reflexional symmetry about the centre of each vortex, which leave the centres undisplaced, because our interest lies in the stability to variations of shape. Stability of the array to disturbances which alter the positions of the vortices, i.e. of the type considered by Lamb (1932, § 156) for point vortices, is a matter for further study. (The effect of finite core size might have a bearing on the fact that Brown & Roshko (1974) did not appear to find the Lamb-type instability.)

It is sufficient to consider the strip $-\frac{1}{2}L < x < \frac{1}{2}L$, $y > 0$ and to use as independent co-ordinates the undisturbed velocity potential and stream function. The strip is $0 < \phi < \frac{1}{2}\Gamma$, $-\infty < \psi < 0$. A deformation of the boundary is described by the curve

$$\psi = \delta(\phi, t), \quad 0 < \phi < \tfrac{1}{2}\Gamma. \tag{5.1}$$

The disturbance to the velocity potential is denoted by $\Phi(\phi, \psi, t)$. Then

$$\partial^2\Phi/\partial\phi^2 + \partial^2\Phi/\partial\psi^2 = 0, \tag{5.2}$$

$$\Phi \to 0 \quad \text{as} \quad \psi \to -\infty. \tag{5.3}$$

For a hollow vortex, the pressure must be constant on its boundary; this gives a dynamic boundary condition

$$\frac{1}{q_0^2}\frac{\partial\Phi}{\partial t} + \frac{\partial\Phi}{\partial\phi} = -\frac{2\pi}{\Gamma}\frac{(b^2-1)^{\frac{1}{2}}}{b-\cos(4\pi\phi/\Gamma)}\delta, \tag{5.4}$$

on $0 < \phi < \frac{1}{2}\Gamma$, $\psi = 0$. In addition there is a kinematic condition

$$\frac{\partial \Phi}{\partial \psi} = \frac{1}{q_0^2}\frac{\partial \delta}{\partial t} + \frac{\partial \delta}{\partial \phi} \tag{5.5}$$

satisfied on the undisturbed vortex.

The symmetry requires that the disturbance has period $\frac{1}{2}\Gamma$ in ϕ. We look for normal modes of the form

$$\Phi = \sum_{-\infty}^{\infty} \Phi_n \sin\left(\frac{4\pi n\phi}{\Gamma} + \omega t\right) \exp\left(\frac{4\pi}{\Gamma}|n|\psi\right), \tag{5.6}$$

$$\frac{\delta}{b - \cos(4\pi\phi/\Gamma)} = \sum_{-\infty}^{\infty} a_n \cos\left(\frac{4\pi n\phi}{\Gamma} + \omega t\right), \tag{5.7}$$

where ω is to be found. Inserting (5.6) and (5.7) into the boundary conditions and carrying out some straightforward algebraic manipulations, we obtain the recursion relation

$$a_{n+1} + \left(\frac{|n|\sinh\beta}{(\sigma+n)^2} - 2\cosh\beta\right)a_n + a_{n-1} = 0, \tag{5.8}$$

for $-\infty < n < \infty$, where $b = \cosh\beta$, $\beta = -\log 2R^2$ and $\sigma = \omega\Gamma/4\pi q_0^2$. The eigenvalues σ are determined by the requirement that $a_n \to 0$ as $n \to \pm\infty$. If σ is complex, the motion is unstable.

In the limit $\beta = \infty$, $R = 0$, the eigenvalues are obviously

$$\sigma = n \pm |\tfrac{1}{2}n|^{\frac{1}{2}}, \quad n = \pm 1, \pm 2, \ldots. \tag{5.9}$$

It is easy to verify directly that these are the natural frequencies of a single hollow vortex. For β large but not infinite, the eigenvalues can be expanded as power series in $e^{-\beta}$, and it is found that σ remains real provided that the regular perturbation scheme remains valid.

For smaller β, numerical means need to be employed, and the method of Laplace (Jeffreys & Jeffreys 1950, p. 486) is convenient. For given β, we assume a value of σ and calculate a_1/a_0 and a_{-1}/a_0 as functions of σ such that $a_n \to 0$ as $|n| \to +\infty$. Substitution into the recursion relation (5.8) for $n = 0$ gives an equation determining σ. The details are as follows. For n positive, define

$$\alpha_n^+ = \left(\frac{n+1}{n+2}\right)^{\frac{1}{2}} \frac{a_{n+1}}{a_n} e^{\beta} - 1. \tag{5.10}$$

It can be shown that $\alpha_n^+ = O(n^{-2})$ for large n when a_n decays as $n \to \infty$. From the recursion relation,

$$\alpha_{n-1}^+ = -1 - e^{\beta}\left[e^{-\beta}\left(1 + \frac{2}{n}\right)^{\frac{1}{2}}(1 + \alpha_n^+) - \left(1 + \frac{1}{n}\right)^{\frac{1}{2}}\left(2\cosh\beta - \frac{n}{(\sigma+n)^2}\sinh\beta\right)\right]^{-1}. \tag{5.11}$$

The asymptotic behaviour of α_n^+ gives a starting value from which $\alpha_0^+(\sigma, \beta)$ can be calculated numerically. We proceed similarly for the a_{-n} $(n > 0)$, defining

$$\alpha_n^- = \left(\frac{n+1}{n+2}\right)^{\frac{1}{2}} \frac{a_{-n-1}}{a_{-n}} e^{\beta} - 1 \tag{5.12}$$

and calculating $\alpha_0^-(\sigma,\beta)$. Because of the symmetry of the recursion relation

$$\alpha_0^-(\sigma,\beta) = \alpha_0^+(-\sigma,\beta). \tag{5.13}$$

The recursion relation for $n = 0$ gives

$$f(\sigma^2,\beta) \equiv \alpha_0^+(\sigma,\beta)+\alpha_0^-(\sigma,\beta) = 2^{\frac{1}{2}}e^{\beta}\cosh\beta - 2. \tag{5.14}$$

Since the left-hand side can be found numerically as a function of σ, the roots of (5.14) are obtained in a straightforward manner as functions of β.

Note that the roots occur in pairs, $\pm\sigma$. The roots are known for large β, so the procedure is to follow the roots numerically as β decreases. The smallest positive root $\sigma_1(\beta)$, say, turns out to be the one of interest. As β decreases, σ_1 decreases from $1-1/2^{\frac{1}{2}}$ at $\beta = \infty$ to zero at $\beta = 0{\cdot}434$. This value can be found analytically as the recursion relation can be solved in closed form (using generating functions) when $\sigma = 0$. For β less than $0{\cdot}434$, equation (5.14) is found to have roots with $\sigma^2 < 0$, demonstrating that there is an exchange of stabilities. It can be shown that the other roots remain real.

The critical value of β at which the array becomes unstable to disturbances of the type considered here gives the same value of R, $0{\cdot}805$, as that at which $A^{\frac{1}{2}}/L$ is a maximum, thereby demonstrating that, when there are two possible configurations, the more deformed is unstable to disturbances for which the less deformed is stable (cf. Moore & Saffman 1971).

This work was supported by the U.S. Army Research Office, Durham, under contract DAHC 04-75-C-0009.

Appendix

Consider a member of the linear array of hollow or stagnant vortices with the geometry as shown in figure 4. We assume periodicity of the array and reflexional symmetry only.

Using the hodograph variable defined by (3.2) we then require that τ satisfies Laplace's equation in the strip $ABCDEF$ and the following boundary conditions:

$$\tau = 0 \quad \text{along} \quad CD, \tag{A 1}$$

$$\tau \quad \text{has period} \quad \tfrac{1}{2}\Gamma \quad \text{in} \quad \phi, \tag{A 2}$$

$$\tau \sim -\log R \quad \text{as} \quad \psi \to -\infty. \tag{A 3}$$

Moreover, we want τ to have the correct behaviour at the stagnation points B and E. Noting that $dw/dz \sim (w-w_0)^{\frac{1}{2}}$ at a stagnation point, we can separate out the singular behaviour of τ at such points by using functions which behave locally as required. Including terms ensuring correct asymptotic behaviour and without violating (A 2), we have

$$\tau = \mathrm{Re}\left\{-\log 2R - \tfrac{1}{2}\log\left(\cos\frac{2\pi}{\Gamma}w + i\sinh\frac{2\pi}{\Gamma}\psi_0\right)\right.$$
$$\left. -\tfrac{1}{2}\log\left(\cos\frac{2\pi}{\Gamma}w - i\sinh\frac{2\pi}{\Gamma}\psi_0\right) - \frac{2\pi}{\Gamma}iw\right\} + H(\phi,\psi),$$

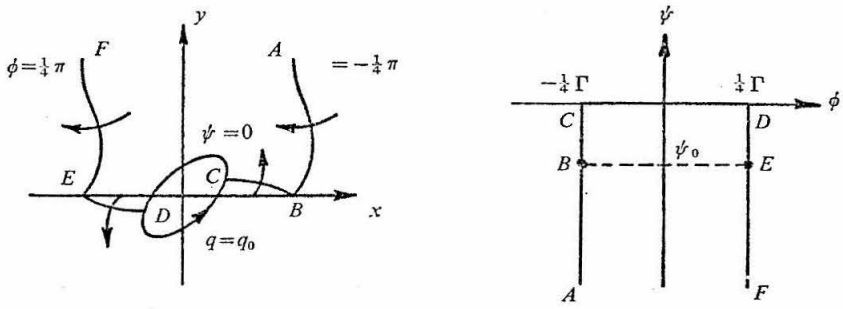

FIGURE 4. Physical and potential planes for an array with reflexional symmetry but not necessarily fore-and-aft symmetry. ψ_0 is the value of the stream function at the stagnation points B and E.

where H satisfies Laplace's equation and (A 2), and is bounded on the strip. Clearly

$$H = \sum_{n=0}^{\infty} \exp(4\pi n\psi/\Gamma)\left(A_n \sin\frac{4\pi n\phi}{\Gamma} + B_n \cos\frac{4\pi n\phi}{\Gamma}\right).$$

Now for τ to satisfy (A 1) we require $A_n = 0$, and hence there is fore-and-aft symmetry. Further,

$$0 = -\log 2R - \tfrac{1}{2}\log\left(\cos^2\frac{2\pi\phi}{\Gamma} + \sinh^2\frac{2\pi\psi_0}{\Gamma}\right) + \sum_{n=0}^{\infty} B_n \cos\frac{4\pi n\phi}{\Gamma},$$

so that the B_n are all uniquely determined. Note that for the correct asymptotic behaviour we require $B_0 = 0$, and so

$$\log 2R + \frac{1}{\Gamma}\int_{-\frac{1}{4}\Gamma}^{\frac{1}{4}\Gamma} \log\left(\cos^2\frac{2\pi\phi}{\Gamma} + \sinh^2\frac{2\pi\psi_0}{\Gamma}\right) d\phi = 0. \tag{A 4}$$

Writing $b = 1 + 2\sinh^2(2\pi\psi_0/\Gamma)$, we find that (A 4) implies

$$b + (b^2-1)^{\frac{1}{2}} = 1/R^2.$$

Since $b > 1$, then $R < 1$.

REFERENCES

BROWN, G. L. & ROSHKO, A. 1974 On density effects and large structure in turbulent mixing layers. *J. Fluid Mech.* **64**, 775.

HILL, F. M. 1975 Ph.D. thesis, Imperial College, London.

JEFFREYS, H. & JEFFREYS, B. S. 1950 *Methods of Mathematical Physics*. Cambridge University Press.

LAMB, H. 1932 *Hydrodynamics*. Cambridge University Press.

MOORE, D. W. & SAFFMAN, P. G. 1971 Structure of a line vortex in an imposed strain. In *Aircraft Wake Turbulence and its Detection* (ed. Olsen, Goldberg & Rogers), p. 339. Plenum.

MOORE, D. W. & SAFFMAN, P. G. 1975 The density of organized vortices in a turbulent mixing layer. *J. Fluid Mech.* **69**, 465.

References

Abramovitz, M. and Stegun, I.A. 1965 Handbook of Mathematical Functions. Dover.

Barker, S. J. and Crow, S. C. 1977 The motion of two-dimensional vortex pairs in ground effect. To be published in J. Fluid Mech.

Chevalier, H. 1973 Flight test studies of the formation and dissipation of trailing vortices. J. Aircraft 10, 14-18.

Chigier, H. B. 1974 Vortices in aircraft wakes. Scientific American 230, 76-83.

Cox, J. 1973 The revolutionary Kasper wing. Soaring 37, 20-23.

Crow, S. C. 1970 Stability theory for a pair of trailing vortices. AIAA J. 8, 2172-2179.

Didden, N. 1977 Untersuchung laminarer, instabiler Ringwirbel mittels Laser-Doppler-Anemometric. Ph.D. Thesis, George-August-Universitat zu Gottingen.

Grabowski, W. J. and Berger, S. A. 1976 Solutions of the Navier-Stokes equations for vortex breakdown. J. Fluid Mech. 75, 525-544.

Hall, M. G. 1972 Vortex breakdown. Annual Review of Fluid Mechanics 4, 195-217.

Karweit, M. 1975 Motion of a vortex pair approaching an opening in a boundary. Phys. Fluids 18, 1604-1606.

Kelvin, Lord. 1880 Vibrations of a columnar vortex. Mathematical and Physical Papers. Cambridge University Press 1910, pp. 152-165.

Krutsch, C. H. 1939 Über eine experimentelle beobachtete Erscheinung an Werbelringen bei ehrer translatorishen Beiregung in Werklechin, Flussigheiter. Ann. Physik 35, 497-523.

Lambourne, N. C. and Bryer, D. W. 1961 The bursting of leading-edge vortices--some observations and discussion of the phenomenon. Aero Res. Counc. R&M 3282.

Landahl, M. T. and Widnall, S. E. 1971 Vortex control. In Aircraft Wake Turbulence and Its Detection (Ed. Olsen, Goldberg, and Rogers), pp. 137-156. Plenum Press.

Lessen, M., Deshpande, N. V. and Hadji-Ohanes, B. 1973 Stability of a potential vortex with nonrotating and rigid body rotating top-hat jet core. J. Fluid Mech. 60, 459-466.

Lin, C. C. 1943 On the motion of vortices in two dimensions. The University of Toronto, Toronto, Canada.

Moore, D. W. 1972 Finite amplitude waves on aircraft trailing vortices. Aero Quart. 23, 307-344.

Moore, D. W. and Griffith-Jones, R. 1974 The stability of an expanding circular vortex sheet. Mathematica 21, 128-133.

Moore, D. W. and Saffman, P. G. 1971 Structure of a line vortex in an imposed strain. In Aircraft Wake Turbulence and Its Detection (Ed. Olsen, Goldberg, and Rogers), pp. 339-354. Plenum Press.

Moore, D. W. and Saffman, P. G. 1972 The motion of a vortex filament with axial flow. Phil. Trans. R. Soc. Lond. A272, 403-429.

Moore, D. W. and Saffman, P. G. 1975 The instability of a straight vortex filament in a strain field. Proc. R. Soc. Lond. A346, 413-425.

Paul, E. 1934 Bewegung eines Wirbels in geradlinig begrenzten gebieten. Z.A.M.M. 14, 105-116.

Polhamus, E. C. 1971 Predictions of vortex-lift characteristics by a leading-edge suction analogy. J. Aircraft 8, 193-199.

Prandtl, L. 1952 Essentials of Fluid Mechanics. Blackie.

Rayleigh, Lord 1916 On the dynamics of revolving fluids. Proc. R. Soc. A 93, 148-154.

Riley, N. 1973 Flows with concentrated vorticity: a report on EUROMECH 41, J. Fluid Mech. 62, 33-39.

Routh, E. J. 1881 Some applications of conjugate functions. Proc. Lond. Math. Soc. 12, 73-89.

Saffman, P. G. 1974 The structure and decay of trailing vortices. Arch. of Mech. 26 423-439.

Saffman, P. G. 1977 The number of waves on unstable vortex rings. Submitted.

Sarpkaya, T. 1971 On stationary and traveling vortex breakdowns. J. Fluid Mech. 45, 545-559.

Scorer, R. S. and Davenport, L. J. 1970 Contrails and aircraft downwash. J. Fluid Mech. 43, 451-464.

Smith, J.H.B. and Clark, R. W. 1975 Nonexistence of stationary vortices behind a two-dimensional normal plate. AIAA J. 13, 1114-1115.

Tombach, Ivar 1973 Observations of atmospheric effects on vortex wake behavior. J. Aircraft 10, 641-646.

Tsai, C-Y. and Widnall, S. E. 1976 The stability of short waves on a straight vortex filament in a weak externally imposed strain field. J. Fluid Mech. 73, 721-733.

Uberoi, M. S., Chow, C. and Narain, J. P. 1972 Stability of coaxial rotating jet and vortex of different densities. Phys. Fluids 15, 1718-1727.

Walton, D. 1974 A brief wind tunnel test of the Kasper airfoil. Soaring 38, 26-27.

Whitham, G. B. 1974 Linear and Nonlinear Waves. Wiley-Interscience.

Widnall, S. E., Bliss, D. B. and Tsai, C-Y. 1974 The instability of short waves on a vortex ring. J. Fluid Mech. 66, 35-47.

Widnall, S. E., Bliss, D. B. and Zalay, A. 1971 Theoretical and experimental study of the stability of a vortex pair. In Aircraft Wake Turbulence and Its Detection (Ed. Olsen, Goldberg, and Rogers), pp. 305-338. Plenum Press.

Widnall, S. E. and Sullivan, J. P. 1973 On the stability of vortex rings. Proc. Roy. Soc. Lond. A332, 335-353.

Widnall, S. E. and Tsai 1977 The instability of the thin vortex ring of constant vorticity. To appear.